João Pedro Verardo Benedetti

Desvendando a região nuclear de NGC 6868: população estelar e gás ionizado

Porto Alegre

2022

João Pedro Verardo Benedetti

Digging deeper into NGC 6868: stellar population and ionized gas

Porto Alegre
2022

João Pedro Verardo Benedetti

Desvendando a região nuclear de NGC 6868: população estelar e gás ionizado

Dissertação submetida ao Programa de Pós-Graduação em Física do Instituto de Física da UFRGS, como requisito parcial para obtenção do título de Mestre em Física, com ênfase em Astrofísica.

Universidade Federal do Rio Grande do Sul

Instituto de Física

Programa de Pós-Graduação em Física

Orientador: Prof. Dr. Rogério Riffel

Porto Alegre

2022

João Pedro Verardo Benedetti

Desvendando a região nuclear de NGC 6868: população estelar e gás ionizado

Dissertação submetida ao Programa de Pós-Graduação em Física do Instituto de Física da UFRGS, como requisito parcial para obtenção do título de Mestre em Física, com ênfase em Astrofísica.

Prof. Dr. Rogério Riffel
Orientador

Porto Alegre
2022

Este trabalho é dedicado às pessoas
que não estão na sala de jantar

Agradecimentos

Os Agradecimentos são talvez o mais próximo que uma dissertação de mestrado se aproxima de uma poesia, onde o trabalho em si fica ao lado para o humano que está entre as linhas precisas e exatas transparecer. Por isso, acho esta uma parte essencial para a completude da obra uma vez que penso que nem o mais egocêntrico dos seres se pensa capaz de ser o paladino da novidade absoluta. Na verdade, eu, assim como este trabalho, sou a síntese daqueles que me cercam e que contribuem para o meu crescimento e conhecimento.

Quero começar agradecendo o Rogério que me acolheu tão bem desde o 2º semestre na graduação. Parece que foi ontem que apareci na tua sala atrás de alguma IC. Obrigado pelo enorme conhecimento, humildade, paciência e incentivo, principalmente quando nada parecia estar fazendo sentido.

Impossível não agradecer meus pais Jaqueline e Luiz Carlos pela fundamental base, suporte, carinho, compreensão, pureza e exemplo. Principalmente, o exemplo. Admiro vocês demais e espero que, através deste trabalho vocês finalmente entendam o que eu estudo (acho que não...)!

Agradeço também a toda a minha família que também nunca entendeu o que eu estudava (não, esta não é uma dissertação sobre culinária), mas se permitiam ficar encantados quando eu tentava (e falhava) resumir algum tópico qualquer. Obrigado especialmente aos meus avós que levo pra sempre no peito.

Obrigado também aqueles que chegaram na minha vida pelas minhas andanças. Os que aprenderam a falar/ler/escrever comigo (Gabi G., João, Carol, Lala, Camily), os que junto comigo vieram desbravar a cativante(?) Porto Alegre (Gian, Martina), os que hoje em dia também tiveram que resolver os exercícios do Halliday (Cris, Eduardo, Mônica, Marcelo, Vitor, Otávio, Henrique, Pedro, Nati, Cata) e os que caíram na minha vida por pura sorte minha e azar de vocês (Júlia e Luiza). Vocês são tudo e podem sempre contar comigo pro que der e vier (ou seja, eu também conto com vocês ok?).

Um obrigado especialmente para o Nicholas que acompanhou todos os altos e baixos possíveis deste trabalho atrás das linhas. Teu suporte e carinho são muito importantes pra mim, pro Figo e pra Caju. Nada disso seria possível sem a tua companhia.

Agradeço a UFRGS também por ser uma instituição que me ensinou o valor da Universidade Pública e o papel transformador que ela cumpre. Espero que através da minha formação eu seja capaz de retribuir ao menos em parte o conhecimento que adquiri nos seus espaços. Agradeço por extensão a todos os professores, colegas e técnicos que

constroem a UFRGS diariamente.

Agradeço também ao CNPq e a CAPES por garantirem que a Pós-Graduação Brasileira exista e terem contribuído financeiramente para a execução deste trabalho. Que no futuro a real contribuição desses órgãos seja de fato valorizada por todos!

De antemão, agradeço aos membros da banca pela disponibilidade na leitura desta dissertação e pelos comentários que certamente enriquecerão o trabalho.

Por fim, quero agradecer aos meus eus passados. Obrigado por me trazerem até aqui e que o eu-presente também seja lembrado pelos eus futuros com o mesmo carinho que tenho por vocês (eus?) hoje.

"Even in a (...) universe where we have hot dogs
for fingers, we get very good with our feet."
(Everything Everywhere All At Once, 2022)

Resumo

Neste trabalho foram usados dados de espectroscopia de campo integral do telescópio Gemini para mapear a população estelar e o gás ionizado na região interna ($\sim 680 \times 470$ pc^2) da galáxia NGC 6868. A fim de entender as propriedades físicas e químicas do seu conteúdo estelar, nós aplicamos síntese de população estelar e medimos e os índices Fe4383, Mg_2, Mg_b, Fe5270, Fe5335 e derivamos Fe3, [MgFe]' e [α/Fe] para todo o campo. Já o gás ionizado foi analisado ajustando-se perfis gaussianos às linhas de emissão e as propriedades físicas deste foram derivadas a partir de razões entre seus fluxos. NGC 6868 é dominada por populações estelares velhas e ricas em metais (12.6 Gyr; 1.0 e 1.6 $Z_\odot$), apresentando um gradiente negativo em metalicidade. Também é detectada uma faixa de poeira que chega a A_V=0.65 mag. Não detectamos sinal de movimento ordenado das estrelas, com o centro caracterizado por alta dispersão de velocidades. Todos os índices apresentam um perfil espacial que varia significativamente através do FoV. Mg_2 apresenta um gradiente pouco inclinado, compatível com a ocorrência de fusões de objetos no passado. Mg_b e Fe3 sugerem diferentes mecanismos de enriquecimento para os elementos traçados por estes índices. Nós observamos três regiões distintas: para R<100 pc e R>220 pc, Mg_2, Mg_b estão anti-correlacionados com Fe3 e [MgFe]' e para 100 pc<R<220 pc eles correlacionam, sugerindo um históricos de enriquecimento distintos. O perfil de [α/Fe] é muito complexo, apresentando um valor central de $\sim$ 0.2 dex. Interpretamos tais achados como o resultado de uma fusão no passado com alguma galáxia com [α/Fe] distinto. A cinemática e morfologia do gás ionizado da galáxia reveladas por *channel maps* são complexas, sugerindo que diferentes processos estão atuando concomitantemente. Detectamos duas componentes onipresentes nas nossas observações: uma larga e uma estreita. A componente estreita traça um disco de gás ionizado enquanto a componente alargada traça um influxo de gás. A distribuição do avermelhamento derivado via razões de linhas se equipara espacialmente com o derivado via síntese de população estelar, porém com valores superiores, provavelmente devido ao obscurecimento do núcleo ativo de baixa luminosidade. Medimos temperaturas eletrônicas para NGC 6868 pela primeira vez, encontrando valores que variam de $\sim$ 14000 K no centro até $\gtrsim$ 20000 K nas regiões externas do FoV. Além disso,a medição da densidade eletrônica mostra um comportamento oposto ao da temperatura, com valores centrais atingindo $\sim$ 800 cm^{-3} e em regiões mais longe do centro de $\sim$ 100 cm^{-3}, sugerindo uma compressão do gás. Todos spaxels da galáxia tem razões de linhas que os classificam com LINER no diagrama BPT. Porém, no diagrama WHAN a região central é classificada como ionizada por um núcleo ativo enquanto que o componente mais extenso é ionizado por estrelas quentes evoluídas, sendo que os resultados cinemáticos não descartam a possibilidade de choques estarem influenciando a ionização do gás.

Palavras-chave: NGC 6868, núcleos de galáxias, populações estelares, gás ionizado

Abstract

We use Gemini integral field unit observations to map the stellar population and ionized gas properties of the inner region ($\sim 680 \times 470$ pc^2) of the galaxy NGC 6868. In order to understand the physical and chemical properties of the stellar content of this galaxy, we performed stellar population synthesis and measured the absorption line indices Fe4383, Mg_2, Mg_b, Fe5270, Fe5335 for the whole FoV, and used them to derive Fe3 and [MgFe]'. These indices were used to derive [α/Fe]. The ionized gas component was analysed via emission-line fitting and the physical properties of the ionized gas were derived using emission line flux ratios. This galaxy is dominated by old metal-rich populations (12.6 Gyr; 1.0 and 1.6 $Z_\odot$) with a negative metallicity gradient. A dust lane with a peak extinction of 0.65 mag is seen. No signs of ordered stellar motion is found and the stellar kinematics is dispersion dominated. All indices show a spatial profile varying significantly along the FoV. Mg_2 shows a shallow gradient, compatible with the occurrence of mergers in the past. Mg_b and Fe3 profiles suggest different enrichment processes for this elements. We observe three distinct regions: for R<100 pc and R>220 pc, Mg_2, Mg_b are anti-correlated with Fe3 and [MgFe]', and for 100 pc<R<220 pc, they are correlated, hinting at different enrichment histories. The [α/Fe] profile is really complex and has a central value of ~ 0.2 dex. We interpret this as the result of a past merger with another galaxy with different [α/Fe] history, thus explaining the [α/Fe] maps. Channel maps reveal complex kinematics and morphology of the ionized gas hinting at different processes acting on NGC 6868. We detect two components ubiquitous in our data: a narrow and a broad component. The narrow component traces an ionized gas disc whereas the broad component traces inflowing gas. The reddening in the V band matches the spatial distribution of the reddening derived by stellar population synthesis however with larger values probably due to the obscuration by dust of the central low-luminosity active galactic nuclei. We are able to measure the electronic temperature for NGC 6868 for the first time, finding values ranging from ~ 14000 K to $\gtrsim 20000$ K in an outward increasing temperature gradient. Also, density measurement shows an inverse behaviour with central values reaching ~ 800 cm^{-3} falling to ~ 100 cm^{-3} towards the edges of the data, hinting at a compression of the gas. This galaxy is entirely classified as a LINER object in the BPT diagram. The WHAN diagram shows that the central region is ionized by a central AGN with an outer extended component ionized by HOLMES. The kinematical findings coupled with the diagrams cannot rule out the presence of shock-heated gas.

Keywords: NGC 6868, galactic nuclei, stellar population, ionized gas

Lista de tabelas

Lista de abreviaturas e siglas

AGB	Ramo Assintótico das Gigantes
AGN	Núcleo Ativo de Galáxia
BPT	Baldwin, Phillips e Terlevich
CALIFA	*Calar Alto Legacy Integral Field Area Survey*
CCG	Galáxia Central de Aglomerados
DAR	Refração diferencial atmosférica
ETG	Galáxia *Early-Type*
EW	Largura Equivalente
FC	*Featureless continuum*
FoV	Campo de Visão
GMOS	*Gemini Multi-Object Spectrograph*
IFS	Espectroscopia de Campo Integral
IFU	Unidade de Campo Integral
IMF	Função Inicial de Massa
IRAF	*Image reduction and analysis facility*
IRAS	*Infrared Astronomical Satellite*
IUE	*International Ultraviolet Explorer*
LINER	Região de Emissão Nuclear de Baixa Ionização
LLAGN	AGN de baixa luminosidade
LOSVD	Distribuição de velocidades na linha de visada
KDC	Núcleo cinemático distinto
HOLMES	Estrelas evoluídas quentes de baixa massa
MaNGa	*Mapping Nearby Galaxies at APO*

MUSE	*Multi Unit Spectroscopic Explorer*
NED	Base de dados Extragaláticos da NASA
NGC	*New General Catalogue*
PA	Ângulo de posição
PCA	Análise de componentes principais
PSF	Função de Espalhamento de Ponto
SAURON	*Spectroscopic Areal Unit for Research on Optical Nebulae*
SDSS	*Sloan Digital Sky Survey*
SFH	Histórico de Formação Estelar
SMBH	Buraco Negro Supermassivo
SN	Supernova
SSP	População Estelar Simples

Sumário

1 Introdução

1.1 Evolução de galáxias e formação das *early-type*

Galáxias podem ser separadas em duas grandes classes: as galáxias passivas, que não estão formando estrelas ativamente e que possuem populações estelares vermelhas e velhas, e as *star-forming*, que são azuis e possuem altas frações de populações estelares jovens. Essa bimodalidade foi encontrada em vários estudos ao longo dos anos (KAUFFMANN et al., 2003; BALDRY et al., 2004; NOESKE et al., 2007; WETZEL; TINKER; CONROY, 2012; WEL et al., 2014), mesmo em altos *redshifts* (BRAMMER et al., 2009; MUZZIN et al., 2013). O problema é que os mecanismos responsáveis por regular a formação estelar (SF) e cessá-la para transformar as galáxias azuis em galáxias vermelhas ainda não são entendidos. Determinar os mecanismos físicos responsáveis por esta transição é um dos maiores desafios da astrofísica moderna (CANO-DÍAZ et al., 2016).

As propriedades fotométricas das galáxias correlacionam inclusive com sua morfologia. As galáxias passivas em geral são chamadas de galáxias *early-type* (ETGs), ou seja, galáxias elípticas e lenticulares, que podem ser divididas em rotadores lentos e rotadores rápidos. Eles, porém, possuem mecanismos de formação distintos, mas complementares. Cappellari (2016) fez uma revisão sistemática das propriedades destas galáxias derivadas a partir de dados de espectroscopia de campo integral e traçou o cenário mais atual para a formação e evolução das ETGS. As ETGs evoluem a partir de dois mecanismos. O primeiro por acreção de gás, sendo o combustível para a SF, assim aumentando a massa da galáxia e aumentando o seu componente esferoidal. E o segundo por canibalismo de galáxias menores, onde estabelece um halo em volta das ETGs, que leva o aumento da sua massa, sem alterar dramaticamente as propriedades da população estelar destes objetos.

Neste sentido, se forma um cenário de formação hierárquica (MO; BOSCH; WHITE, 2010). No universo primordial, os maiores halos de matéria escura foram também os que mais rapidamente acretaram gás que devido a sua natureza dissipativa consegue radiar energia e perder momento angular, sendo então convertido em estrelas. Este processo fez com que estes halos acumulassem muita matéria, formando assim muitas estrelas. Porém forma-se um halo de gás quente, que é aquecido pelo choque do gás que adentra a galáxia. Contudo, esse fenômeno inibe a SF, uma vez que cria uma "barreira" para entrada de gás nesta galáxia (KEREŠ et al., 2005; DEKEL; BIRNBOIM, 2006). As rotadoras rápidas, no entanto, tem uma via um pouco diferente de formação. Os halos menos massivos de matéria escura acabam tendo um regime de acreção mais lento, formando discos ricos em gás turbulento, podendo migrar para o centro da galáxia em formação e assim criando o seu bojo. Isso faz com que estes objetos tenham uma formação menos violenta quando

comparada às rotadoras lentas. Quando estes objetos entram nos halos que hospedam as rotadoras lentas, o gás é arrancado e a SF cessada. Devido a suas altas velocidades em relação ao halo principal que ocupam, elas vão sofrer poucas fusões no decorrer do tempo, mesmo no caso de uma fusão entre dois grupos ou aglomerados. As rotadores lentas, no entanto, através da fusão hierárquica continuam a crescer em massa através destes eventos, uma vez que ocupam o centro destes aglomerados.

Este cenário, apesar de explicar a maior parte das observações e as tendências observadas, possuem vários gargalos. Observações de ETGs já mostraram que estes objetos não são completamente desprovidos de gás (molecular, atômico e ionizado) como se acreditava anteriormente (CALDWELL, 1984; PHILLIPS et al., 1986). Descobertas recentes também detectaram que as ETGs possuem uma evolução mais diversa do que se acreditava, possuindo em alguns casos SF ativa, mesmo que diminuta, ou sinais de episódios de formação no seu passado (KOKUSHO et al., 2017). Portanto, estudar detalhadamente ETGs ainda se faz necessário para entendermos mais precisamente de que forma ocorrem as suas histórias evolutivas.

Outros problemas para entender este cenário de formação vem das das simulações cosmológicas, um dos maiores adventos da astrofísica do século XXI. Através delas, várias das hipóteses e observações de formação e evolução de galáxias foram confirmadas, porém em outros aspectos o atual modelo cosmológico padrão foi posto em cheque devido a discordâncias com as observações (BULLOCK; BOYLAN-KOLCHIN, 2017). Dentre estas discordâncias, as simulações preveem um número muito maior de galáxias satélites que não são observadas nos halos. Além disso, quando a função de luminosidade teórica das galáxias é comparada com a observada, se percebe que, apesar dela descrever relativamente bem galáxias com a luminosidade da Via-Láctea, ela sobre-estima tanto o número de galáxias de menor massa quanto de maior massa. Estes dois problemas, porém, têm em comum um aspecto: ambos podem ser resolvidos quando processos de *feedback* são incluídos nos modelos.

1.2 Feedback: soluções e desafios

Processos de *feedback*, de maneira geral, são processos relacionados à matéria bariônica que injetam energia no seu entorno. Eles podem ser de origem estelar, através dos ventos produzidos pelas Supernovas (SN) que expulsam as suas camadas externas injetando energia mecânica e radiativa no meio interestelar, ou de um núcleo ativo, que pode produzir jatos e ventos. Atualmente considera-se que eles desempenham um papel fundamental na evolução das galáxias. A modelagem de tais processos ainda é muito debatida e as simulações cosmológicas dependem de tais modelos para descrever os dados observacionais.

Desde a descoberta de correlações entre a massa do Buraco Negro Supermassivos (SMBH) e propriedades da galáxia hospedeira, como a dispersão de velocidades e a massa do componente esferoidal (MAGORRIAN et al., 1998; GEBHARDT et al., 2000; HÄRING; RIX, 2004) e com o aumento das evidências de que as diferentes manifestações dos Núcleos Ativos de Galáxias (AGN) estavam na verdade relacionados ao SMBH, um cenário de coevolução e interação entre eles surgiu (FABIAN, 2012; KORMENDY; HO, 2013; HECKMAN; BEST, 2014). A injeção de energia pelos AGNs mais energéticos tem fundamental importância em cessar a SF (CROTON et al., 2006; SEGERS et al., 2016) através da expulsão do material disponível para formar estrelas. A maior parte dos estudos tentando relacionar SF e AGNs foi feito em objetos relativamente brilhantes como Seyferts e quasares (NAYAKSHIN; ZUBOVAS, 2012) e, portanto, o efeito de AGNs de baixa luminosidade (LLAGN) na região circum-nuclear ainda é incerta. Este, inclusive, é a principal manifestação de AGNs no Universo local, estando presente em $\sim 1/3$ de todas as galáxias e representa $\sim 2/3$ de todos os tipos de AGN (HO, 2008). Portanto, estes objetos em especial precisam ser estudados para entendermos o seu impacto na região circum-nuclear.

Apesar do exato mecanismo de formação dos SMBH ainda ser desconhecido, já não é novidade que o *feedback* de AGN, resultado de uma acreção de matéria para o SMBH, desempenha um papel importantíssimo na regulação da SF (MATTEO; SPRINGEL; HERNQUIST, 2005; HOPKINS; ELVIS, 2010; HARRISON, 2017; STORCHI-BERGMANN; SCHNORR-MÜLLER, 2019; RIFFEL et al., 2021; ELLISON et al., 2021). O gás que alimenta a SF também alimenta o SMBH, disparando-o e injetando energia no meio interestelar que expulsa o gás e cessa a SF (FABIAN, 2012; KING; POUNDS, 2015; ZUBOVAS; BOURNE, 2017; TRUSSLER et al., 2020). Este processo se manifesta inclusive nas simulações cosmológicas. Quando elas não incluem alguma forma de *feedback*, a função de luminosidade não consegue ser reproduzida, tanto as maiores quanto as menores galáxias acabam mais massivas do que se observa nos dias atuais (SPRINGEL et al., 2005), sem contar que a idade da população estelar nas galáxias mais massivas é subestimada quando comparada as observações (CROTON et al., 2006). Apesar destas evidências darem conta de que algum processo de *feedback* deve estar atuando nestes objetos, distinguir a natureza física deles ainda é desafiador. O problema é que as simulações incluem estes efeito de uma maneira *ad hoc* (SCHAYE et al., 2015), ou seja, apenas para reproduzir os dados observacionais uma vez que não têm resolução suficiente para traçar os processos físicos a partir de primeiros princípios. Portanto, uma descrição completa deste impacto ainda é necessária pra separarmos os efeitos do *feedback* tanto do AGN quanto de SN, sendo necessários estudos detalhados de alta resolução espacial na vizinhança de SMBHs para delinear as propriedades tanto do gás ionizado quando da população estelar submetida a influência dele (RIFFEL et al., 2021).

Estudos tentaram estabelecer uma relação observacional direta entre SF e AGNs,

mas os resultados são controversos. SF parece ser comum em AGNs (RIFFEL et al., 2009; RUSCHEL-DUTRA et al., 2017; MALLMANN et al., 2018; RIFFEL et al., 2021; BURTSCHER et al., 2021; DAHMER-HAHN et al., 2021; RIFFEL et al., 2022) e alguns estudos mostram uma relação entre a fração de populações jovens e a luminosidade do AGN, sendo que os mais luminosos também apresentam as maiores frações (RIFFEL et al., 2009; RUSCHEL-DUTRA et al., 2017; ZUBOVAS; BOURNE, 2017; MALLMANN et al., 2018). Apesar disso, a emissão de raios-X duros (14-195 keV) das galáxias não aparenta estar correlacionada com a fração de populações jovens. Na verdade, o material jogado no meio interestelar pelas estrelas de idade intermediária parece ser importante na alimentação do AGN (RIFFEL et al., 2022).

1.3 O paradigma atual das LINERs

As Regiões de Emissão Nuclear de Baixa Ionização (LINER) foram primeiramente descritas por Heckman (1980) apresentando fortes linhas de íons de baixa ionização (O I, por exemplo) e linhas fracas de íons de alta ionização (O III, por exemplo). Mesmo que neste trabalho inicial já era reconhecida a natureza diversa dos objetos classificados como LINER, Através das décadas surgiu algum consenso frente a vários estudos que determinavam que estes objetos eram núcleos Seyfert em regimes de luminosidades menores (FERLAND; NETZER, 1983; HALPERN; STEINER, 1983; HO; FILIPPENKO; SARGENT, 1996; HO et al., 1997; CONSTANTIN; VOGELEY, 2006). Ou seja, a emissão observada era devido a um LLAGN. A detecção de núcleos rádio na escala de parsecs em 50% dos LINERs e jatos em escalas de subparsec (NAGAR; FALCKE; WILSON, 2005) e, mais recentemente, a detecção de *outflows* de gás ionizado em aproximadamente 48% das LINERs relacionadas com um SMBH (MUÑOZ et al., 2022) alimentaram este cenário. Estudos em raios-X, porém indicam que AGNs não podem ser os únicos responsáveis pelas intensidades das linhas observadas (FLOHIC et al., 2006).

Com estudos com resolução espacial melhor, assinaturas do tipo LINER foram encontradas não apenas na região nuclear das galáxias (< 1 kpc), mas também nas suas periferias, por isso novos termos foram adotados por alguns autores para descrever estes objetos: os LIERs ou LI(N)ERs. (SINGH et al., 2013; BELFIORE et al., 2016). Neste contexto, outros mecanismos de ionização são necessários para explicar as observações, como por exemplo: choques galáticos ou devido a *outflows* (HECKMAN, 1980; DOPITA; SUTHERLAND, 1995; HO et al., 2014; HO et al., 2016); galáxias *starbursts* dominadas por estrelas Wolf-Rayet (BARTH; SHIELDS, 2000); e estrelas HOLMES (BINETTE et al., 1994). Este último mecanismo tem ganhado cada vez mais suporte como o principal mecanismo de ionização em objetos com emissão estendida do tipo LINER (STASIŃSKA et al., 2008; FERNANDES et al., 2011; YAN; BLANTON, 2012; SINGH et al., 2013) com evidências fortes, como a correlação entre a emissão em Hα e propriedades da população

estelar em galáxias passivas (HSIEH et al., 2017), sugerindo uma origem estelar para as assinaturas LINER, e a falta de fótons ionizantes suficientes para explicar a emissão do tipo LINER devido apenas a LLAGN (ERACLEOUS; HWANG; FLOHIC, 2010). Neste sentido, LINERs (ou LIERs) podem ser encontradas em diferentes objetos, podendo diferentes fenômenos produzir assinaturas semelhantes. Por este motivo, não é possível agrupar estes objetos como uma classe homogênea (HERPICH et al., 2016).

A espectroscopia de campo integral (IFS) tem sido utilizada há cerca de uma década para ajudar no nosso entendimento sobre estes objetos, uma vez que é uma ferramenta poderosa para discernir espacialmente os diferentes mecanismos de ionização presentes em objetos com emissão do tipo LINER. Sarzi et al. (2010), usando o levantamento de dados SAURON de IFS feito com o objetivo de, dentre outros, entender melhor o componente do gás ionizado presente em ETGs dentro de $\tilde{1}$ raio efetivo, encontraram uma forte correlação entre a densidade superficial de massa estelar e a densidade superficial de emissão de Hβ, sugerindo uma origem estelar por trás dos fenômenos de ionização observados. Loubser e Soechting (2013) analisando os kpc centrais de galáxias centrais de aglomerados (CCG) evidenciou que LLAGN podem sim explicar a ionização observada, mas que choques ou fotoionização por estrelas HOLMES não poderiam ser descartadas. Ricci, Steiner e Menezes (2014a), Ricci, Steiner e Menezes (2014b), Ricci, Steiner e Menezes (2015a), Ricci, Steiner e Menezes (2015b) analisaram extensivamente os parsecs centrais de um grupo de 10 galáxias próximas usando o instrumento GMOS de vários tipos morfológicos classificadas como LINERs e encontraram evidências sólidas da presença de AGNs em ao menos 8 dos objetos avaliados. Apesar disso, descobriu-se discos de gás ionizado em 7 delas sendo que em 3 a fonte mais provável de ionização dos discos provinha de estrelas HOLMES. Belfiore et al. (2015) estudou 14 galáxias do levantamento MaNGa, que observou as galáxias até 2.5 raios efetivos, e encontrou componentes estendidos de gás ionizado consistentes com a emissão por estelar HOLMES. Hsieh et al. (2017) usando uma subamostra deste levantamento também encontrou uma correlação entre a densidade superficial de massa estelar e densidade superficial de Hα, indicando o mesmo cenário que aquele derivado utilizando SAURON. Estudos usando o levantamento de dados CALIFA (KEHRIG et al., 2012; PAPADEROS et al., 2013; SINGH et al., 2013; GOMES et al., 2016) encontraram estrelas velhas e quentes onipresentes e raros buracos negros acretando matéria. Um estudo mais recente de Menezes et al. (2022) usando a amostra mini-DIVING^{3D} foram capazes de separar a região nuclear da região circum-nucelar, podendo assim fazer um tratamento diferenciado entre cada um dos componentes devido a alta resolução dos seus dados. Eles reportaram que 23% da galáxias na mostra possuem emissão do tipo LINER e destas 69% tem sinais de atividade de AGNs. Lagos et al. (2022) usando dados do MUSE para estudar ETGs dominantes em seus grupos encontraram que a região central é mais influenciada por LLAGNs e as regiões externas ionizada por estrelas HOLMES. É claro que LINERs, como já dito, possuem uma natureza diversa e separar todos os fenômenos que ocorrem

concomitantemente só podem ser possíveis através de uma inspeção meticulosa de dados de IFS.

1.4 O caso de NGC 6868 e objetivos

Frente à necessidade de análises detalhadas da região nuclear de galáxias próximas, a fim de entender melhor tanto as conexões entre o SMBH e a galáxia hospedeira, quanto os processos por trás das assinaturas LINER, apresentamos aqui um estudo da população estelar e do gás ionizado da região central de NGC 6868.

NGC 6868 é uma galáxia elíptica (TULLY et al., 2013) do universo local (VAUCOULEURS et al., 1991), sendo o membro mais brilhante do grupo *Telescopium* e já foi observado em diversos comprimentos de onda. Alguns parâmetros extraídos do NED[1] podem ser vistos na tabela 1.

Tabela 1 – Tabela mostrando alguns parâmetros basicos de NGC 6868

Parameter	NGC 6868
RA (J2000)	$20^h09^m54^s.07$
Dec. (J200)	-48°22´46.4´´
Morphology[a]	E3
R (mag)[b]	7.91
M_R (mag)[b]	-24.7
Diameter (kpc)[c]	73.0
L_X (erg s^{-1})[d]	$8.54 \cdot 10^{40}$
Nuclear Activity[e]	LINER
Radio classification[f]	Flat-Spectrum Radio Source
A_V[g] (mag)	0.152
Radial Velocity[h] (km s^{-1})	2854
Distance[i] (Mpc)	27.70
Redshift[h] (z)	0.00952

Data available in NED
[a](VAUCOULEURS et al., 1991)
[b](CARRASCO; OLIVEIRA; INFANTE, 2006)
[c](LAUBERTS; VALENTIJN, 1989)
[d](BABYK et al., 2018)
[e](RICKES; PASTORIZA; BONATTO, 2008)
[f](HEALEY et al., 2007)
[g](SCHLAFLY; FINKBEINER, 2011)
[h](RAMELLA; FOCARDI; GELLER, 1996)
[i](TULLY et al., 2013)

Rickes, Pastoriza e Bonatto (2008) analisaram NGC 6868 através de observações em fenda longa e mostraram que ela exibe uma emissão do tipo LINER em seu centro

[1] O NED é operado pelo *Jet Propulsion Laboratory*, *California Institute of Technology* contratados pela *National Aeronautics and Space Administration*

que foi atribuída a uma combinação de LLAGN e choques. Eles também investigam a distribuição de metalicidade e do gás ionizado. Segundo eles, os índices apresentam um gradiente negativo, indicando sobreabundância de Fe, Mg, Na e TiO na região central em relação às bordas. Mg_2 correlaciona com Fe5270 e Fe5335, sugerindo processos de enriquecimento parecidos. O gradiente de Mg_2 sugere que esta galáxia elíptica foi formada através de fusões. A população estelar apresenta ao menos dois componentes com idades próximas de 13 e 5 Gyr.

NGC 6868 esteve incluída numa série de artigos analisando-a com dados de fotometria e espectroscopia de fenda longa (BUSON et al., 1993; ZEILINGER et al., 1996; MACCHETTO et al., 1996; CAON; MACCHETTO; PASTORIZA, 2000). Eles reportaram um disco de gás ionizado alinhado ao campo de velocidades das estrelas. Porém, para um dos seus ângulo de posição (PA), eles encontram um um disco interno que apresenta uma contra-rotação. Além disso, um núcleo cinemático distinto (KDC) é reportado nos 3" internos, uma vez que as estrelas internas aparentam contra-rotar com respeito as estrelas nas regiões externas. Eles encontram também que o gás ionizado em NGC 6868 tem uma morfologia do tipo "regular estendida" com possíveis filamentos pequenos.

Veron-Cetty e Veron (1988) detectaram uma uma faixa de poeira no centro de NGC 6868. Bregman et al. (1998) posteriormente detectaram poeira fria usando dados do IRAS. A massa média estimada de poeira quente, usando observações no infravermelho, foi de 70 $M_\odot$ (FERRARI et al., 2002). Observações no rádio (SLEE et al., 1994; MAUCH et al., 2003; HEALEY et al., 2007) revelaram uma fonte rádio com espectro plano de baixa potência no seu centro ($\alpha \sim 0.07$) cujo brilho, temperatura e inclinação é inconsistente com regiões H II, sendo um AGN a fonte mais provável para a emissão observada.

Hansen, Jorgensen e Norgaard-Nielsen (1991) examinaram esta galáxia usando fotometria de banda larga e estreita, e um espectro do IUE de baixa resolução, detectando uma faixa de poeira e alguns filamentos espirais emergindo a partir dela. Além disso, eles reportam que a distribuição de Lyα segue a poeira de maneira surpreendente. Tudo isso leva os autores a acreditar que NGC 6868 recentemente capturou uma companheira rica em gás. Machacek et al. (2010) usando dados do em raios-X do satélite Chandra encontraram fortes evidências de um encontro entre NGC 6868 e NGC 6861 que aconteceu aproximadamente há uma centena de milhões de anos, detectando caudas de maré, "cascas" e cavidades no raio-X, um indicativo de episódios energéticos do AGN no passado, que pode inclusive ter sido despertado pela interação. Rose et al. (2019) analisaram o gás molecular no centro de NGC 6868 e concluiram que ele está se arrastando em órbitas não circulares.

O nosso estudo portanto quer analisar, pela primeira vez com espectroscopia de campo integral, a região central da galáxia NGC 6868 para destrinchar todos estes processos que estão ocorrendo concomitantemente em seu centro. Os objetivos específicos deste

trabalho serão:

- Através da síntese de população estelar estimar a população estelar presente na região central de NGC 6868.
- Entender a evolução química desta população e como se relaciona a seu passado de formação.
- Estudar a cinemática do gás ionizado identificando possíveis inomogeneidades que expliquem os resultados passados.
- Entender a fonte de ionização presente em NGC 6868 e como se encaixa com resultados encontrados na população estelar.

2 Observações e tratamento dos dados

NGC 6868 foi observada no dia 04 de maio de 2013 com o telescópio *Gemini* usando o instrumento GMOS no modo IFU (ALLINGTON-SMITH et al., 2002; HOOK et al., 2004). Estes dados fazem parte do levantamento de dados DIVING^{3D} que fez observações da região central de 170 galáxias no hemisfério sul celeste com magnitude $B < 12.0$ e a longitude galática $|b| > 15°$. Para mais detalhes, Steiner et al. (2022) dão uma descrição completa do levantamento. A configuração de uma fenda foi usada para a observação, resultando num FoV de 5.0×3.5 arcsec^2. A rede de difração utilizada para a observação foi a B600-G5323 com um comprimento de onda central de 5620 Å indo de 4260 Å até 6795 Å. A resolução espectral é de 1.8 Å estimada através da linha do céu O I λ5577 Å. Exposições de *flat-field*, *bias* e os espectros da lâmpada de CuAr foram adquiridas para a calibração e redução. O *seeing* da observação foi estimado utilizando as estrelas presentes na imagem de aquisição na banda r (sistema do SDSS) da galáxia, tiradas com o imageador GMOS. Além disso, a anã branca DA EG 27 (HAMUY et al., 1992) foi observada a fim das calibrações espectrofotométricas serem feitas. Mais informações sobre a observação podem ser conferidas na tabela 2.

Processos padrão do IRAF (TODY, 1986; TODY, 1993) foram seguidos para reduzir os dados usando as tarefas contidas no pacote Gemini IRAF. *Bias*, *flat-fields*, calibração em comprimento de onda, correção da dispersão e calibração em fluxo foram aplicados nos dados. Para remover raios cósmicos, nós utilizamos o software LACOS (DOKKUM, 2001). Por fim, o cubo de dados final foi construído com uma amostragem espacial de 0.05 arcsec.

Depois da redução padrão, outros processos foram aplicados no cubo de dados a fim de melhorar a visualização dos dados como descrito em Menezes et al. (2019): remoção de ruídos de alta frequência através de um filtro BUTTERWORTH, correção da DAR, remoção de *fingerprints* instrumentais através da técnica de PCA e deconvolução Richardson-Lucy.

A remoção do ruído de alta frequência na dimensão espacial foi feita convoluindo cada imagem do cubo de dados com um filtro BUTTERWORTH (GONZALEZ; WOODS, 2008; RICCI; STEINER; MENEZES, 2014a). A ordem do filtro usado foi $n = 2$ e a

Tabela 2 – Tabela mostrando alguns parâmetros observacionais.

Parameter	NGC 6868
Observation date	2013 May 04
Gemini Programme	GS-2013A-Q-52
Seeing (arcsec)	0.77
Airmass	1.056
T_{exp} (s)	1800

frequência de corte $F_c = 0.14\ F_{Ny}$, sendo que F_{Ny} é a frequência *Nyquist* que corresponde a 0.5 spaxel^{-1}. Esta frequência de corte foi escolhida para remover apenas as frequências espaciais maiores que a PSF do cubo de dados, certificando que nenhuma informação cientifica válida seria perdida neste processo.

A correção da DAR consiste em corrigir o desvio que diferentes comprimentos de onda sofrem ao atravessar a atmosfera. Assim, este método desloca os planos das imagens do cubo de dados a fim de que o espectro num determinado ponto ocupe a mesma posição em todos os comprimentos de onda. A correção do DAR em NGC 6868 foi feita utilizando as equações de Bönsch e Potulski (1998) e Filippenko (1982) que assume um modelo de atmosfera plano-paralelo e calcula em função da distância zenital o índice de refração e outros parâmetros atmosféricos.

A técnica de tomografia PCA (STEINER et al., 2009) aplica PCA em cubos de dados. Este procedimento procura por correlações espectro-espaciais através do cubo de dados. Ele retorna portanto os auto-vetores (ou auto-espectros) que mostram as correlações entre os comprimentos de onda causadas tanto por um fenômeno físico quanto por uma *fingerprint* instrumental e os tomogramas que correspondem a projeções do cubo de dados em cada um dos autovetores encontrado. Esta é uma transformação ortogonal, ou seja, é garantido que sua inversa também exista. Os auto-vetores são classificados em relação a quanto cada um é capaz de explicar a variância do cubo de dados, portanto o primeiro autovetor é aquele que explica a maior parte da variância e assim por diante. Usando esta técnica, as *fingerprints* instrumentais podem aparecer como um dos autovetores que estariam sobrepostos aos dados. Assim, podem ser isolados e um cubo de dados recriado apenas com a inclusão do autovetor relacionado ao *fingerprint*. Este pode então ser descontado do cubo original, removendo o *fingerprint*.

Depois da remoção dos *fingerprints* instrumentais, o avermelhamento causado pela poeira dentro da Via-Láctea foi corrigido usando a lei CCM (CARDELLI; CLAYTON; MATHIS, 1989) e $A_V = 0.152$ mag (SCHLAFLY; FINKBEINER, 2011). As linhas telúricas também foram removidas e os espectros foram corrigidos pela velocidade de afastamento da galáxia, sendo trazidos ao referencial de repouso usando o desvio para o vermelho da tabela 1.

Por último, a deconvolução Richardson-Lucy (RICHARDSON, 1972; LUCY, 1974) é um processo iterativo que tem como objetivo reconstruir a imagem da galáxia antes de ser convoluída com a PSF quando passa pela atmosfera e os aparelhos óticos do telescópio. Após 10 iterações, a PSF final foi de 0.71 arcsec, estimada a partir do perfil espacial obtido a partir da asa vermelha na componente largo de Hα.[1]

[1] Esta parte do trabalho foi realizado pelo Prof. Dr. Tiago Ricci

3 Metodologia

3.1 STARLIGHT

Para derivar o SFH da região central de NGC 6868, nós utilizamos o código STARLIGHT (FERNANDES et al., 2004; FERNANDES et al., 2005; FERNANDES et al., 2013; FERNANDES, 2018) que ajusta o contínuo do espectro combinando em proporções diferentes a contribuição de SSPs, levando em conta o avermelhamento e parâmetros cinemáticos. Em outras palavras, ele tenta ajustar o espectro observado (O_λ) com um modelado (M_λ), dado por

$$M_\lambda = M_{\lambda_0} \left[\sum_{j=1}^{N_*} x_j b_{j,\lambda} r_\lambda \right] \otimes G(v_*, \sigma_*), \tag{3.1}$$

sendo que M_{λ_0} é a densidade de fluxo média dentro de um intervalo de normalização predeterminado[1], N_* é o número de elementos na base de SSPs utilizada, x_j é contribuição em luz do j-ésimo elemento da base de SSPs no comprimento de onda de normalização, $b_{j,\lambda}$ é o espectro do j-ésimo elemento da base de SSPs, r_λ é o fator de avermelhamento dado por $r_\lambda = 10^{-0.4(A_\lambda - A_{\lambda_0})}$ e $A_\lambda = A_V q_\lambda$, sendo q_λ a lei de extinção avaliada em λ. Por último, o código convolui o espectro modelado com uma Gaussiana para levar em conta a LOSVD do componentes estelar no espectro, onde v_* é a velocidade estelar na linha de visada e σ_* é a dispersão de velocidades estelar na linha de visada. Para determinar qual o melhor ajuste, o código procura, variando todos estes parâmetros, a combinação que minimiza a função

$$\chi^2 = \sum_\lambda [(O_\lambda - M_\lambda)\omega_\lambda]^2 \tag{3.2}$$

onde ω_λ é o peso e pode ser usado tanto para mascarar ($\omega_\lambda = 0$) determinadas características do espectro, como problemas no CCD ou intervalos dominados por emissão de outros componentes, como as linhas de emissão do gás ionizado, ou para dar maior peso estatístico para determinados intervalos do espectro (certas absorções estelares características para permitir estimativas cinemáticas melhores, se este for o objetivo pretendido). Para além de mascarar os locais das emendas dos CCDs e linhas de emissão presentes no nosso cubo de dados, a absorção de Mg I λ5200 Å e NaD λ5894 Å também foram omitidas na síntese. Isso foi feito para tentar isolar a contaminação por processos de *α-enhancement* da determinação da metalicidade e do meio interestelar.

Um dos ingredientes fundamentais neste método é base de SSPs usada. Nós construímos a nossa base de elementos com os modelos da biblioteca MILES (VAZDEKIS

[1] Nós normalizamos o espectro na região de 5700 Å, devido à falta de absorções estelares significativas e ter um bom S/N em todo FoV.

et al., 2016) usando as isócronas de Girardi et al. (2000) e a IMF de Kroupa (2001). Estes modelos foram escolhidos porque o intervalo de comprimento de onda abrangido pelos modelos se sobrepões aos nossos dados e têm uma resolução espectral melhor quando comparados com outros modelos de SSPs (BRUZUAL; CHARLOT, 2003; MARASTON; STRÖMBÄCK, 2011; CONROY; GUNN; WHITE, 2009). Esta alta resolução espectral é fundamental para modelar as absorções estelares e permitir um estudo preciso da cinemática do gás quando o contínuo estelar for descontado. A base final de SSPs abrange 15 idades (0.0631, 0.1, 0.16, 0.28, 0.50, 0.89, 1.26, 1.41, 2.51, 3.98, 6.31, 7.94, 10.0, 11.2, 12.6 Gyr) e seis metalicidades (0.005, 0.02, 0.2, 0.4, 1.0, 1.6 $Z_{\odot}$), sendo $Z_{\odot} = 0.019$ (GIRARDI et al., 2000).

Os modelos MILES, porém, não contam com SSPs jovens, sendo a SSP de menor idade a de 63 Myr. A fim de testarmos se NGC 6868 possui estes componentes muito jovens, nós fizemos testes com os modelos de Bruzual e Charlot (2003) que possuem resolução espectral menor, mas incluem modelos de SSPs com até 0.1 Myr. Nós não encontramos nenhuma contribuição significativa para SSPs mais jovens que 63 Myr. Utilizamos a lei de extinção CCM (CARDELLI; CLAYTON; MATHIS, 1989, R_V=3.1) para modelar a atenuação por poeira (A_V) intrínseca ao nosso objeto. Além disso, para levar em conta um possível FC devido a presença de um AGN, nós incluímos na nossa base um espectro de uma lei de potência do tipo $f \sim \nu^{-1.5}$. Foram testados também FCs com diferentes expoentes, indo de -1.75 até -1.0, porém nenhuma contribuição significativa destes componentes foi encontrada.

Por fim, para melhor entender a distribuição de idade e metalicidade nesta galáxia, nós calculamos a idade média $\langle t \rangle_L$ e a metalicidade média $\langle Z \rangle_L$ em cada spaxel (FERNANDES et al., 2005), sendo a idade média pesada por luz

$$\langle t \rangle_L = \sum_j x_j \log(t_j), \tag{3.3}$$

e a metalicidade média pesada por luz

$$\langle Z \rangle_L = \sum_j x_j Z_j. \tag{3.4}$$

Decidimos não mostrar as quantidades pesadas em massa uma vez que já é sabido que esta galáxia é dominada por estrelas velhas de baixa massa. Ao usar as quantidades pesadas em luz, os parâmetros ficam mais sensíveis à presença das estrelas mais jovens, tornando mais fácil sua detecção.

Para otimizar o gerenciamento dos dados, nós utilizamos o código MEGACUBE (MALLMANN et al., 2018; RIFFEL et al., 2021) que tem como entrada o cubo de dados e prepara-o para fazer a síntese, executa a síntese e também computa os parâmetros para análise preliminar (por exemplo, calcula as Eq. 3.3 e 3.4) além de montar os mapas num novo cubo com os resultados para análise posterior.

3.2 Medição de índices

A fim de melhor entender a história de formação de NGC 6868, principalmente através dos processo de α-*enhancement*, nós medimos os índices para as linhas de absorção. Nós medimos os índices para Fe4383, Mg_2, Mg_b, Fe5270, Fe5335 usando as definições apresentadas em Riffel et al. (2019) que são baseadas em Worthey et al. (1994). Estes índices foram então utilizados para derivar Fe3[2] e [MgFe]′[3]. Para que uma medição precisa dos índices fosse feita, todos os spaxeis foram corrigidos pela velocidade na linha de visada derivada pelo STARLIGHT e alargadas com uma gaussiana para coincidir com a resolução do sistema Lick/IDS de 8.2 Å (ROSA et al., 2007).

O código PACCE (RIFFEL; VALE, 2011) foi usado para medir as EWs destes índices. O código usa bandas predefinidas em volta das absorções e ajusta uma reta como pseudo-contínuo. Uma vez ajustada, os EW são calculados através de

$$W_\lambda = \left(1 - \frac{A_2}{C}\right)(\lambda_u - \lambda_i)\,, \tag{3.5}$$

sendo W_λ o EW medido, A_2 e C são as áreas integradas abaixo das absorções e do pseudo contínuo, respectivamente, e λ_u e λ_i são comprimentos de onda predeterminados inicial e final da banda de absorção. O método de integração do trapézio foi implementado e o cálculo do EW de todos os índices foi feito em todo o cubo.

Um problema enfrentado durante a síntese foi a contaminação das linhas [N I] λ 5197, 5200 Å que ficam entre a absorção de Mg I e a definição das bandas de ajuste do pseudo contínuo para medição de Mg_b. Para conseguir corrigir por este problema, nós modelamos as linhas e subtraímos sua contribuição dos spaxeis. Na figura 1, um exemplo de um spaxel deste desconto é dado, mostrando a diferença no fluxo estimado no espectro com a contaminação pela linha de emissão e depois da modelagem. Na seção 3.3 explicamos como se deu o processo de ajuste destas linhas.

Com todos os índices medidos, nós queríamos derivar o [α/Fe] da população estelar. Nós seguímos os procedimentos descritos em Barbera et al. (2013) usando os índices Mg_b, Fe3 e a idade média pesada pela luminosidade, derivada pelo STARLIGHT para medir Z_{Mg_b} e Z_{Fe3}. Isto foi feito interpolando os modelos de Vazdekis et al. (2015) e criando grades variando a metalicidade e as idades dos modelos. Como mencionado em Barbera et al. (2013),pode ser necessário extrapolar as grades em populações α-*enhanced*. Assim, calculamos o *proxy* $[Z_{Mg_b}/Z_{Fe3}] = Z_{Mg_b}\text{-}Z_{Fe3}$ que finalmente pode ser usado para calcular [α/Fe] através de (TREVISAN; MAMON; KHOSROSHAHI, 2017)

$$[\alpha/\mathrm{Fe}] = -0.07 + 0.51[Z_{Mg_b}/Z_{Fe3}]. \tag{3.6}$$

[2] Fe3 = (Fe4383 + Fe5270 + Fe5335)/3 (KUNTSCHNER, 2000)

[3] $[\mathrm{MgFe}]' = \sqrt{Mg_b}\,(0.72 \times \mathrm{Fe5270} + 0.28 \times \mathrm{Fe5335})$ (THOMAS; MARASTON; BENDER, 2003)

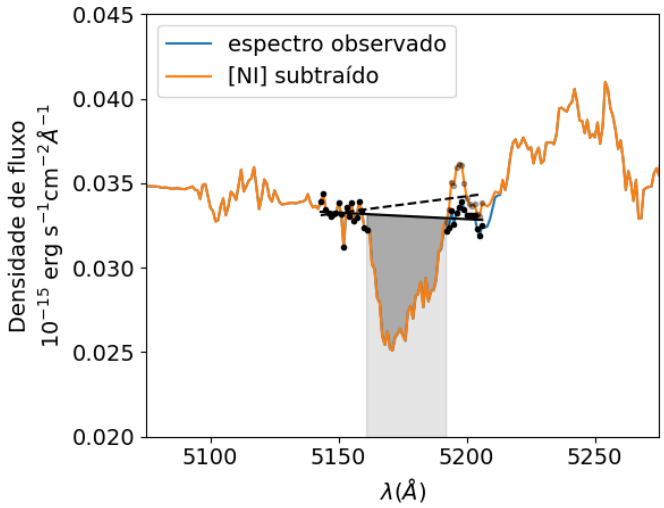

Figura 1 – Exemplo de espectro mostrando o espectro observado e depois de descontada a linha [NI]. A linha pontilhada mostra o continuo se não tivesse sido feita a correção e a linha continua onde de fato foi traçado o contínuo. Podemos ver que este efeito é muito significativo para fazer esta medição.

3.3 IFSCube: Ajuste dos perfis de linha

Uma vez que a análise da população estelar foi concluída e o contínuo estelar modelado com precisão, partimos para a análise do gás ionizado. O componente do gás ionizado pode ser isolado descontando a emissão estelar, sendo possível analisar apenas as linhas de emissão.

Após a subtração do contínuo estelar, porém nós acabamos com uma razão sinal-ruído (S/N) muito baixa em algumas regiões do espectro, principalmente nas bordas do FoV. A fim de melhorar o S/N utilizamos *voronnoi binning* (CAPPELLARI; COPIN, 2003) que agrupa os dados, preservando a máxima resolução espacial dado um S/N mínimo predefinido que deve ser atingido em todo o FoV. O sinal foi medido como sendo o fluxo médio entre 6528-6615 Å que engloba as linhas de emissão [N II] $\lambda 6548, 6584$+Hα. O ruído foi estimado como o desvio padrão entre 4800-4845 Å. Nós optamos por usar esta região do espectro porque ela está do lado azul do espectro e, portanto, é também mais ruidosa, funcionando assim como um limite superior para o ruído em todo o espectro. O alvo do S/N utilizado foi 30.

A síntese, apesar da precisão, pode levar a discrepâncias entre os dados e o contínuo estelar. Isso pode ser contornado ajustando-se um pseudo-contínuo não físico na forma de um polinômio alta ordem no espectro descontado da população estelar. Para fazer este ajuste, nós mascaramos os intervalos onde temos as linhas de emissão e botamos peso em dobro em bandas de 20 Å do espectro em volta de cada uma das linhas, assegurando que nestas regiões o contínuo seria bem ajustado. Várias configurações foram testadas, mas

acabamos com um polinômio de grau 13 para ajustar nossos dados.

Depois deste pré-processamento, fomos então para o ajuste das linhas de emissão de fato. Esta é uma das principais funções do IFSCube (RUSCHEL-DUTRA; OLIVEIRA, 2020)[4], que ajusta as diferentes linhas usando funções gaussianas. O código permite estabelecer vínculos entre as diferentes linhas assegurando que o ajuste final tenha uma motivação física. Grupos cinemáticos é um dos jeitos de estabelecer estes vínculos, fazendo com que as diferentes linhas mantenham os mesmos parâmetros cinemáticos através do processo de ajuste (velocidade e dispersão de velocidades).

O espectro de NGC 6868 é rico em linhas de emissão, permitindo-nos caracterizar suas propriedades físicas. As linhas identificadas que conseguimos ajustar foram H I Hα, Hβ e Hγ, [N II] λ5755, 6548, 6583 Å, [O III] λ4959, 5007 Å, [O I] λ6300, 6360 Å, [N I] λ5197, 5200 Å e [S II] λ6716, 6731 Å. A cinemática do gás ionizado deste objeto já foi estudada através de espectroscopia de fenda longa (CAON; MACCHETTO; PASTORIZA, 2000; ZEILINGER et al., 1996) e eles encontraram uma cinemática complexa. Além disso, temos uma diversidade enorme nos perfis de linha detectados. Portanto, vários testes foram feitos com diferentes configurações até chegarmos em um modelo consistindo em dois componentes cinemáticos para cada linha: uma estreita e uma larga. Esta configuração foi aplicada em todos os spaxeis.

Para reduzir a degenerescência do nosso ajuste, nós fizemos algumas suposições e estabelecemos outros vínculos nos nossos modelos. Primeiramente, utilizamos razões de linhas bem conhecidas (OSTERBROCK; FERLAND, 2006): [N II] λ6583 Å = 3.06 [N II] λ6548 Å, [O III] λ5007 Å = 2.94 [O III] λ4959 Å e [O I] λ6300 Å = 3.05 [O I] λ6360 Å. Em um primeiro momento, estabelecemos grupos cinemáticos apenas entre linhas produzidas pelos mesmo íons. Porém, percebemos que as linhas produzidas por diferentes íons acabaram com a cinemática e a distribuição de fluxo parecidas entre si. Assim, para reduzir novamente a degenerescência, deixamos o ajuste apenas com dois grupos cinemáticos, ou seja, o grupo de linhas estreitas precisa ter a mesma velocidade e dispersão de velocidade através das diferentes linhas produzidas pelos diferentes íons. Isso ajuda o perfil modelado a ficar mais preciso, principalmente as linhas mais fracas, uma vez que o ajuste precisará apenas variar a amplitude destas linhas para reproduzi-las.

3.4 PyNeb: Determinação de parâmetros físicos

As linhas de emissão, para além das informações cinemáticas do gás carregam informações sobre o estado físico dele. Assim, razões de linhas podem ser utilizadas para derivarmos parâmetros físicos e as condições de onde está este gás. Temperatura (T_e) e densidade(n_e) eletrônicas foram computadas usando PyNeb (LURIDIANA; MORISSET;

[4] Disponível em: https://github.com/danielrd6/ifscube

SHAW, 2015) através das razões de linha [N II] λ5755, 6583 Å e [S II] λ6716, 6731 Å além das razões de linha [N II] λ6583/Hα, [S II] λ6716, 6731/Hα, [O I] λ6300/Hα, [O III] λ5007/Hβ.

O avermelhamento também foi derivado usando PyNeb. Considerando o caso B de recombinação e algumas estimativas aproximadas para a temperatura e densidade do gás, como primeira aproximação (n_e=100 cm^{-3} e T_e=10000 K), nós estimamos o valor teórico $\mathrm{F_{H\alpha}/F_{H\beta}} = 2.87$. Assumindo a lei de extinção (f_λ) CCM (CARDELLI; CLAYTON; MATHIS, 1989, $\mathrm{R_V}$=3.1) e seguindo Riffel et al. (2021), chegamos às seguintes relações:

$$\begin{aligned} \mathrm{E(B-V)} &= \frac{E(\mathrm{H\beta}-\mathrm{H\alpha})}{f_\lambda(\mathrm{H\beta})-f_\lambda(\mathrm{H\alpha})} \\ &= \frac{2.5}{3.1\cdot(1.164-0.818)}\log\left(\frac{(\mathrm{F_{H\alpha}/F_{H\beta}})^{\mathrm{obs}}}{(\mathrm{F_{H\alpha}/F_{H\beta}})^{\mathrm{theo}}}\right) \end{aligned} \tag{3.7}$$

$$A_\mathrm{V} = 7.22\log\left(\frac{(\mathrm{F_{H\alpha}/F_{H\beta}})^{\mathrm{obs}}}{2.87}\right). \tag{3.8}$$

Portanto, usando as linhas de recombinação de Balmer (Hα, Hβ), nós derivamos o avermelhamento na banda V (A_V) e corrigimos os fluxos das linhas de emissão pelo avermelhamento derivado através de

$$\mathrm{F_{int}} = \mathrm{F_{obs}}10^{0.4\cdot \mathrm{A}_\lambda} = \mathrm{F_{obs}}10^{0.4\cdot \mathrm{A_V}\cdot f_\lambda}. \tag{3.9}$$

onde f_λ é o valor da lei de extinção no comprimento de onda da linha que estamos corrigindo.

4 A População Estelar de NGC 6868

No capítulo que segue apresentamos os resultados da análise do conteúdo estelar de NGC 6868. Esse artigo já foi submetido para a MNRAS e está em processo de revisão.

MNRAS **000**, 1–13 (2022) Preprint 24 January 2023 Compiled using MNRAS LATEX style file v3.0

Digging deeper into NGC 6868 I: stellar population

João P. V. Benedetti,[1] ⋆ Rogério Riffel,[1] † Tiago Ricci,[2] Marina Trevisan,[1] Rogemar A. Riffel,[3] Miriani Pastoriza,[1] Luis G. Dahmer-Hahn,[4] Daniel Ruschel-Dutra,[5] Alberto Rodríguez-Ardila,[6] Jose A. Hernandez-Jimenez[7] and João Steiner[8] ‡

[1]*Departamento de Astronomia, Universidade Federal do Rio Grande do Sul. Av. Bento Gonçalves 9500, 91501-970 Porto Alegre, RS, Brazil*
[2]*Universidade Federal da Fronteira Sul, 97900-000 Campus Cerro Largo, RS, Brazil*
[3]*Departamento de Física, Universidade Federal de Santa Maria, Centro de Ciências Naturais e Exatas, 97105-900 Santa Maria, RS, Brazil*
[4]*Shanghai Astronomical Observatory, Chinese Academy of Sciences, 80 Nandan road, Shanghai 200030, China*
[5]*Departamento de Física - CFM - Universidade Federal de Santa Catarina, 476, 88040-900 Florianópolis, SC, Brazil*
[6]*Laboratório Nacional de Astrofísica/MCT - Rua dos Estados Unidos 154, Bairro das Nacões. CEP 37504-364 Itajubá, MG, Brazil*
[7]*Universidade do Vale do Paraíba, Av. Shishima Hifumi, 2911, Zip Code 12244-000, São José dos Campos, SP, Brazil*
[8]*Instituto de Astronomia, Geofísica e Ciências Atmosféricas, Universidade de São Paulo, 05508-900 São Paulo, Brazil*

Accepted XXX. Received YYY; in original form ZZZ

ABSTRACT

We use Gemini integral field unit observations to map the stellar population properties in the inner region ($\sim 680 \times 470$ pc^2) of the galaxy NGC 6868. This is the most massive galaxy from the Telescopium Group. In order to understand the physical and chemical properties of the stellar content of this galaxy, we performed stellar population synthesis using the STARLIGHT code with the MILES simple stellar population models. We measured the absorption line indices Fe4383, Mg_2, Mg_b, Fe5270, Fe5335 for the whole FoV, and used them to derive Fe3 and [MgFe]'. These indices were used to derive [α/Fe]. This galaxy is dominated by old metal-rich populations (12.6 Gyr; 1.0 and 1.6 $Z_\odot$) with a negative metallicity gradient. A dust lane with a peak extinction of 0.65 mag is seen. No signs of ordered stellar motion are found and the stellar kinematics is dispersion dominated. All indices show a spatial profile varying significantly along the FoV. Mg_2 shows a shallow gradient, compatible with the occurrence of mergers in the past. Mg_b and Fe3 profiles suggest different enrichment processes for these elements. We observe three distinct regions: for R<100 pc and R>220 pc, Mg_2, Mg_b anti correlate with respect to Fe3 and [MgFe]', and for 100 pc<R<220 pc, they correlate, hinting at different enrichment histories. The [α/Fe] profile is really complex and has a central value of $\sim$ 0.2 dex. We interpret this as the result of a past merger with another galaxy with a different [α/Fe] history, thus explaining the [α/Fe] maps.

Key words: galaxies: individual (NGC 6868), galaxies: nuclei, galaxies: elliptical and lenticular, cD, galaxies: stellar content

1 INTRODUCTION

Galaxies can widely be defined as either *passive*, that are not actively forming stars and host a red and old stellar population, and *star-forming* galaxies, that are blue, hosting large fractions of young stellar populations. This bi-modality was found in many studies over the years (e.g. Kauffmann et al. 2003; Baldry et al. 2004; Noeske et al. 2007; Wetzel et al. 2012; van der Wel et al. 2014), even at high redshifts ($z > 2.5$ Brammer et al. 2009; Muzzin et al. 2013, for example). However, it is not yet clear which mechanisms are regulating star formation and transforming the blue galaxies into *red-and-dead* ones. A major challenge in modern astrophysics is to determine the physical mechanism acting in quenching star formation in galaxies.

Nowadays, it is established that active galactic nuclei (AGN) feedback plays an important role in regulating the star formation (SF) of its host galaxy (Di Matteo et al. 2005; Hopkins & Elvis 2010; Harrison 2017; Storchi-Bergmann & Schnorr-Müller 2019; Riffel et al. 2021; Ellison et al. 2021). The gas inflowing, responsible for SF, also feeds the supermassive black hole (SMBH), triggering the AGN episode that can either heat (or expel) the gas, thus shutting down the SF (Fabian 2012; King & Pounds 2015; Zubovas & Bourne 2017; Trussler et al. 2020). In cosmological simulations without including AGN and stellar feedback, the observed luminosity function of galaxies cannot be reproduced: the larger and smaller galaxies end up with higher masses than observed in the present-day universe (Springel et al. 2005). Also, the ages of the stars from the most massive galaxies are underestimated when compared with observations (Croton et al. 2006). These results show that some form of gas striping or heating must be taking place in these objects. However, distinguishing the nature of such processes is still challenging, once the simulations cannot reach the physical scales involved and use *ad hoc* prescriptions to account for these mechanisms (Schaye et al. 2015). In order to really disentangle the effects of supernova (SN) feedback and AGN we need to look at the vicinity of SMBH and trace the star formation history (SFH) of that population in order to understand the effect of the AGN in the stellar population (Riffel et al. 2021).

⋆ E-mail: joao.benedetti@ufrgs.br (JPVB)
† E-mail: riffel@ufrgs.br (RR)
‡ In Memorian.

Past studies have tried to establish this link, but the results have been controversial. Despite SF being common in AGNs (Riffel et al. 2009; Ruschel-Dutra et al. 2017; Mallmann et al. 2018; Riffel et al. 2021; Burtscher et al. 2021; Dahmer-Hahn et al. 2021; Riffel et al. 2022), the time scale for starting the star formation ($\sim$ 100 Myr, Hickox et al. 2014; Burtscher et al. 2021) is far greater than for the AGN triggering ($\sim 0.1 - 1$ Myr, Novak et al. 2011; Schawinski et al. 2015), preventing us from connecting the two. Some studies show a correlation between the fraction of young populations and the AGN luminosity, where the most luminous sources present the highest fraction (Riffel et al. 2009; Ruschel-Dutra et al. 2017; Zubovas & Bourne 2017; Mallmann et al. 2018). However, the hard X-ray (14-195 keV) luminosity from the galaxies does not seem to correlate with the fraction of young populations (Burtscher et al. 2021). Instead, mass loss from intermediate-age stars seems to be important in AGN feeding (Riffel et al. 2022).

Most of the previous studies have been done on relatively bright objects. However, the most common form of AGN in the local Universe is low luminosity AGN (LLAGN) in massive galaxies (Ho 2008). Most of them are classified as low-ionization nuclear emission-line region (LINER) objects (Heckman 1980). However, despite their significance, the physical nature of these objects is still poorly understood. Since their discovery, many mechanisms have been purposed to explain the LINER signature beyond the LLAGN paradigm (Ferland & Netzer 1983; Halpern & Steiner 1983), once many other physical processes can mimic the same spectral signatures without the LLAGN (these objects are known as LIERs Cid Fernandes et al. 2011; Belfiore et al. 2016) such as shocks (Heckman 1980), hot low-mass evolved stars (HOLMES) (Binette et al. 1994; Yan & Blanton 2012; Papaderos et al. 2013; Singh et al. 2013; Belfiore et al. 2016) and starbursts with ages between 3 and 5 Myr, dominated by Wolf-Rayet stars (Barth & Shields 2000). With current observational technology, one can disentangle the different ionization mechanisms by performing detailed spatially resolved studies analysing both the stellar population and the ionized gas components.

Even in the LLAGN hypothesis, the effects of such objects in their host galaxy are still uncertain as most studies focusing on the AGN impact over galaxies are performed with high-luminosity AGN (e.g. Seyferts and quasars, e.g. Nayakshin & Zubovas 2012). With the rising importance of LINERs, new studies have been analysing such impacts, although a complete picture is yet to be drawn and further research is needed.

IFU spectroscopy has expanded our view towards early-type galaxies, their formation and evolution. This technique allowed to better constrain the stellar population and the kinematical structure in this objects, with the emergence of KDCs, counter-rotating stellar discs and so on (see Cappellari 2016, for a review). Despite previous studies being able to reproduce the stellar population parameters of ETGs with a rapid in-situ conversion of gas into stars (e.g. Chiosi & Carraro 2002) with including a fully consistent chemical evolution (e.g. Vazdekis et al. 1997), the emergence of this structures has been seen as evidence for the importance of merger processes in ETG formation. Dry minor mergers have already been established as a subsequent growth pathway for ETGs (the two phases of galaxy formation Oser et al. 2010; Navarro-González et al. 2013), however they rarely affect the central regions of galaxies. Therefore, studying this structures in galactic cores may help us further elucidate the formation and evolution of ETGs (e.g. Krajnović et al. 2015).

From the above, it is clear that detailed studies thoroughly analysing the nuclear regions of galaxies probing the stellar population and gas content are fundamental to elucidate the impact of the AGN with respect to the galaxy evolution. In this sense, an "artisanal" approach is better at analysing the details that would otherwise be missed in large surveys. With this in mind, here we present a detailed GMOS IFU study of the galaxy NGC 6868. A nearby (27.70 Mpc, Tully et al. 2013) elliptical galaxy (E2, de Vaucouleurs et al. 1991). Some basic parameters extracted from NED can be seen in table 1 and three images from NGC 6868 in different scales are shown in Fig. 1. NGC 6868 is the brightest member of the Telescopium group. In addition, Rickes et al. (2008) have shown that NGC 6868 exhibits LINER emission in its centre, which has been attributed to a combination of an LLAGN and shocks. They also investigate this galaxy's metallicity distribution and ionized gas by means of long-slit spectroscopy and stellar population synthesis. According to the authors, Lick indices present a negative gradient indicating an overabundance of Fe, Mg, Na and TiO in the central parts with respect to the external regions. Mg_2 correlates with Fe5270 and Fe5335, suggesting that these elements probably underwent the same enrichment process in NGC 6868. The lack of correlation between computed galaxy mass and the Mg_2 gradient suggests that this elliptical galaxy was formed by merger events. The stellar population synthesis shows the presence of at least two populations with ages of 13 and 5 Gyr old. The fact that this galaxy apparently has multiple ionization scenarios behind it and also shows signs of complex star formation history makes NGC 6868 an excellent candidate to further investigate the mechanisms behind LINER emission and the processes involved in the evolution of early-type galaxies.

NGC 6868 was already observed in different wavelengths. Machacek et al. (2010) using X-ray data found strong evidence of a past encounter between NGC 6868 and NGC 6861, displaying tidal tails and shells. Moreover, they found X-ray cavities, indicative of past AGN activity. Hansen et al. (1991) studied NGC 6868 using CCD images and an International Ultraviolet Explorer (IUE) low-resolution spectrum, and they found a dust lane in the centre of the galaxy with an extended dust component with spiral features.

Table 1. Table showing some basic parameters of the galaxy NGC 6868.

Parameter	NGC 6868
RA (J2000)	$20^h09^m54^s.07$
Dec. (J200)	-48°22´46.4´´
Morphology[a]	E2
R (mag)[b]	7.91
M_R (mag)[b]	-24.7
Diameter (kpc)[c]	73.0
L_X (erg s^{-1})[d]	$8.54 \cdot 10^{40}$
Nuclear Activity[e]	LINER
Radio classification[f]	Flat-Spectrum Radio Source
A_V (mag)[g]	0.152
Radial Velocity (km s^{-1})[h]	2854
Distance (Mpc)[i]	27.70
Redshift (z)[h]	0.00952
Velocity dispersion (km·s^{-1}) [j]	250

Data available in NED[1]
[a]de Vaucouleurs et al. (1991) [b]Carrasco et al. (2006)
[c]Lauberts & Valentijn (1989) [d]Babyk et al. (2018)
[e]Rickes et al. (2008) [f]Healey et al. (2007)
[g]Schlafly & Finkbeiner (2011) [h]Ramella et al. (1996)
[i]Tully et al. (2013) [j]Wegner et al. (2003)

[1] The NASA/IPAC Extragalactic Database (NED) is operated by the Jet Propulsion Laboratory, California Institute of Technology, under contract with the National Aeronautics and Space Administration

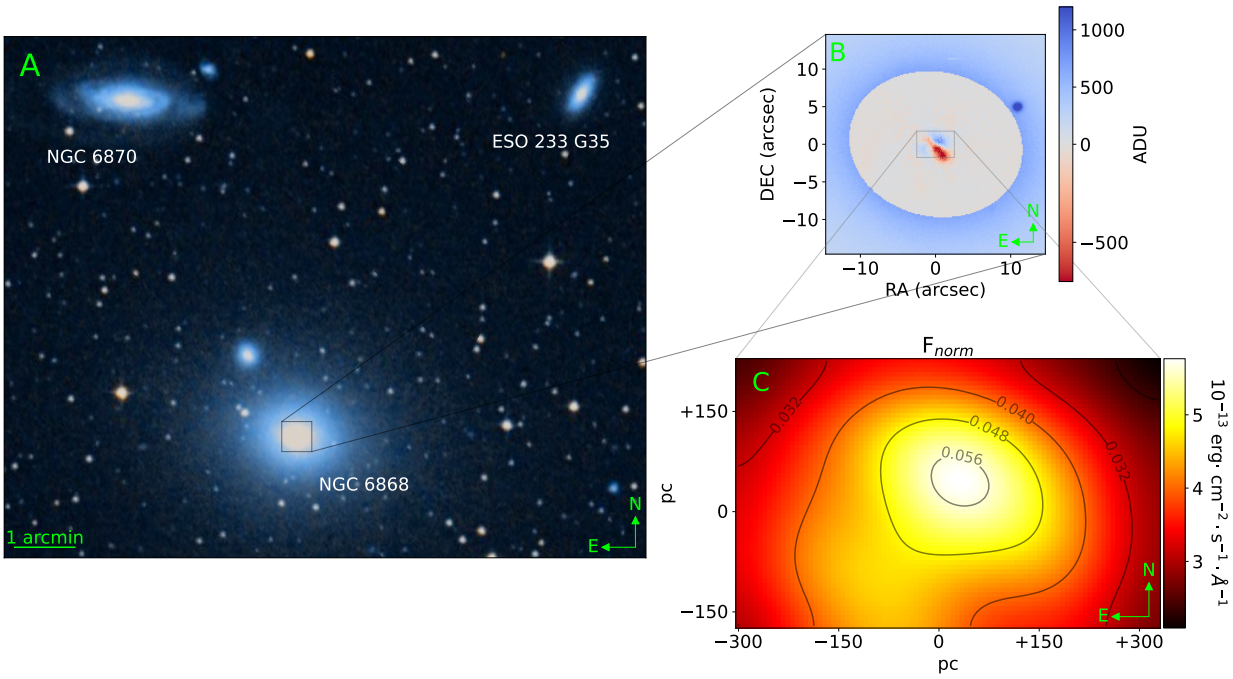

Figure 1. Images from NGC 6868 in three different scales. (a) Composite DSS image showing NGC 6868 and close neighbours. It is the brightest group member from the Telescopium group (AS0851). (b) Residuals from the photometric modeling of the acquisition image in the r band. A clear dust lane, also reported by Veron-Cetty & Veron (1988), is seen in the center of NGC 6868. At ~11"W and 5"N a stellar-like object is found and, according to Hansen et al. (1991), may be a cannibalised galaxy from which spiral features are emerging. (c) Continuum image from NGC 6868 extracted from our GMOS data cube at 5700 Å exhibiting an irregular light profile with a distortion in the SE direction. The (0,0) is defined as the peak in the continuum image corrected by extinction, as can be seen in Fig. 13.

A series of papers have reported the presence of ionized gas, finding a disturbed morphology and complex kinematics for the galaxy with a possible counter-rotating disc (Buson et al. 1993; Zeilinger et al. 1996; Macchetto et al. 1996). Caon et al. (2000) have analysed long-slit observations with distinct position angles (PAs). They reported a rotating disc of ionized gas, in agreement with the stellar velocity field. However, in a different PA, a counter-rotating gas disc with respect to the stars is found, displaying an inner component that shows a counter-rotation. Also, a kinematically decoupled stellar core was seen where the kinematical break radius is at 3". Bregman et al. (1998) using IRAS data confirmed the presence of cold dust. NGC 6868 has been observed in the radio by Slee et al. (1994) at 2.3, 5, and 8.4 GHz and Mauch et al. (2003) at 843 MHz and Healey et al. (2007) reported a low-power flat spectrum radio source in its centre ($\alpha \sim 0.07$). The brightness, temperature and spectral slope are inconsistent with HII regions, so an AGN was the most likely source of the radio emission. Rose et al. (2019) using ALMA observations detected molecular gas in the centre of NGC 6868 drifting in non-circular motions. Also, they reported an HI absorption.

In this paper, the first of a series aimed at studying in detail this object, we will focus on the stellar content of NGC 6868. It is organized as follows: in § 2, we describe the observations and the reduction procedures; in § 3, we present the employed methodology; in § 4, the results are presented and a comparison with data from other studies. Discussion of the results is made in § 5 and the conclusion and summary are made in § 6. Throughout this paper, we assume that solar metallicity corresponds to $Z_\odot = 0.019$ (Girardi et al. 2000).

2 OBSERVATION AND DATA REDUCTION

NGC 6868 was observed on 2013 May 04 with the Gemini South Telescope using the Gemini Multi-Object Spectrograph (GMOS) in the IFU mode (Allington-Smith et al. 2002; Hook et al. 2004). This object is part of the DIVING^{3D} survey, which made observations of the central regions of all 170 galaxies in the Southern hemisphere with $B < 12.0$ and $|b| > 15°$ (see Steiner et al. 2022 for more details). The one slit set-up was used for the observations, resulting in an FoV of 5.0 × 3.5 arcsec^2. The B600-G5323 grating was used with a central wavelength of 5620 Å and a spectral range from 4260 Å to 6795 Å. The spectral resolution is 1.8 Å, estimated with the O I λ5577Å sky line. Flat-field exposures, bias and CuAr lamp spectra were acquired for calibration and correction purposes. The seeing of observation was estimated using stars that are present in the acquisition image of the galaxy, taken with the GMOS imager in the r-band (SDSS system). Moreover, the DA white dwarf EG 274 (Hamuy et al. 1992) was observed in order to perform the spectrophotometric calibration. These and some other basic information regarding the observation is given in table 2.

Standard IRAF procedures (Tody 1986, 1993) were followed to reduce the data using the tasks contained in the Gemini IRAF package. Bias, flat-fields, wavelength calibration, dispersion correction, and flux calibration procedures were applied to the science data. To remove cosmic rays, we used the LACOS software (van Dokkum 2001). The data cube was constructed with a spatial sampling of 0.05 arcsec.

After the standard reduction procedures, other data treatments were applied by means of improving the visualization of the data as described in Menezes et al. (2019): removal of the high spatial noise using a Butterworth filter, the correction of the differential atmospheric refraction (DAR), instrumental fingerprint removal through PCA Tomography and Richardson-Lucy deconvolution.

The removal of high-frequency noise from the spatial dimension was performed by convolving each image of the data cube with a Butterworth filter (Gonzalez & Woods 2008; Ricci et al. 2014). The filter order used was $n = 2$ and the cut-off frequency was $F_c = 0.14\ F_{Ny}$ where F_{Ny} is the Nyquist frequency, corresponding to 0.5 spaxel^{-1}. This cut-off frequency was chosen to remove only spatial frequencies higher than the PSF of the data cube, assuring that no valid scientific information was lost in this process.

The correction of the differential atmospheric refraction (DAR) consists of spatially shifting the wavelength planes of the data cube so that the spectrum of a given point in the galaxy occupies always the same position at all wavelengths. The correction of the differential refraction effect on the data cube of NGC 6868 was performed using the equations from Bönsch & Potulski (1998) and Filippenko (1982), which assume a plane parallel atmosphere and calculate the displacement of the centroid of the galaxy for each wavelength as a function of the zenith distance, the refraction index and other atmospheric parameters.

The PCA Tomography technique (Steiner et al. 2009, and references therein) applies Principal Component Analysis (PCA) to data cubes. This procedure searches for spectro-spatial correlation across a given data cube. The results are the eigenvectors (or eigenspectra), which show the correlations between the wavelengths caused by some physical phenomenon or an instrumental fingerprint, and the tomograms, which correspond to the projection of the data cube onto each eigenvector. This is an orthogonal transform meaning it can be reversed. The eigenvectors are ordered by how much of the variance in the data cube they are able to explain, meaning the first eigenvector explains most of the variance and so on. Using this technique, the instrumental fingerprints may appear as one of the eigenvectors that would otherwise be entangled with the data. This instrumental signature may be isolated by building a data cube containing only this issue. In the end, we subtract this fingerprint from the science data cube.

After the removal of the instrumental fingerprints, the reddening caused by the dust within the Milky Way was corrected using the CCM law (Cardelli et al. 1989) and $A_V = 0.152$ mag (Schlafly & Finkbeiner 2011). The telluric lines were also removed and the spectra were brought to the rest frame using the redshift shown in Table 1.

Lastly, the Richardson-Lucy deconvolution (Richardson 1972; Lucy 1974) is an iterative process that aims at reconstructing the image of the galaxy before its convolution with the PSF when it passes through the atmosphere and the optical apparatus of the telescope. After 10 iterations, the final estimated PSF was 0.71 arcsec, estimated from a spatial profile obtained along the red wing of the broad Hα emission. An image from the continuum of NGC 6868, extracted from the final data cube, is shown in Fig. 1.

3 METHODOLOGY

3.1 Stellar population synthesis

In order to derive the SFH (star formation history), we used the STARLIGHT code (Cid Fernandes et al. 2004, 2005, 2013; Cid Fernandes 2018) which fits the continuum spectra by combining in different proportions the contribution from different simple stellar populations (SSPs), taking into account reddening and kinematical parameters. In other words, it tries to match the observed spectrum (O_λ) with a modelled one (M_λ), described by

$$M_\lambda = M_{\lambda_0}\left[\sum_{j=1}^{N_*} x_j b_{j,\lambda} r_\lambda\right] \otimes G(v_*, \sigma_*), \quad (1)$$

where M_{λ_0} is the flux in a predetermined normalization wavelength, N_* is the number of elements in the SSP base, x_j is the j-th component of the population vector ($\vec{x}$) that stores the light contribution from each SSP (with respect to the normalization wavelength[2], λ_0). $b_{j,\lambda}$ is the spectrum of the j-th component, r_λ is the reddening factor, defined by $r_\lambda = 10^{-0.4(A_\lambda - A_{\lambda_0})}$) and $A_\lambda = A_V q_\lambda$, where q_λ is the extinction law evaluated at λ. Lastly, there is a convolution with a Gaussian distribution to take into account the line-of-sight velocity distribution (LOSVD) of the stellar component in the spectra, where v_* is the line-of-sight stellar velocity and σ_* is the stellar velocity dispersion. To determine the best fit, the code tries to minimize a χ^2 defined by

$$\chi^2 = \sum_\lambda [(O_\lambda - M_\lambda)\omega_\lambda]^2 \quad (2)$$

where ω_λ is the weight. Using this parameter, we are able to mask ($\omega_\lambda = 0$) spurious features or contributions from other non-stellar components (e.g. emission lines from the ionized gas) or give more weight to important regions of our spectra (e.g. characteristic adsorptions that allow better kinematical predictions, if that is the intended objective). Along with the emission lines present in our spectra, the Mg I absorption was masked during the synthesis in order to minimize the α-enhancement effects in the determination of the metallicity.

One of the fundamental ingredients in this method is the SSPs used in the fit. We constructed our base with the models developed by Vazdekis et al. (2016, hereafter E-MILES), using the evolutionary tracks of Girardi et al. (2000) and the Kroupa (2001) initial mass function. These models were chosen because their wavelength range overlaps with our data and have a better spectral resolution (2.51 Å FWHM) when compared to other stellar population models (e.g. Bruzual & Charlot 2003; Maraston & Strömbäck 2011; Conroy et al. 2009). The high resolution is fundamental to model the stellar absorptions allowing a precise study of the gas kinematics when discounting the stellar component. The final SSPs span 15 ages (0.0631, 0.1, 0.16, 0.28, 0.50, 0.89, 1.26, 1.41, 2.51, 3.98, 6.31, 7.94, 10.0, 11.2, 12.6 Gyr) and six metallicities (0.005, 0.02, 0.2, 0.4, 1.0, 1.6 $Z_\odot$).

The E-MILES models, however, lack really young and hot stars,

Table 2. Table displaying some basic observational parameters

Parameter	NGC 6868
Observation date	2013 May 04
Gemini Programme	GS-2013A-Q-52
Seeing (arcsec)	0.77
Airmass	1.056
T_{exp} (s)	1800
Number of exposures	1

[2] We normalized our spectra in the 5700 Å region, due to the lack of significant stellar absorption bands and having good S/N in the whole FOV.

having only SSPs with ages greater than 63 Myr. In order to assess the possibility of such a young population in NGC 6868, we performed stellar synthesis with the Bruzual & Charlot (2003) models, which include stars as young as 0.1 Myr in the whole FoV. We found that there is no contribution from components with less than 63 Myr.

Since this object does not have any ongoing star formation, we decided to use the reddening law from Cardelli et al. (1989) to model the dust attenuation (A_V) intrinsic to our object. To account for a possible featureless continuum (FC) emission of an AGN, we followed Riffel et al. (2009) and a power-law spectrum with $f \sim \nu^{-1.5}$ was added to the base. In other test runs, we have included FC with different exponents, ranging from -1.75 to -1.0, however, no significant contribution from any of these components was found.

Finally, to better understand the age and metallicity spatial distribution, we calculated the light-weighted mean stellar age ($< t >_L$) and metallicity ($< Z >_L$, Cid Fernandes et al. 2005), as:

$$< t >_L = \sum_j x_j \log(t_j), \tag{3}$$

and the light-weighted mean stellar metallicity

$$< Z >_L = \sum_j x_j Z_j. \tag{4}$$

To optimize the data management, we used the MEGACUBE tool (Mallmann et al. 2018; Riffel et al. 2021) which takes as input the data cube and prepares the data for the synthesis procedure, executes the synthesis and also performs the preliminary analysis (e.g. calculate the equations 3 and 4) as well as mounting the maps with the important parameters.

3.2 Indices measurements and Alpha-enhancement

To better constrain the assembly history of NGC 6868, especially the α-enhancement, we have measured indices for the absorption lines. We measured the indices for Fe4383, Mg_2, Mg_b, Fe5270, Fe5335 using the definitions presented in Riffel et al. (2019) which are based on Worthey et al. (1994) and were subsequently used to derive Fe3[3] and [MgFe]'[4]. All spaxels were corrected to the rest frame using the line-of-sight Doppler shift velocity derived by STARLIGHT. In a first moment, we decide not to correct the effects due to the velocity dispersion.

The in-house PACCE code (Riffel & Borges Vale 2011) was used to perform the equivalent widths (EW) measurements of these indices. The code uses predefined continuum bands around a given line and fits a pseudo-continuum line. Once the line is fitted, the EW is calculated through

$$W_\lambda = \left(1 - \frac{A_2}{C}\right)(\lambda_u - \lambda_i) \tag{5}$$

being W_λ the measured width of the line, A_2 and C are the integrated areas below the absorption and below the pseudo-continuum, respectively, and λ_u and λ_i are the predetermined final and initial wavelength of the absorption feature. The trapezium integration method is used and the calculation of W_λ is iterated over the whole cube.

A problem we faced during these measurements was the contamination from the weak [N I] λ 5199 Å emission line which is located between the Mg I absorption and the pseudo continuum definition of Mg_b. We were able to work this around by modelling the emission line profile and subtracting this contribution from the spaxels. In order to properly model this component, we discounted the previously derived stellar spectra and fitted the remaining continuum with a high-order polynomial. Afterwards, we adjusted this line using the IFSCUBE package (Ruschel-Dutra & Oliveira 2020). We modelled the [N I] λ 5199 Å emission line using two Gaussian components and coupled its kinematics with the [N II] $\lambda\lambda$6548, 6583 Å. Additional details on emission line fitting will be presented in Benedetti et al. (*in preparation*). Once the lines were properly fitted we were able to discount this emission and remeasure the Mg I indices.

We wanted to derive the [α/Fe] of the population to further help us constrain the assembly history of NGC 6868. In this sense, in order to match the spectral resolution of the V15 models (2.51 Å FWHM, Vazdekis et al. 2015), we broadened our spectra to match this resolution and re-measured the indices. Afterwards, we followed the procedures described in La Barbera et al. (2013) using the indices Mg_b, Fe3 and the luminosity-weighted age derived from STARLIGHT to measure Z_{Mg_b} and Z_{Fe3}. Firstly, the measured indices were corrected by the velocity dispersion following de la Rosa et al. (2007). With the corrected values, the Vazdekis et al. (2015) models were interpolated, creating grids varying the metallicities and ages from the models. The resulting grids derived from Vazdekis et al. (2015) used to calculate Z_{Mg_b} and Z_{Fe3} are shown in Fig. 2. As mentioned in La Barbera et al. (2013), one may need to extrapolate the grids in α-enhanced populations. This is represented as the dotted lines in the same figure. Afterwards, we calculated the proxy $[Z_{Mg_b}/Z_{Fe3}]$= Z_{Mg_b}-Z_{Fe3} which finally can be used to get (Vazdekis et al. 2015):

$$[\alpha/\mathrm{Fe}] = 0.02 + 0.56[Z_{Mg_b}/Z_{Fe3}]. \tag{6}$$

4 RESULTS

4.1 Stellar population synthesis

We present an example of the fits for an individual, nuclear spaxel in Fig. 3. A good matching between the observed (black) and modelled (red) spectra can be seen. The quality of the fits over the full FoV is ensured by the signal-to-noise (S/N) ratio map and can be certified in the χ^2 and Adev[5] maps (Fig. 4).

The resulting stellar population derived over the full FoV by the fitting procedure resulted in a contribution of mainly 3 components: two old metal-rich (12.6 Gyr; 1.0 and 1.6 $Z_\odot$) and a negligible contribution of a very young also metal-rich (63.1 Myr; 1.6 $Z_\odot$). The spatial distribution of each component is shown in Fig. 5. It is clear that the central region is dominated by an old stellar population ($\sim$ 12 Gyr), as is to be expected for the massive early-type galaxies. However, this contribution is divided into two different components with different metallicities, having 1.0 and 1.6 $Z_\odot$ each. They also exhibit a distinct spatial distribution, with more metal-rich stars dominating the central region of our FoV.

One last contribution of a young metal-rich component (63.1 Myr; 1.6 $Z_\odot$) is also observed. Residual star formation can be found in some elliptical galaxies and how common they are is still a matter of debate. Salvador-Rusiñol et al. (2020) have detected young stars in red massive galaxies probably related with recycled material within

[3] Fe3 = (Fe4383 + Fe5270 + Fe5335)/3 (Kuntschner 2000)

[4] $[\mathrm{MgFe}]' = \sqrt{\mathrm{Mg_b}\,(0.72 \times \mathrm{Fe5270} + 0.28 \times \mathrm{Fe5335})}$ (Thomas et al. 2003)

[5] Adev is the Allan deviation and serves as a quality indicator of the fit. It corresponds to the percentage mean $|O_\lambda - M_\lambda|/O_\lambda$ deviation over all fitted pixels.

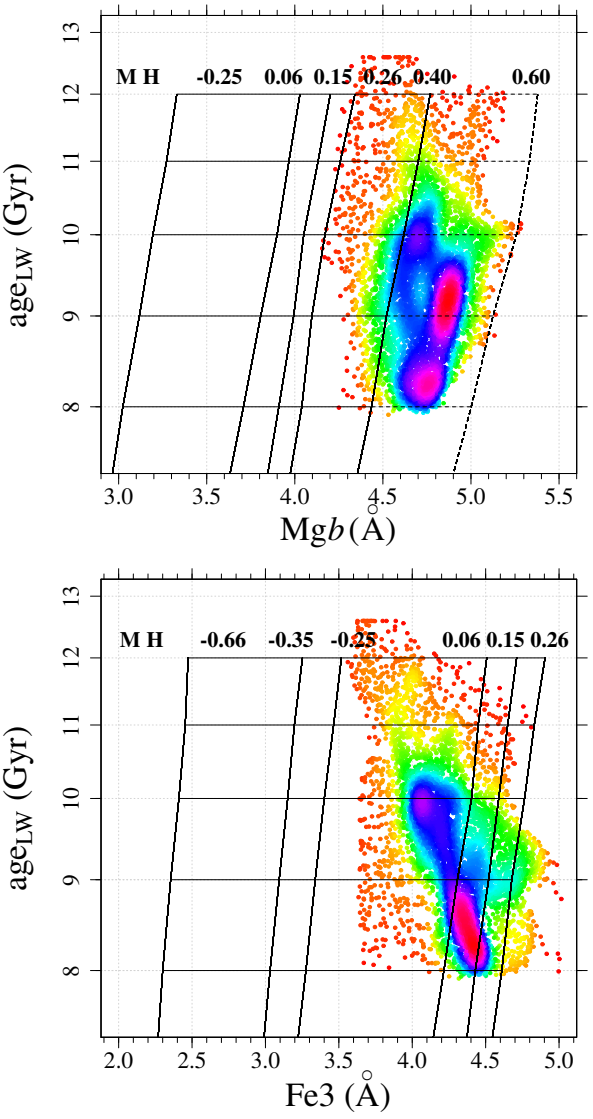

Figure 2. Diagrams showing the grids used to derive the Z_{Mgb} (top) and the Z_{Fe3} (bottom) in each spaxel, represented by the red dots. The light-weighted mean age derived from STARLIGHT was used and the measured EW from each absorption.

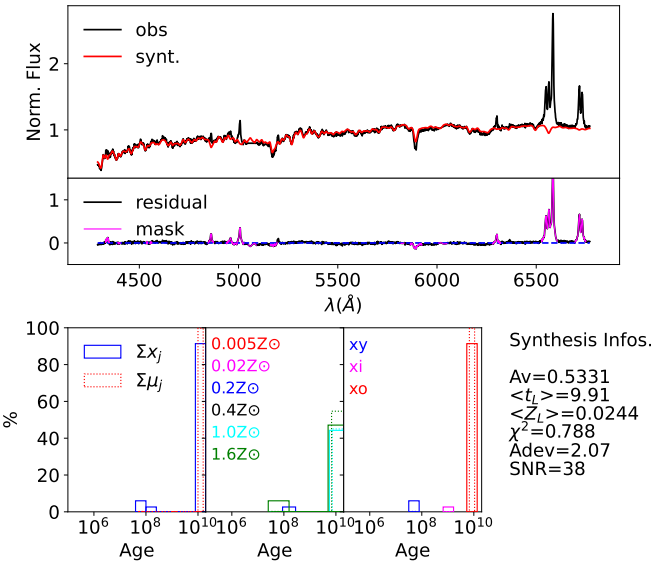

Figure 3. Top: Example spectra extracted from the spaxel with the highest continuum flux. The observed spectra (black) and the synthesised spectrum (red) are shown as well as the residuals (blue) and the masked pixels (pink). **Bottom:** Histograms showing the stellar population composition found by STARLIGHT. Continuous lines show light-weighted parameters and dashed lines, mass-weighted parameters. From left to right, the sum of contributions of components with the same age but different metallicities; contribution from each SSP in the base; age and metallicities contribution summed in predefined age bins, being xi SSPs between 0.1 Myr until 100 Myr, x, 100 Myr until 2 Gyr and xo, 2 Gyr until 13.7 Gyr. Further right are other parameters derived by the synthesis: The reddening in the V band, light- and mass-weighted mean age, light- and mass-weighted mean metallicity, χ^2, Adev and the S/N measured between 5670-5730 Å. The code clearly indicates the presence of old populations followed by a small fraction of young populations.

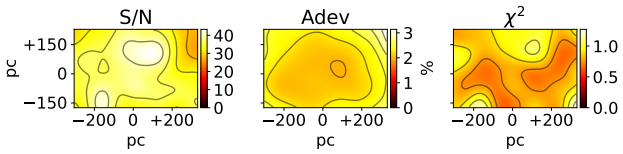

Figure 4. Maps displaying the statistical parameters derived from the stellar population synthesis. From left to right: the signal-to-noise ratio (measured between 5670-5730 Å), Adev and χ^2. Together they attest to the robustness of the modelled population.

the galaxy with mass fraction $\tilde{0}.5$ % whereas Simonian & Martini (2017) interprets early-type galaxies which typically are UV-weak as lacking younger components with HOLMES stars being responsible for this residual UV emission. Using the M/L from the E-MILES models, and summing over the contributions from all SSPs with 2 Gyr or less, we get a median mass contribution in our FoV of $\tilde{0}.2$ %. This insipient contribution may come from younger stars, however other mechanisms (e.g. HOLMES stars) may be enough to account for it. However, we interpret this detection as due to the lack of an old blue population, probably related to the horizontal branch, that current stellar population models do not account for (Cid Fernandes & González Delgado 2010). This results in an excess blue light that the code computes as a younger component. This interpretation is supported by the fact that this component is co-spatial with the older metallic component. Also, Bica et al. (1996) using IUE spectra classified this galaxy as a UV-weak source and found no contribution from young stellar populations.

Rickes et al. (2008) have also conducted stellar population synthesis studies in NGC 6868 in a larger scale ($R < 17$ arcsec) and also found an ubiquitous old population. However, they also report an intermediate-age stellar population of 5 Gyr which peaks in the centre of the galaxy, contradicting our findings. However, their data ranges from 5100 – 6800 Å therefore lacking the bluer end of the spectrum in order to constrain the presence of intermediate and young stars. Also, their SSP base consists of very few elements, that most likely do not portray all the different SFH a galaxy can have. Therefore, the discrepancies seen are most likely the result of better data and the evolution of the synthesis method.

Despite the different arrangements of FCs we tried in our base, we did not find any contribution from an AGN. As this is a galaxy classified as a LINER, the supermassive black hole is likely accret-

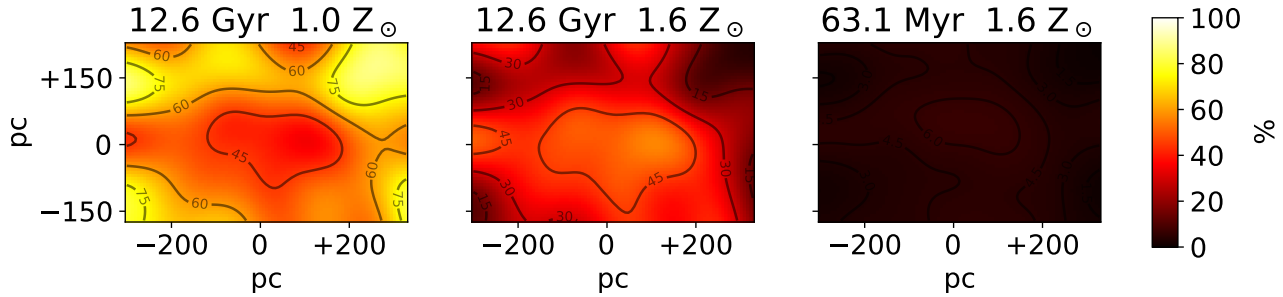

Figure 5. Maps displaying the light contribution from the three most significant components for the spectral synthesis in our FoV. The younger component is likely a spurious effect from the fit. The two older components establish a spatial anti-correlation.

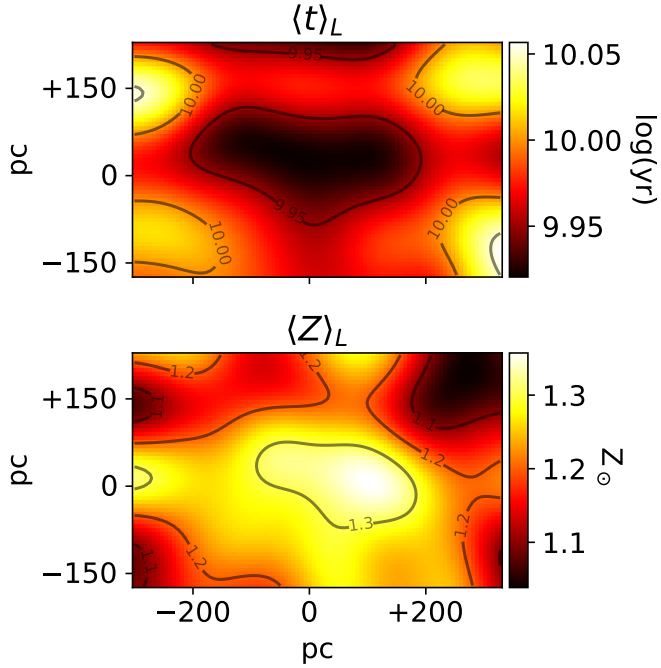

Figure 6. Mean age (left) and mean metallicity (right) maps derived from STARLIGHT output. Both are luminosity-weighted quantities. The mean age seems to be affected by the younger component found in the synthesis and the mean metallicity map clearly shows the gradient metallicity in this galaxy.

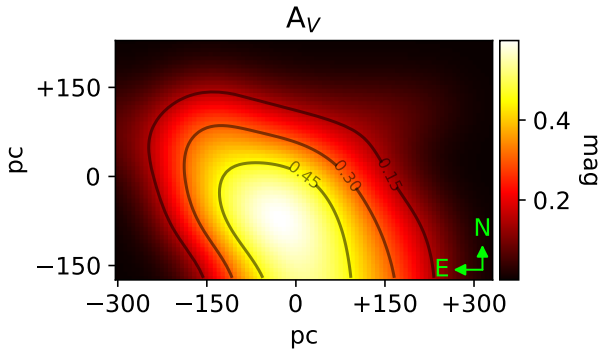

Figure 7. Map of the reddening in the V band extracted using STARLIGHT. The morphology resembles a dust lane in the line of sight of the observer. This amount of dust has disturbed the continuum image, making it seem like a double core.

ing at a really low rate, making its contribution to the continuum undetectable.

In order to represent the galaxy's age and metallicity in a single map, we have derived the $< t >_L$ and $< Z >_L$ maps, which are shown in Fig. 6. In these maps, one can observe that the galaxy's mean age is slightly smaller and the metallicity higher in the nucleus. Finally in Fig. 7 we show the reddening map (A_V). It reaches a peak of ~0.65 mag in the centre of the image and its morphology resembles a dust lane embedded in the centre of the galaxy. This is in agreement with literature results (e.g. Veron-Cetty & Veron 1988; Hansen et al. 1991; Buson et al. 1993).

STARLIGHT also outputs the line of sight velocity and velocity dispersion. These maps are shown in Fig. 8. It is evident that NGC 6868 does not display a rotation profile or any ordered motion. Instead, it appears that the stars are in random motions, as can be seen in the σ_* distribution, showing a clear peak ~ 290 km s^{-1} in the centre of the galaxy. In order to verify our results, we have also performed the fits using pPXF (Cappellari & Emsellem 2004; Cappellari 2017) with the same SSP base and got the exact same results.

In past studies (Caon et al. 2000), the stellar kinematics was measured using long-slit data and they found (1) a shallow rotation profile with a peak velocity of ~ 45 km s^{-1} at a radius of 42 arcsec (~ 5.8 kpc), (2) a kinetically decoupled core (KDC) which exhibits a counter rotation with respect to the outer regions and (3) a drop in velocity dispersion at the centre of the galaxy, only seen in one of their PAs. Our data is not consistent with this drop in σ_* reported. However, comparing the derived velocity dispersion profiles from other PAs in their data, there is also no evidence of this behaviour. This too is the case for the KDC, where the velocities within it do not reach 10 km s^{-1}. The most probable explanation for their findings is the high variation between different PAs as can be seen in Fig. 8. Depending on the angle observed, a rotation (or counter rotation) can or cannot be observed, due to the high-velocity dispersion in that region. Moreover, our FoV is too small to compare the kinematics in the inner region with the kinematics in the outer parts of the galaxy, so a larger FoV would be necessary to be certain about this behaviour.

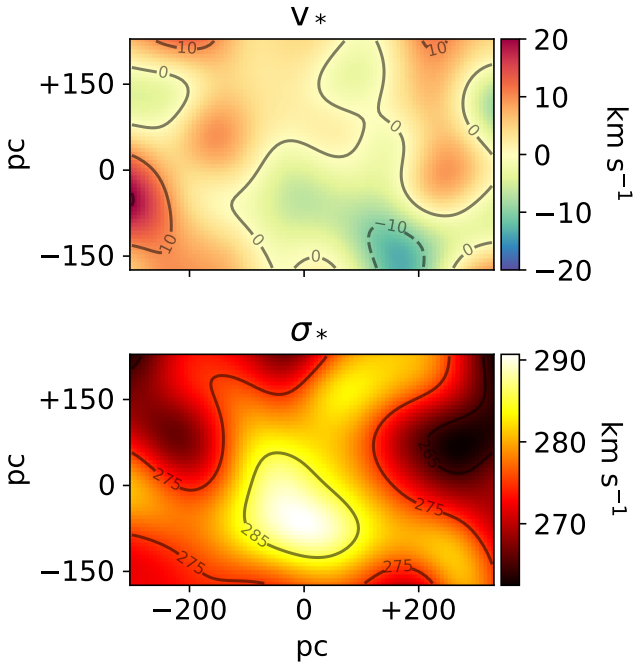

Figure 8. Kinematical maps regarding the LOSVD of the stellar component. The velocity map (left) does not seem to follow any particular geometry or distribution and the velocity dispersion (right) has a more defined profile with a clear peak at the centre of the distribution.

4.2 Absorption line indices

The maps for the absorption line indices calculated in the Lick/IDS resolution are shown in Fig. 9. All the values shown were corrected by the intrinsic velocity dispersion found with STARLIGHT, except for the Mg_2 index because it is almost insensitive to Doppler broadening. In our case, this correction would be smaller than the intrinsic error of the method (< 0.003, e.g. Kuntschner 2000), so we chose not to apply any correction. This is not the case for the other indices. The correction factors for each spaxel follow the spatial distribution from the velocity dispersion (Fig.8). The derived correction factors for the Mg_b index are in the range 1.09-1.14; Fe4383, 1.12-1.17; Fe5270, 1.23-1.29; Fe5335, 1.40-1.54. The maximum error found for each index was Mg_2: 0.0044 mag, Mg_b: 0.15 Å, Fe4383: 0.36 Å, Fe5270: 0.14 Å, Fe5335: 0.18 Å, Fe3: 0.14 Å e [MgFe]': 0.17 Å. These errors leave all the following reported gradients unaffected.

In order to assess how precise our results turned out, we made extractions matching PAs from the literature (Carollo et al. 1993; Rickes et al. 2008) matching the spatial extent of our data. This comparison can be seen in Fig. 10 and the error bars displayed for the values derived in this work are the standard deviation measured within each bin which is greater than the systematic errors. Mg_2 presents an offset of at least -0.5 mag between Rickes et al. (2008) and our extractions, with both showing a negative gradient. The likely explanation for this offset is the different ways to measure the continuum applied in each work: they chose custom continuum bands and we followed Riffel et al. (2019). Carollo et al. (1993), on the other hand, matches all our data within the error bars for both of their PAs. Fe5270 and Fe5335 also present an offset between Rickes et al. (2008) and our measurements, again preserving gradients probably related to the continuum definitions, as previously said. Carollo et al. (1993) measured Fe5270 (transparent points in Fig. 10) and verified it was not in the Lick system. Therefore they derived a correction to be applied for their data in the form δFe5270 = 0.87(±0.07) · Fe5270 – 2.67(±0.02), resulting in δFe5270 ~ 0.5 Å. The corrected points are the full circles in Fig. 10 which, once again, match all our data within the error bars. Carollo et al. (1993) did not measure Fe5335.

In contrast to the parameters derived in the stellar population synthesis (Fig. 6), the spatial variation of the measured indices is far more intricate. Therefore to gauge the mean behaviour of each index, in Fig. 11 we plot the median of each index in circular apertures of δr = 0.05 arcsec (7 pc) using the peak in Mg_2 as the origin. Mg_2 has the clearest spatial correlation when compared to all the other indices, monotonically decreasing across the majority of the FoV. Two peculiar regions deviate from this trend, however: one at NW (+120 pc,+175 pc) in the border of the FoV, and another one SW at (+170 pc, -140 pc). Unfortunately, we do not have any literature results in these areas, however, given that our method resulted in an excellent agreement with past studies, we are convinced of this detection. The Mg_b profile closely resembles Mg_2 also showing the distinct regions previously cited. Fe3 is particularly interesting because it does not follow the metallicity map as previously shown (Fig. 6), already a hint of α-enhancement processes at play. The most curious result is that in the same SW region previously mentioned, there is a depletion of this index. The [MgFe]' map closely resembles the $< Z_L >$ map indicating that the centre of this galaxy really is metal-rich and exhibits a negative gradient.

One curious behaviour that can easily be seen in Fig. 11 is that for R < 100 pc the Mg_2 and Mg_b anti-correlate with Fe3 and [MgFe]' reaching their peaks at R ~ 100 pc away from the centre. Until ~ 220 pc we actually observe a correlation between the two indices which turns again into an anti-correlation beyond R ~ 220 pc, however shallower when compared to the inner region.

Rickes et al. (2008) found that Mg_2 and Fe5270 or Fe5335 establish a strong correlation which lead them to conclude that the elements traced by both of these indices suffered the same enrichment processes. This can be the case for bigger scales, but in our FoV, we observe a distinct behaviour.

4.3 Alpha-enhancement

The grids used to derive the [α/Fe] are seen in Fig. 2 as well as our measurements. As we only find old stellar populations, the most significant variation is given by the indices. Using these values, the [α/Fe] map is shown in Fig. 12. It is clear that the whole FoV presents α-enhanced stellar populations with values between ~ +0.07 and +0.24 dex. Also, we find a really structured profile with diverse morphology. Using once again the peak in Mg_2 as our reference, we plot the median profile of the [α/Fe] using circular apertures that can also be seen in Fig. 12. What becomes apparent is that the centre of NGC 6868 shows a peak in α-enhancement followed by a region of shallower [α/Fe] which again is followed by another region with values as big as the ones in the centre, producing the "U" shape found in the median profile.

The only other paper where there is a measurement of the [α/Fe] from NGC 6868 is Rickes et al. (2008). According to them, the central parts of NGC 6868 present lower [α/Fe], between -0.3 and 0.0 dex and an above-solar metallicity ([$Z/Z_\odot$] ~ +0.3 dex. Moreover, the external parts present higher [α/Fe] values (~ +0.3 dex) and lower metallicities ([$Z/Z_\odot$] ~ −0.33 dex). In order to obtain these values, they use the Mg_2, Fe5270 and Fe5335. However, as we already showed in § 4.2, these indices, despite agreeing with the gradients

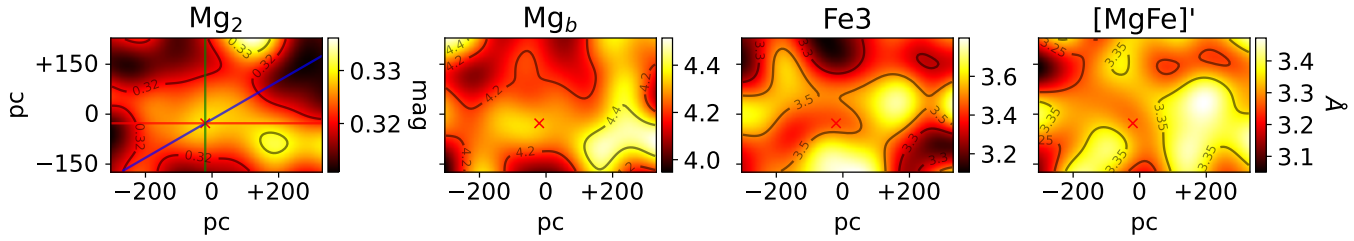

Figure 9. Results for the index measurement. From left to right: Mg_2, Mg_b, Fe3 and [MgFe]'. The indices show complex profiles in contrast to the results from the stellar population synthesis. In the Mg_2 map we over-plotted lines indicating the extractions done in our cube in order to compare with the literature results (Fig. 10). The red "x" in the panels is the location of the peak Mg_2.

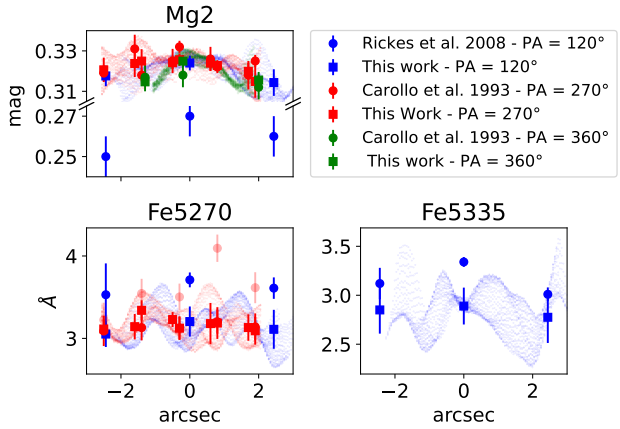

Figure 10. Comparison of our Mg_2, Fe5270 and Fe5335 results to past studies using long-slit spectroscopy for different PAs (Rickes et al. 2008; Carollo et al. 1993). Each PA is represented by a colour, literature results are shown as circles and our measurements are shown as squares. The smaller scatter points correspond to the spaxels within the artificial slit observed. As can be seen, even inside the artificial slits there is significant variation.

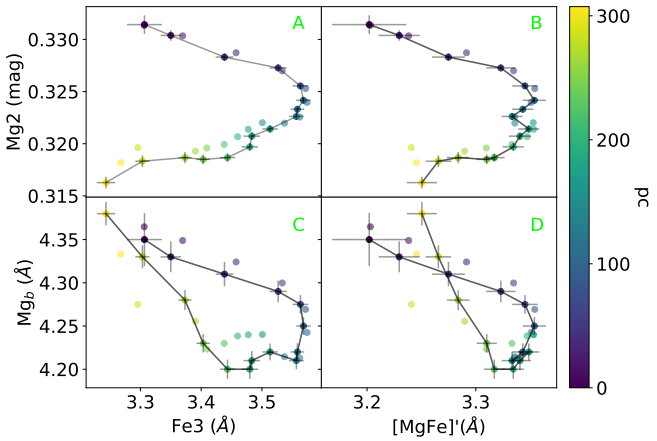

Figure 11. Correlations between Mg_2, Mg_b, Fe3 and [MgFe]' indices. These are the median values within $\delta r = 0.05$ arcsec apertures that have been colour-coded for the distance from the centre. For $R < 100$ pc and $R > 220$ pc the Mg_2 and Mg_b anti-correlate , with Fe3 and [MgFe]'. The intermediate region displays a correlation. The transparent points indicate the mean of each index in each radial bin. This hints at different possible enrichment processes in each region.

found in other studies, the values present a normalization problem probably due to the continuum bands used to compute the indices. If this shift in measurements were accounted for, the values of [α/Fe] would increase, reaching the α-enhanced region in their diagram, thus matching our observations. This would not affect the negative gradient in metallicity nor the positive gradient in [α/Fe] which are in agreement with observations of other early-type galaxies (e.g. Kuntschner et al. 2010).

5 DISCUSSION

5.1 Stellar population synthesis

NGC 6868 is an early-type galaxy and so what is expected is that it had a fast phase of intense SF that suddenly stopped, forming the bulk of its stellar mass with a subsequent growth attributed to dry minor mergers. Therefore it is expected that the isophotes are not severely disturbed by the accreted galaxies. NGC 6868 at first inspection appears to deviate from this hypothesis, exhibiting a significant distortion in its continuum image (Fig. 1) in the SE direction which could be interpreted as another galaxy's nucleus in the process of fusing with NGC 6868. However, when corrected by the stellar reddening found in the synthesis procedure, the actual morphology is revealed as an undisturbed spheroidal, as shown in Fig. 13. Therefore, no deviation from the expected spheroidal is found in the isophotes of NGC 6868.

The dust found in our data (Fig. 7) is probably related to the cannibalism of a small gas-rich companion as proposed by Hansen et al. (1991). The molecular (Rose et al. 2019), atomic (Rose et al. 2019) and ionized gas (e.g. Buson et al. 1993) detected are probably related with this event. For instance, as can be seen in figure 2 of Hansen et al. (1991), there are dust filaments with spiral features that can be followed in a ring-like structure around the galaxy centre with a connection at NE which is aligned with the dust lane detected in the present study (Fig. 7). The ring is also connected to a stellar-like object in NW that they proposed is a cannibalised galaxy. Curiously, despite evidence for this violent process, we do not detect any signs of recent SF in this galaxy. Either there is not enough gas to collapse or it is constantly being heated preventing the collapse. This gas is most likely the reason behind the triggering of the AGN which is producing the LINER emission that is detected in the centre of the galaxy. This however is highly speculative and a thorough analysis of

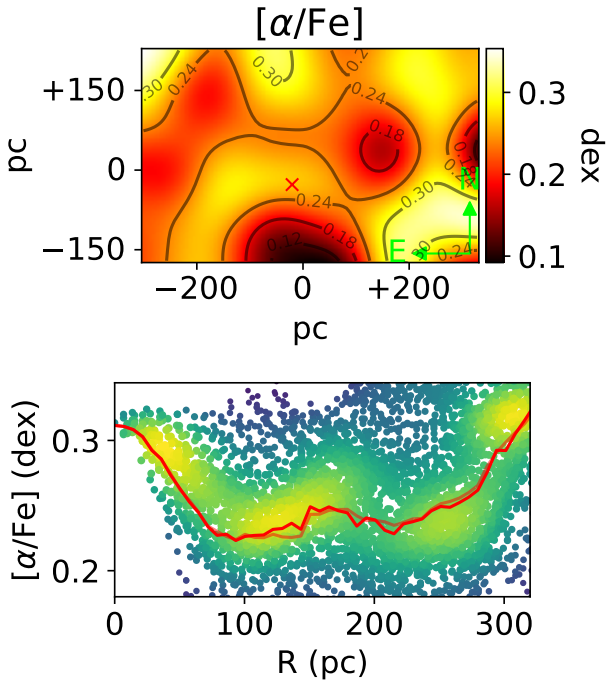

Figure 12. Top panel: Derived [α/Fe] for the whole FoV where it becomes clear that α-enhancement processes are ubiquitous. This parameter shows a really complex morphology, with a clear peak towards the centre, but also alpha-enhanced populations at larger radii. **Bottom panel:** Radial profile of [α/Fe] with the median (red) and mean (red, transparent) of the distribution over-plotted. It is clear that the profile exhibits a peak in the centre, followed by a region with smaller [α/Fe] followed again by an α-enhanced region. The red "x" in the top panel is the peak in Mg_2 following Fig. 11 and is used as the reference to trace the profile in the bottom panel

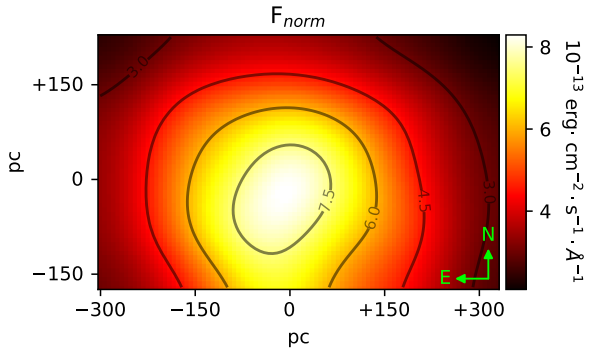

Figure 13. Continuum image extracted from our GMOS data of NGC 6868. The apparent double core (Fig. 1) vanishes when considering the reddening by the dust.

the ionized gas component will be carried out in an upcoming paper (Benedetti et al. *in preparation*).

In the synthesis, despite including an FC component and testing with different exponents, the code does not find any significant contribution of an AGN to the continuum. This however does not mean there is not an AGN in the centre of NGC 6868 as the emission can be obscured by dust, or the SMBH might not be accreting matter at a sufficiently high rate. As was already pointed out, this galaxy presents AGN evidence from past studies in radio (Slee et al. 1994; Mauch et al. 2003). We already know this is a LINER source, therefore the SMBH cannot be accreting at high rates. However, it is already known that when comparing AGN detection in the radio and optical the ratio of detection is not a 1:1 relation (Comerford et al. 2020).

According to our analysis, the SFH of this galaxy is characterized by a short burst in the early Universe with no major episodes of star formation since then (Fig. 6). This means that NGC 6868 probably did not experience any encounters with star-forming galaxies as they would leave signatures in the SFH from this galaxy. However, a merger with another galaxy in the distant universe could certainly have happened without signatures in the SFH from the galaxy detectable in the present-day Universe.

The mean metallicity map (Z_L, Fig. 6) is consistent with the scenario that massive early-type galaxies are able to retain the material expelled by SN thus fixating the elements produced during stellar evolution into new stars, creating also a gradient where central regions tend to be more metal-rich when compared to outer regions. This is the case for the majority of early-type galaxies (Kuntschner et al. 2010). They also show that for fast-rotators characterized by only old populations (>9 Gyr), a stellar disc is embedded in the stellar population of the galaxy characterized by higher metallicity and lower [α/Fe], including the central regions.

The kinematic revealed by STARLIGHT matches what is expected for a cD galaxy. We do not find any clear sign of rotation or strong ordered motion. Actually, the v_* map displays values that are below our uncertainty. Using the spectral resolution from our data and 5000 Å as our reference wavelength, we come to the conclusion that we are not able to distinguish any velocities with less than 100 km·s^{-1}. It is clear that our whole FoV presents values for the velocity in the line of sight which we are not able to confirm, however, for completeness we decided to show it in Fig. 8. The velocity dispersion, on the other hand, does not face this problem as all values derived are > 250 km·s^{-1}. Despite past studies reporting a KDC in this object, we cannot confirm this result due to our small FoV. What remains clear is the fact that the central region of NGC 6868 is really dispersion dominated and no kinematically decoupled structure is found.

5.2 Absorption line indices and alpha-enhancement

Analysing the profiles derived for the indices (Fig. 9), it is clear that they are far more structures when compared to the ones derived in the synthesis (Fig. 6). Moreover, the variation in each index is heavily dependent on the PA one decides to look at. This hints at a more chaotic assembly history when compared to what is derived in the synthesis that shows only contributions from old metal-rich populations. The [MgFe]' resembles the $< Z >_L$ profile probably because we were able to partially isolate the sensitivity to the α-enhancement processes from the synthesis.

This hypothesis is further endorsed by Fig. 11, where at least three distinct chemically enrichment regimes are clear, with two anti-correlations ($R \lesssim 100$ pc and $R \gtrsim 220$ pc) and a correlation ($R \gtrsim 100$ pc and $R \lesssim 220$ pc), clearer in the Mg_b-[MgFe]' plot. What this tells us, again is that a simple monolithic collapse cannot explain

our findings, otherwise we would expect the elements sensitive to the indices measured would have followed similar enrichment processes, thus producing matching gradients. This appears to be the case for larger scales (Rickes et al. 2008), however, this is not true for our FoV. A deviation from past studies that [MgFe]' reveals is a slight dip in the metallicity of the galaxy towards the very centre (R<100 pc, Fig. 11) that is also apparent in Fe3. As this index is insensitive to [α/Fe] what we observe is that the central region is depleted in metals with respect to the outer (100 pc < R <220 pc) region. This behaviour is unexpected as shown by past studies (e.g. Kuntschner et al. 2010).

One way of distinguishing the formation scenario, as noted by Carollo et al. (1993) is measuring the Mg_2 gradient (d Mg_2/d log r). Using only r>1 arcsec we find a gradient of d Mg_2/d log r≈-0.024, which is a shallow gradient, incompatible with the monolithic collapse scenario according to the authors.

The [α/Fe] map (Fig. 12) also presents a complex profile. However, looking at the median curve we see a much clear behaviour. The central (R<100 pc) and outer (R>260 pc) regions appear to be significantly more α-enhanced than the intermediate region. These regions agree with our findings from the indices. What becomes clear is that the signatures in the stellar populations of the centre of NGC 6868 cannot be described only by a burst of star formation in the early universe with a passive evolution since then.

5.3 Possible formation scenario for NGC 6868

From our findings, NGC 6868 presents compelling evidence that its assembly history was not just comprised of a single burst of star formation without any significant evolution ever since. The [α/Fe] map is especially suited to understanding this galaxy. A close inspection reveals that the regions where it is smaller are also the more metallic regions. Kuntschner et al. (2010) found stellar populations with these exact same features (high metallicity and low [α/Fe]) in discs of fast-rotator early-type galaxies. Some of these discs show signs of recent star formation, however, they also find these characteristics in galaxies depleted of gas and dominated only by old stellar populations (<9 Gyr).

Therefore, our hypothesis is that in the past NGC 6868 could have suffered an episode of merger with another galaxy with lower [α/Fe], such as the ones previously described. This would explain why we see such structured maps in [α/Fe], the slight increase in metallicity outside from the centre and the absence of a detectable subsequent star formation episode or a lack of gradient in the mean age across our FoV. The fact that we do not observe any clear kinematical signature is probably because we are looking at a really small region and cannot compare with outer regions, despite a KDC being previously reported (Caon et al. 2000). However, we do find an imprinted chemical signature. We emphasize that, in this hypothesis, the accreted galaxy could not have a mass comparable with NGC 6868, because, despite different maps showing structured profiles, Mg_2 shows a (shallow) negative gradient. Therefore, this enrichment process must have disturbed the stars from NGC 6868 only to a certain extent. Simulations could be used to test our predictions, however, this analysis is beyond the scope of this paper.

Finally, this might not be the only disturbance NGC 6868 has suffered. We notice some regions that stand out, mainly in the SW in the [α/Fe] map which display a $\sim$ +0.25 dex and, as can be seen in the Fe3 map (Fig. 9) it is depleted in [Fe/H]. This can be a recently captured small galaxy, however, this is unlikely due to its scale and the region it is encountered. We would need more data to properly characterize this region which is also beyond the scope of this paper.

6 CONCLUDING REMARKS

In this paper, we analysed GMOS-IFU data of the inner region of the ETG NGC 6868 mapping for the first time the physical and chemical properties of the stellar content of this source. This, together with an absorption-line indices analysis has allowed us to constrain the assembly history of this object. Our results can be summarized as follows:

- This galaxy is dominated by an old metal-rich (12.6 Gyr; 1.0 and 1.6 $Z_\odot$) stellar population and presents a negative gradient in metallicity. This is further endorsed by the [MgFe]'. We do not find any signs of star formation apart from a burst of star formation in the early Universe.
- The apparent distortion in the continuum image is due to a dust lane embedded in the centre of the galaxy and reaches a peak in $A_V\sim$ 0.65 mag. This structure is coincident with the one found in other studies.
- No evidence of an FC continuum is found, probably meaning the AGN in the centre of NGC 6868 is accreting at really low rates.
- The kinematics in the centre of NGC 6868 is characterized by high dispersion velocities and no apparent circular motion of the stars is seen.
- The indices Mg_2, Mg_b, Fe3 and [MgFe]' all present structured profiles, with Mg_2 presenting the steepest negative gradient. However, it is too shallow to support a formation history due to a monolithic collapse.
- Three distinct regions can be found when cross-correlating the indices: anti-correlations for R$\lesssim$ 100 pc and R$\gtrsim$ 220 pc and a correlation for 100 pc$\lesssim$R$\lesssim$ 220 pc. This reveals different enrichment histories in these regions.
- The [α/Fe] map also does not present a clear gradient. However, the median appears to also show three distinct regions: the central (R<100 pc) and outer (R>260 pc) regions appear to be significantly more α-enhanced than the intermediate region.

These findings suggest that NGC 6868 was not formed on a single collapse and passively evolved since then. Rather we propose that it has suffered a past merge with another galaxy. This can explain the findings in the α-enhancement and the different regions in the indices correlations together with the stellar population synthesis ones, such as the metallicity gradient and ubiquitous old ages. We do not find evidence of a distinct kinematic component either because this merger supposedly happened too long ago or we would need a larger FoV to asses if this region really is a KDC as other studies have previously reported.

ACKNOWLEDGEMENTS

This work was supported by Brazilian funding agencies Conselho Nacional de Desenvolvimento Científico e Tecnológico (CNPq) and Coordenação de Aperfeiçoamento de Pessoal de Nível Superior (CAPES) and by the *Programa de Pós-Graduação em Física* (PPGFis) at UFRGS. JPVB acknowledges financial support from CNPq and CAPES (Proj. 0001). RR thanks to CNPq (Proj. 311223/2020-6, 304927/2017-1 and 400352/2016-8), Fundação de amparo à pesquisa do Rio Grande do Sul (FAPERGS, Proj. 16/2551-0000251-7 and 19/1750-2) and CAPES (Proj. 0001). TVR thanks CNPq for support under grant 306790/2019-0. MT thanks the support of CNPq (process 312541/2021-0) and the programme L'Oréal UNESCO ABC *Para Mulheres na Ciência*. RAR acknowledges the support from Conselho Nacional de Desenvolvimento Científico e Tecnológico

and Fundação de Amparo à pesquisa do Estado do Rio Grande do Sul. JAHJ acknowledges support from FAPESP, process number 2021/08920-8.

Based on observations obtained at the international Gemini Observatory and processed using the Gemini IRAF package, a programme of NSF's NOIRLab, which is managed by the Association of Universities for Research in Astronomy (AURA) under a cooperative agreement with the National Science Foundation on behalf of the Gemini Observatory partnership: the National Science Foundation (United States), National Research Council (Canada), Agencia Nacional de Investigación y Desarrollo (Chile), Ministerio de Ciencia, Tecnología e Innovación (Argentina), Ministério da Ciência, Tecnologia, Inovações e Comunicações (Brazil), and Korea Astronomy and Space Science Institute (Republic of Korea).

DATA AVAILABILITY

The data are publicly available on GEMINI archive under the project GS-2013A-Q-52.

REFERENCES

Allington-Smith J., et al., 2002, Publications of the Astronomical Society of the Pacific, 114, 892
Babyk I. V., McNamara B. R., Nulsen P. E. J., Hogan M. T., Vantyghem A. N., Russell H. R., Pulido F. A., Edge A. C., 2018, The Astrophysical Journal, 857, 32
Baldry I. K., Glazebrook K., Brinkmann J., Ivezić , Lupton R. H., Nichol R. C., Szalay A. S., 2004, The Astrophysical Journal, 600, 681
Barth A. J., Shields J. C., 2000, Publications of the Astronomical Society of the Pacific, 112, 753
Belfiore F., et al., 2016, Monthly Notices of the Royal Astronomical Society, 461, 3111
Bica E., Bonatto C., Pastoriza M. G., Alloin D., 1996, Astronomy and Astrophysics, 313, 405
Binette L., Magris C. G., Stasińska G., Bruzual A. G., 1994, Astronomy and Astrophysics, 292, 13
Brammer G. B., et al., 2009, The Astrophysical Journal, 706, L173
Bregman J. N., Snider B. A., Grego L., Cox C. V., 1998, The Astrophysical Journal, 499, 670
Bruzual G., Charlot S., 2003, Monthly Notices of the Royal Astronomical Society, 344, 1000
Burtscher L., et al., 2021, Astronomy & Astrophysics, 654, A132
Buson L. M., et al., 1993, Astronomy and Astrophysics, 280, 409
Bönsch G., Potulski E., 1998, Metrologia, 35, 133
Caon N., Macchetto D., Pastoriza M., 2000, The Astrophysical Journal Supplement Series, 127, 39
Cappellari M., 2016, Annual Review of Astronomy and Astrophysics, 54, 597
Cappellari M., 2017, Monthly Notices of the Royal Astronomical Society, 466, 798
Cappellari M., Emsellem E., 2004, Publications of the Astronomical Society of the Pacific, 116, 138
Cardelli J. A., Clayton G. C., Mathis J. S., 1989, The Astrophysical Journal, 345, 245
Carollo C. M., Danziger I. J., Buson L., 1993, Monthly Notices of the Royal Astronomical Society, 265, 553
Carrasco E. R., Oliveira C. M. d., Infante L., 2006, The Astronomical Journal, 132, 1796
Chiosi C., Carraro G., 2002, Monthly Notices of the Royal Astronomical Society, 335, 335
Cid Fernandes R., González Delgado R. M., 2010, Monthly Notices of the Royal Astronomical Society, 403, 780
Cid Fernandes R., Gu Q., Melnick J., Terlevich E., Terlevich R., Kunth D., Rodrigues Lacerda R., Joguet B., 2004, Monthly Notices of the Royal Astronomical Society, 355, 273
Cid Fernandes R., Mateus A., Sodré L., Stasińska G., Gomes J. M., 2005, Monthly Notices of the Royal Astronomical Society, 358, 363
Cid Fernandes R., Stasińska G., Mateus A., Vale Asari N., 2011, Monthly Notices of the Royal Astronomical Society, 413, 1687
Cid Fernandes R., et al., 2013, Astronomy & Astrophysics, 557, A86
Cid Fernandes R., 2018, Monthly Notices of the Royal Astronomical Society, 480, 4480
Comerford J. M., et al., 2020, The Astrophysical Journal, 901, 159
Conroy C., Gunn J. E., White M., 2009, The Astrophysical Journal, 699, 486
Croton D. J., et al., 2006, Monthly Notices of the Royal Astronomical Society, 365, 11
Dahmer-Hahn L. G., et al., 2021, Monthly Notices of the Royal Astronomical Society, 509, 4653
Di Matteo T., Springel V., Hernquist L., 2005, Nature, 433, 604
Ellison S. L., et al., 2021, Monthly Notices of the Royal Astronomical Society: Letters, 505, L46
Fabian A., 2012, Annual Review of Astronomy and Astrophysics, 50, 455
Ferland G. J., Netzer H., 1983, The Astrophysical Journal, 264, 105
Filippenko A. V., 1982, Publications of the Astronomical Society of the Pacific, 94, 715
Girardi L., Bressan A., Bertelli G., Chiosi C., 2000, Astronomy and Astrophysics Supplement Series, 141, 371
Gonzalez R. C., Woods R. E., 2008, Digital image processing, 3rd ed edn. Prentice Hall, Upper Saddle River, N.J
Halpern J. P., Steiner J. E., 1983, The Astrophysical Journal, 269, L37
Hamuy M., Walker A. R., Suntzeff N. B., Gigoux P., Heathcote S. R., Phillips M. M., 1992, Publications of the Astronomical Society of the Pacific, 104, 533
Hansen L., Jorgensen H. E., Norgaard-Nielsen H. U., 1991, Astronomy and Astrophysics, 243, 49
Harrison C. M., 2017, Nature Astronomy, 1, 1
Healey S. E., Romani R. W., Taylor G. B., Sadler E. M., Ricci R., Murphy T., Ulvestad J. S., Winn J. N., 2007, The Astrophysical Journal Supplement Series, 171, 61
Heckman T. M., 1980, Astronomy and Astrophysics, 87, 152
Hickox R. C., Mullaney J. R., Alexander D. M., Chen C.-T. J., Civano F. M., Goulding A. D., Hainline K. N., 2014, The Astrophysical Journal, 782, 9
Ho L. C., 2008, Annual Review of Astronomy and Astrophysics, 46, 475
Hook I. M., Jørgensen I., Allington-Smith J. R., Davies R. L., Metcalfe N., Murowinski R. G., Crampton D., 2004, Publications of the Astronomical Society of the Pacific, 116, 425
Hopkins P. F., Elvis M., 2010, Monthly Notices of the Royal Astronomical Society, 401, 7
Kauffmann G., et al., 2003, Monthly Notices of the Royal Astronomical Society, 341, 54
King A., Pounds K., 2015, Annual Review of Astronomy and Astrophysics, 53, 115
Krajnović D., et al., 2015, Monthly Notices of the Royal Astronomical Society, 452, 2
Kroupa P., 2001, Monthly Notices of the Royal Astronomical Society, 322, 231
Kuntschner H., 2000, Monthly Notices of the Royal Astronomical Society, 315, 184
Kuntschner H., et al., 2010, Monthly Notices of the Royal Astronomical Society, 408, 97
La Barbera F., Ferreras I., Vazdekis A., de la Rosa I. G., de Carvalho R. R., Trevisan M., Falcón-Barroso J., Ricciardelli E., 2013, Monthly Notices of the Royal Astronomical Society, 433, 3017
Lauberts A., Valentijn E. A., 1989, The surface photometry catalogue of the ESO-Uppsala galaxies. https://ui.adsabs.harvard.edu/abs/1989spce.book.....L
Lucy L. B., 1974, The Astronomical Journal, 79, 745
Macchetto F., Pastoriza M., Caon N., Sparks W. B., Giavalisco M., Bender R., Capaccioli M., 1996, Astronomy and Astrophysics Supplement Series, 120, 463
Machacek M. E., O'Sullivan E., Randall S. W., Jones C., Forman W. R., 2010,

The Astrophysical Journal, 711, 1316
Mallmann N. D., et al., 2018, Monthly Notices of the Royal Astronomical Society, 478, 5491
Maraston C., Strömbäck G., 2011, Monthly Notices of the Royal Astronomical Society, 418, 2785
Mauch T., Murphy T., Buttery H. J., Curran J., Hunstead R. W., Piestrzynski B., Robertson J. G., Sadler E. M., 2003, Monthly Notices of the Royal Astronomical Society, 342, 1117
Menezes R. B., Ricci T. V., Steiner J. E., da Silva P., Ferrari F., Borges B. W., 2019, Monthly Notices of the Royal Astronomical Society, 483, 3700
Muzzin A., et al., 2013, The Astrophysical Journal, 777, 18
Navarro-González J., Ricciardelli E., Quilis V., Vazdekis A., 2013, Monthly Notices of the Royal Astronomical Society, 436, 3507
Nayakshin S., Zubovas K., 2012, Monthly Notices of the Royal Astronomical Society, 427, 372
Noeske K. G., et al., 2007, The Astrophysical Journal, 660, L47
Novak G. S., Ostriker J. P., Ciotti L., 2011, The Astrophysical Journal, 737, 26
Oser L., Ostriker J. P., Naab T., Johansson P. H., Burkert A., 2010, The Astrophysical Journal, 725, 2312
Papaderos P., et al., 2013, Astronomy & Astrophysics, 555, L1
Ramella M., Focardi P., Geller M. J., 1996, Astronomy and Astrophysics, 312, 745
Ricci T. V., Steiner J. E., Menezes R. B., 2014, Monthly Notices of the Royal Astronomical Society, 440, 2442
Richardson W. H., 1972, JOSA, 62, 55
Rickes M. G., Pastoriza M. G., Bonatto C., 2008, Monthly Notices of the Royal Astronomical Society, 384, 1427
Riffel R., Borges Vale T., 2011, Astrophysics and Space Science, 334, 351
Riffel R., Pastoriza M. G., Rodríguez-Ardila A., Bonatto C., 2009, Monthly Notices of the Royal Astronomical Society, 400, 273
Riffel R., et al., 2019, Monthly Notices of the Royal Astronomical Society, 486, 3228
Riffel R., et al., 2021, Monthly Notices of the Royal Astronomical Society, 501, 4064
Riffel R., et al., 2022, Monthly Notices of the Royal Astronomical Society, 512, 3906
Rose T., et al., 2019, Monthly Notices of the Royal Astronomical Society, 489, 349
Ruschel-Dutra D., Oliveira B. D. D., 2020, danielrd6/ifscube: Modeling, doi:10.5281/ZENODO.4065550, https://zenodo.org/record/4065550
Ruschel-Dutra D., Rodríguez Espinosa J. M., González Martín O., Pastoriza M., Riffel R., 2017, Monthly Notices of the Royal Astronomical Society, 466, 3353
Salvador-Rusiñol N., Vazdekis A., La Barbera F., Beasley M. A., Ferreras I., Negri A., Dalla Vecchia C., 2020, Nature Astronomy, 4, 252
Schawinski K., Koss M., Berney S., Sartori L. F., 2015, Monthly Notices of the Royal Astronomical Society, 451, 2517
Schaye J., et al., 2015, Monthly Notices of the Royal Astronomical Society, 446, 521
Schlafly E. F., Finkbeiner D. P., 2011, The Astrophysical Journal, 737, 103
Simonian G. V., Martini P., 2017, Monthly Notices of the Royal Astronomical Society, 464, 3920
Singh R., et al., 2013, Astronomy & Astrophysics, 558, A43
Slee O. B., Sadler E. M., Reynolds J. E., Ekers R. D., 1994, Monthly Notices of the Royal Astronomical Society, 269, 928
Springel V., et al., 2005, Nature, 435, 629
Steiner J. E., Menezes R. B., Ricci T. V., Oliveira A. S., 2009, Monthly Notices of the Royal Astronomical Society, 395, 64
Steiner J. E., et al., 2022, Monthly Notices of the Royal Astronomical Society, 510, 5780
Storchi-Bergmann T., Schnorr-Müller A., 2019, Nature Astronomy, 3, 48
Thomas D., Maraston C., Bender R., 2003, Monthly Notices of the Royal Astronomical Society, 339, 897
Tody D., 1986, in Crawford D. L., ed., Society of Photo-Optical Instrumentation Engineers (SPIE) Conference Series Vol. 627, Instrumentation in astronomy VI. Crawford, David L., Tucson, p. 733, doi:10.1117/12.968154, http://proceedings.spiedigitallibrary.org/proceeding.aspx?doi=10.1117/12.968154
Tody D., 1993, in Astronomical Data Analysis Software and Systems I. p. 173, https://ui.adsabs.harvard.edu/abs/1993ASPC...52..173T
Trussler J., Maiolino R., Maraston C., Peng Y., Thomas D., Goddard D., Lian J., 2020, Monthly Notices of the Royal Astronomical Society, 491, 5406
Tully R. B., et al., 2013, The Astronomical Journal, 146, 86
Vazdekis A., Peletier R. F., Beckman J. E., Casuso E., 1997, The Astrophysical Journal Supplement Series, 111, 203
Vazdekis A., et al., 2015, Monthly Notices of the Royal Astronomical Society, 449, 1177
Vazdekis A., Koleva M., Ricciardelli E., Röck B., Falcón-Barroso J., 2016, Monthly Notices of the Royal Astronomical Society, 463, 3409
Veron-Cetty M.-P., Veron P., 1988, Astronomy and Astrophysics, Vol. 204, p. 28-38 (1988), 204, 28
Wegner G., et al., 2003, The Astronomical Journal, 126, 2268
Wetzel A. R., Tinker J. L., Conroy C., 2012, Monthly Notices of the Royal Astronomical Society, 424, 232
Worthey G., Faber S. M., Gonzalez J. J., Burstein D., 1994, The Astrophysical Journal Supplement Series, 94, 687
Yan R., Blanton M. R., 2012, The Astrophysical Journal, 747, 61
Zeilinger W. W., et al., 1996, Astronomy and Astrophysics Supplement Series, 120, 257
Zubovas K., Bourne M. A., 2017, Monthly Notices of the Royal Astronomical Society, 468, 4956
de Vaucouleurs G., de Vaucouleurs A., Corwin Herold G. J., Buta R. J., Paturel G., Fouque P., 1991, Third reference catalogue of bright galaxies. Springer-Verlag, New York
de la Rosa I. G., de Carvalho R. R., Vazdekis A., Barbuy B., 2007, The Astronomical Journal, 133, 330
van der Wel A., et al., 2014, The Astrophysical Journal, 788, 28
van Dokkum P., 2001, Publications of the Astronomical Society of the Pacific, 113, 1420

This paper has been typeset from a TEX/LATEX file prepared by the author.

5 O Gás Ionizado de NGC 6868

No capítulo seguinte analisamos as propriedades físicas, mecanismos de ionização e cinemática do gás ionizado de NGC 6868. Esse artigo encontra em fase final de redação e deverá ser submetido para a MNRAS muito em breve.

MNRAS **000**, 1–11 (2022) Preprint 24 January 2023 Compiled using MNRAS LATEX style file v3.0

Digging deeper into NGC 6868 II: ionized gas and excitation mechanism

João P. V. Benedetti,[1] ⋆ Rogério Riffel,[1] † Tiago Ricci,[2] Rogemar A. Riffel,[3] Miriani Pastoriza,[1] Marina Trevisan,[1] Luis G. Dahmer-Hahn,[4] Daniel Ruschel-Dutra,[5] Alberto Rodríguez-Ardila,[6] Jose A. Hernandez-Jimenez[7] and João Steiner[8] ‡

[1]*Departamento de Astronomia, Universidade Federal do Rio Grande do Sul. Av. Bento Gonçalves 9500, 91501-970 Porto Alegre, RS, Brazil*
[2]*Universidade Federal da Fronteira Sul, 97900-000 Campus Cerro Largo, RS, Brazil*
[3]*Departamento de Física, Universidade Federal de Santa Maria, Centro de Ciências Naturais e Exatas, 97105-900 Santa Maria, RS, Brazil*
[4]*Shanghai Astronomical Observatory, Chinese Academy of Sciences, 80 Nandan road, Shanghai 200030, China*
[5]*Departamento de Física - CFM - Universidade Federal de Santa Catarina, 476, 88040-900 Florianópolis, SC, Brazil*
[6]*Laboratório Nacional de Astrofísica/MCT - Rua dos Estados Unidos 154, Bairro das Nacões. CEP 37504-364 Itajubá, MG, Brazil*
[7]*Universidade do Vale do Paraíba, Av. Shishima Hifumi, 2911, Zip Code 12244-000, São José dos Campos, SP, Brazil*
[8]*Instituto de Astronomia, Geofísica e Ciências Atmosféricas, Universidade de São Paulo, 05508-900 São Paulo, Brazil*

Accepted XXX. Received YYY; in original form ZZZ

ABSTRACT

We study the ionized gas in the inner region ($\sim 680 \times 470$ pc^2) of the galaxy NGC 6868 by means of Gemini/GMOS integral field unit observations. We performed emission-line fitting via IFSCUBE using Gaussian profiles and derived the electron density and temperature of the ionized gas using PyNeb. Channel maps reveal complex kinematics and morphology hinting at different processes acting on NGC 6868. We detect two components ubiquitous in our data: a narrow and a broad component. The narrow component traces an ionized gas disc whereas the broad component traces inflowing gas. The reddening, derived via emission line ratios, matches the spatial distribution of the one derived by stellar population synthesis (from Paper I), however, it has larger values. We are able to measure the electronic temperature for NGC 6868 for the first time, finding values ranging from $\sim$ 14000 K in the very centre to $\gtrsim$ 20000 K in an outward increasing temperature gradient. Also, the electron density measurement shows an inverse behaviour with central values reaching $N_e \sim 800$ cm^{-3} falling to $N_e \sim 100$ cm^{-3} towards the edges of the field of view. Using BPT diagrams all spaxels of our data cube are classified as LINER. When using the WHAN diagram we are able to separate different ionization sources within the LINER regime: a central AGN ionizes the central region with an extended outer component ionized by HOLMES. The kinematical findings coupled with the diagrams cannot rule out the presence of shock-heated gas.

Key words: galaxies: individual (NGC 6868), galaxies: nuclei, galaxies: elliptical and lenticular, cD, galaxies: ISM, galaxies: kinematics and dynamics

1 INTRODUCTION

Since the discovery of tight correlations of central black-hole (BH) mass and galaxy properties, such as central velocity dispersion and bulge mass (Magorrian et al. 1998; Gebhardt et al. 2000; Häring & Rix 2004) and with the ever-growing evidence that the different manifestations of active galactic nuclei (AGN) were the counterpart of BHs, a picture of co-evolution and interaction between the two components has emerged (Fabian 2012; Kormendy & Ho 2013; Heckman & Best 2014). The injection of energy by the most energetic AGN in the interstellar medium (ISM) has a crucial role in quenching the star formation (SF) mainly in the most massive galaxies (e.g. Croton et al. 2006; Segers et al. 2016) by heating and expelling the available gas for star-formation. However, studies trying to link SF and AGN activity were done in relatively bright objects (e.g. Seyferts and quasars, e.g. Nayakshin & Zubovas 2012) and the effect of low-luminosity AGN (LLAGN) in the circumnuclear stellar population remains uncertain. A class of this LLAGNs are classified as LINERs (Low-Ionization Nuclear Emission Regions) and proved to be numerous in the nearby Universe, being present in 1/3 of all galaxies and 2/3 of all different types of AGN (Ho 2008). Hence detailed studies of the circumnuclear region are needed to improve our knowledge of the impact of these objects in their vicinity.

LINERs were formerly described by Heckman (1980) as having strong lines from low-ionization species (e.g. O I) and weaker strong ionization lines (e.g. O III). Over the decades with compiling evidence (Ferland & Netzer 1983; Halpern & Steiner 1983; Ho et al. 1996, 1997; Constantin & Vogeley 2006) a growing consensus was formed over the picture that they were toned down versions of Seyfert nuclei, meaning the ionized gas features were due to the photoionization of a low-luminosity active galactic nucleus (LLAGN). Detection

⋆ E-mail: joao.benedetti@ufrgs.br (JPVB)
† E-mail: riffel@ufrgs.br (RR)
‡ In Memorian.

of parsec-scale radio nuclei in 50% of LINERs and subparsec jets further endorsed this picture (Nagar et al. 2005) and, more recently, the detection of ionized gas outflows in approximately ∼46% of LINERs in the sample from Muñoz et al. (2022) related with the central supermassive black-hole despite X-ray studies hinting that AGN could not be the sole responsible for the optical emission-line intensities observed (Flohic et al. 2006).

With improved spatial resolution studies, LINER-like signatures were found not only in the nuclear regions of galaxies (< 1 kpc) but also at greater distances, hence the terms LIER or LI(N)ER adopted by some authors (e.g. Singh et al. 2013; Belfiore et al. 2016). In this scenario other ionization mechanisms need to be taken into account, such as shocks (galactic or from an outflow, Heckman 1980; Dopita & Sutherland 1995; Ho et al. 2014, 2016), starbursts dominated by Wolf-Rayet stars (Barth & Shields 2000) and post-asymptotic giant branch stars (pAGB, Binette et al. 1994). The latter scenario has been gaining support as the dominant ionization mechanism in objects with LINER-like extended emission (Stasińska et al. 2008; Cid Fernandes et al. 2011; Yan & Blanton 2012; Singh et al. 2013) with compelling evidence, such as correlations between Hα and the stellar population has been found in red-and-dead galaxies (e.g. Hsieh et al. 2017), hinting at a stellar origin for the LINER signature and the lack of ionizing photons due to LLAGN to explain the LINER spectra (Eracleous et al. 2010). In this sense, LINERs (or LIERs) can be found in different objects and phenomena in different parts of the spectra and, despite the similarity in spectral signatures, cannot be grouped as a homogeneous class (Herpich et al. 2016).

In this sense, Integral Field Spectroscopy (IFS) has been used in the past decade to improve our understanding of these objects as it is a powerful tool to disentangle the different ionization mechanisms present in objects with LI(N)ER-like emission. Sarzi et al. (2010) using the SAURON IFS survey aimed at understanding the ionized-gas component present in early-type galaxies found a tight correlation between stellar mass surface density and Hβ surface density hinting at a stellar origin behind the ionization process. Loubser & Soechting (2013) analysing central cluster galaxies has found that LLAGN can explain the observed ionization, but shocks and pAGB photoionization could not be ruled out. Ricci et al. (2014a,b, 2015a,b) have extensively analysed a group of 10 LINER galaxies from a range of morphological types. In these objects, they found convincing AGN presence in at least 8 of the objects. However, they also report discs of ionized gas in 7 of them, with 3 having the most probable source of ionizing photons for this disc component from pAGB stars. Belfiore et al. (2015) studied 14 galaxies and found extended ionized gas components, consistent with emission from pAGB stars. Hsieh et al. (2017) using a larger subset of MaNGa also found a correlation between the stellar surface density and Hα surface density, indicating the same scenario as the one derived using SAURON. Studies using the CALIFA survey (Kehrig et al. 2012; Papaderos et al. 2013; Singh et al. 2013; Gomes et al. 2016) found "ubiquitous hot evolved stars and rare accreting black-holes". A more recent study from Menezes et al. (2022) using the mini-DIVING^{3D} sample was able to separate the nuclear from the circumnuclear region, thus allowing a different treatment for each component due to the high spatial resolution for their data. From their sample, 23% present LINER-like emission of which 69% have signs of AGN activity. Lagos et al. (2022) using MUSE data to study group-dominant early-type galaxies found central regions are more influenced by LLAGNs with outer regions ionized by pAGB stars. It is clear that LINERs have a diverse nature and disentangling their nature can only be possible through meticulous inspection of IFS data.

It is clear that in order to fully understand the nature behind objects classified as LINERs and what the impact of an LLAGN is in its host galaxy, one needs to engage in detailed spatially resolved studies, tracing both the properties of the ionized gas and the underlying stellar population focused on the region surrounding the SMBH. Therefore we present a detailed GMOS IFU study of the stellar content of NGC 6868 (Benedetti et al. *submitted*, hereafter Paper I, see below for more details). NGC 6868 was chosen because it is a nearby (27.70 Mpc, Tully et al. 2013) elliptical galaxy (E2, de Vaucouleurs et al. 1991), presents LINER-like signature and an odd ionization profile (Rickes et al. 2008). A detailed study of its central regions has not been presented yet. Some basic parameters extracted from NED can be seen in table 1 and NGC 6868 is shown in different scales in Fig. 1.

Table 1. Table showing some basic parameters of the galaxy NGC 6868.

Parameter	NGC 6868
RA (J2000)	$20^h09^m54^s.07$
Dec. (J200)	-48°22´46.4´´
Morphology[a]	E3
R (mag)[b]	7.91
M_R (mag)[b]	-24.7
Diameter (kpc)[c]	73.0
L_X (erg s^{-1})[d]	$8.54 \cdot 10^{40}$
Nuclear Activity[e]	LINER
Radio classification[f]	Flat-Spectrum Radio Source
A_V[g] (mag)	0.152
Radial Velocity[h] (km s^{-1})	2854
Distance[i] (Mpc)	27.70
Redshift[h] (z)	0.00952

Data available in NED[1]
[a]de Vaucouleurs et al. (1991) [b]Carrasco et al. (2006)
[c]Lauberts & Valentijn (1989) [d]Babyk et al. (2018)
[e]Rickes et al. (2008) [f]Healey et al. (2007)
[g]Schlafly & Finkbeiner (2011) [h]Ramella et al. (1996)
[i]Tully et al. (2013)

NGC 6868 is the brightest member from the Telescopium group and was already observed in different wavelengths. It was featured in a series of papers investigating the ISM on early-type galaxies through long-slit spectroscopy (e.g. Buson et al. 1993; Zeilinger et al. 1996; Macchetto et al. 1996; Pizzella et al. 1997; Ferrari et al. 1999; Caon et al. 2000; Ferrari et al. 2002). They found that the ionized gas in NGC 6868 has a "regular extended" morphology with possible small filaments. Also, the stars present a kinematically decoupled core (KDC) as the stars in the central region counter-rotate with respect to the stars in the outer regions. Moreover, they found NGC 6868 harbours complex ionized gas kinematics with the superposition of two ionized gas discs. Lastly, the hot dust mass estimated from the mid-IR is 70 $M_\odot$ (Ferrari et al. 2002). Veron-Cetty & Veron (1988) have detected a dust lane in the centre of NGC 6868 further endorsed by Bregman et al. (1998) who detected cold dust using IRAS data. Hansen et al. (1991) has examined this galaxy using CCD images and an International Ultraviolet Explorer (IUE) low-resolution spectrum, detecting a dust lane with spiral features emerging from it. Also, they report that the Lyα distribution follows that of the dust. All this leads the authors to suggest that NGC 6868 has captured a gas-rich galaxy. Machacek et al. (2010) using X-ray data found strong

[1] The NASA/IPAC Extragalactic Database (NED) is operated by the Jet Propulsion Laboratory, California Institute of Technology, under contract with the National Aeronautics and Space Administration

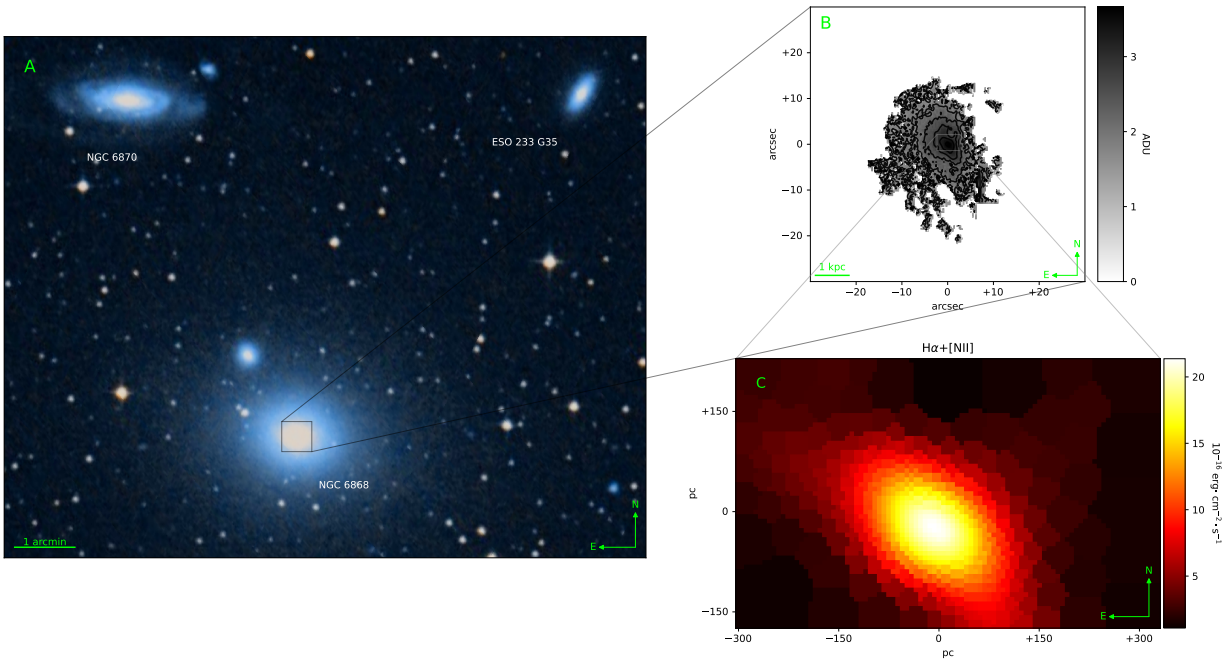

Figure 1. Images from NGC 6868 in three different scales. (a) Composite DSS image showing NGC 6868 and close neighbours. It is the brightest group member from the Telescopium group (AS0851). (b) Recreation of Hα+[N II] image present in Macchetto et al. (1996) using NTT+EFOSC2. They describe the galaxy as having a "regular extended" morphology where small filaments may be present. (c) Hα+[N II] image extracted from the final GMOS data cube. The (0,0) is kept the same as in Paper I for consistency.

evidence of a past encounter between NGC 6868 and NGC 6861 in the past hundred Myr, displaying tidal tails and shells. Moreover, they found X-ray cavities, indicative of past AGN activity triggered by the interaction. Radio observations (Slee et al. 1994; Mauch et al. 2003; Healey et al. 2007) revealed a low-power flat spectrum radio source in its centre ($\alpha \sim 0.07$) and the brightness, temperature and spectral slope are inconsistent with HII regions, thus hinting at an AGN as the most likely source of the emission. Rose et al. (2019) have analysed molecular gas in the centre of NGC 6868 and concluded it is drifting in non-circular motions.

In Paper I we have already studied the stellar content of this galaxy through stellar population synthesis and indices calculation. We found that this galaxy is dominated by old high-metallicity stars (~12 Gyr; 1.0-1.6 Z$\odot$) and no evidence of a featureless continuum was found. The kinematics in the centre of the galaxy is dispersion dominated and no apparent ordered rotation was detected. The indices profile reveals that this object has a complex chemical evolution, further endorsed by the [α/Fe] map showing regions with very distinct enrichment. This has led us to conclude that only past mergers would be able to explain these findings.

In this paper, we will focus on the ionized gas content of NGC 6868 which is organized as follows: in § 2, we describe the observations and the reduction procedures; in § 3, we present the methodology; in § 4, the results are presented. Discussion of the results is made in § 5 and the conclusion and summary are made in § 6. Throughout this paper, we assume that solar metallicity corresponds to $Z_{\odot} = 0.019$ (Girardi et al. 2000).

2 OBSERVATION AND DATA REDUCTION

The acquisition of the observational data, the reduction processes and subsequent data processing steps were already thoroughly described in Paper I. Briefly, NGC 6868 was observed as a part of the DIVING^{3D} survey (Steiner et al. 2022) on 2013 May 04 using the Gemini Mutli-Object Spectrograph (GMOS) in the IFU mode mounted on the Gemini South Telescope. The resulting FoV was 3.5×5.0 arcsec^2 as the one slit setup was used. Moreover, the grating B600-G5323 was used with a central wavelength of 5620 Å ranging from 4260 - 6795 Å. The spectral resolution was estimated with the O I λ5577Å line resulting in 1.8 Å. Using the acquisition image from GMOS in the r-band (SDSS system) and field stars present, the seeing was measured at 0.77 Å. Lastly, the DA white dwarf EG 274 (Hamuy et al. 1992) was observed to perform the spectrophotometric calibrations. Standard IRAF procedures (Tody 1986, 1993) were followed to reduce the data using the GEMINI IRAF package and the LACOS software (van Dokkum 2001) was used to remove cosmic rays. The final sampling of the data cube was 0.05 arcsec.

Other data treatments were applied to improve data visualisation as described in Menezes et al. (2019). The removal of high-frequency spatial noise using a Butterworth filter (Gonzalez & Woods 2008; Ricci et al. 2014a) with an order n=2 and a cut-off frequency of 0.14 of the Nyquist frequency (0.5 spaxel^{-1}). Then the correction by the differential atmospheric correction using the equations from Bönsch & Potulski (1998) and Filippenko (1982). The PCA Tomography technique (Steiner et al. 2009, and references therein) was applied to remove instrumental fingerprints. The data cube was then corrected by the Galactic reddening using the CCM law (Cardelli et al.

1989) and $A_V = 0.152$ mag (Schlafly & Finkbeiner 2011). Telluric lines were removed and using the redshift from NED ($z = 0.00952$, Ramella et al. 1996) the spectra were brought to rest frame velocities. To improve the PSF from our data, the Richardson-Lucy deconvolution (Richardson 1972; Lucy 1974) was applied and after 10 iterations a PSF of 0.71 arcsec was achieved, estimated using the red wing of the broad Hα component. In Fig. 1 a map from [N II]+Hα extracted from the final data cube after the subtraction of the stellar component can be seen.

3 EMISSION LINE FITTING

In Paper I we have fitted the underlying absorption line continuum of this source, to analyse the pure emission line spectrum, we subtracted the modelled stellar continuum from our data. After the subtraction, we had low signal-to-noise ratios, mainly in the borders of our FoV and a distinct region that will be described in detail in the following sections. To improve the S/N, we used the Voronoi binning technique (Cappellari & Copin 2003) which bins the data preserving the maximum spatial resolution given a minimum S/N to be achieved throughout the FoV. We measured the signal as the mean flux density between 6528-6615 Åwhich encompasses the [N II] λ6548, 6584+Hα emission. The noise was estimated as the standard deviation between 4800-4845 Å. We opted to use this region of the spectrum because it is on the bluer side of our spectra and therefore is noisier, functioning as an upper limit to noise in the whole spectrum. The target S/R was 30.

The stellar synthesis, despite its precision, can lead to discrepancies between the data and the stellar continuum. This can be worked around by fitting a high-degree polynomial to the discounted spectra to model a non-physical continuum that can affect our measurements. We masked the emission lines we would want to measure and added and doubles the weight in arbitrary continuum bands of 20 Åof width surrounding each line. We took extra care to avoid adsorptions or emission lines within these bands. We tested different configurations for the fit and ended up with a 13th-degree polynomial as our pseudo-continuum. After this pre-processing, we measured the emission-line fluxes using IFSCube package (Ruschel-Dutra & Oliveira 2020)[2], which fits the different emission lines using Gaussian functions with predefined components.

The spectrum from NGC 6868 is rich in emission lines as can be seen in Fig. 2. The identified lines that we were able to properly fit were the H I Hα, Hβ and Hγ, [N II] λ5755, 6548, 6583 Å, [O III] λ4959, 5007 Å, [O I] λ6300, 6360 Å, [N I] λ5197, 5200 Å and [S II] λ6716, 6731 Å. By looking at Fig. 4 one can see the immense diversity in line profiles from this galaxy[3]. We carried out a series of tests with different configurations and ended up with a model consisting of two distinct kinematical components for each line: a narrow component and a broad component to better describe the emission-line profiles. As will be further discussed in the following sections, the narrow component traces an ionized gas disc whereas the broader component can be attributed to different phenomena, depending on the region of the FoV. This has been applied for all the spaxels and some example fits can be seen in Fig. 4.

In order to reduce the degeneracy from our fit, we made some assumptions and established some constraints to our models. First, we used the following well-known line ratios (Osterbrock & Ferland 2006): [N II] λ6583 Å = 3.06 [N II] λ6548 Å, [O III] λ5007 Å = 2.94 [O III] λ4959 Å, [O I] λ6300 Å = 3.05 [O I] λ6360 Å and [N I] λ5197 Å = 2.32 [N I] λ5200 Å. On the first try, we only established kinematical groupings with components from lines produced by the same ion. We noticed, however, that all lines ended up with really similar kinematical and flux distributions among different ions. To further reduce the degeneracies, we constrained that each component from all the lines fitted would be in the same kinematical group e.g. the blue-shifted component needs to have the same velocity and velocity dispersion among all the different lines. This helps to disentangle the different components in weaker lines as the kinematical information from stronger lines is used to improve the fit.

Electron temperature (T_e) and density (n_e) were computed using PyNeb (Luridiana et al. 2015) with line-ratios [N II] λ5755, 6583 Å and [S II] λ6716, 6731 Å. We also calculated the emission line ratios of [N II] λ6583/Hα, [S II] λ6716, 6731/Hα, [O I] λ6300/Hα , [O III] λ5007/Hβ. We derived the reddening also using the PyNeb package. Considering the case B recombination and rough estimates of both density and temperature, as a first approximation, (100 cm^{-3}; 10000 K). Using this parameters, we estimate the theoretical value of $F_{H\alpha}/F_{H\beta} = 2.87$. Assuming, a CCM extinction law (f_λ; Cardelli et al. 1989, R_V=3.1) and following Riffel et al. (2021), we get

$$E(B-V) = \frac{E(H\beta - H\alpha)}{f_\lambda(H\beta) - f_\lambda(H\alpha)} \quad (1)$$

$$= \frac{2.5}{3.1 \cdot (1.164 - 0.818)} \log\left(\frac{(F_{H\alpha}/F_{H\beta})^{obs}}{(F_{H\alpha}/F_{H\beta})^{theo}}\right)$$

$$A_V = 7.22 \log\left(\frac{(F_{H\alpha}/F_{H\beta})^{obs}}{2.87}\right). \quad (2)$$

Therefore, using the Balmer recombination lines (Hα, Hβ), we derived the reddening in the V band (A_V) and deredden all emission lines, following

$$F_{int} = F_{obs} 10^{0.4 \cdot A_\lambda} = F_{obs} 10^{0.4 \cdot A_V \cdot f_\lambda}. \quad (3)$$

4 RESULTS

4.1 Gas Kinematics

4.1.1 Channel Maps

In order to better assess the kinematically distinct regions from our FoV, we produced channel maps from the Hα emission line (Fig. 3). This was done by slicing the data cube in 2.0 Å(~91 km·s^{-1}) regions and taking the mean flux density in each one of them. We masked all spaxels that had flux values smaller than 3 times the value of the standard deviation as calculated in § 3. We have applied the same procedure for the [O III] λ5007 Å line and have not found significant differences between both lines.

The central region of NGC 6868 displays several distinct features. In the high-velocity maps (+411 and +502 km·s^{-1}), a rather spherical distribution emerges and its centre coincides with our estimation from Paper I. In the lowest velocity map (-319 km·s^{-1}), the same centrally concentrated region however with a slight perturbation to the NW that can be followed in the maps of -228 and -137 km·s^{-1}. In the maps from -228 to +228 km·s^{-1} a signature of a disc can be traced, going from the SW to NE. In the +319 km·s^{-1} a distortion in the central profile can also be seen in the NE region, that appears to be independent of the disc as such a profile does not emerge in the -319 km·s^{-1} map. Lastly, a region in the N region, we have not

[2] Available at: https://github.com/danielrd6/ifscube

[3] The ionized gas kinematics from this object have already been studied through long-slit spectroscopy (e.g. Caon et al. 2000; Zeilinger et al. 1996) and they all found intricate kinematics.

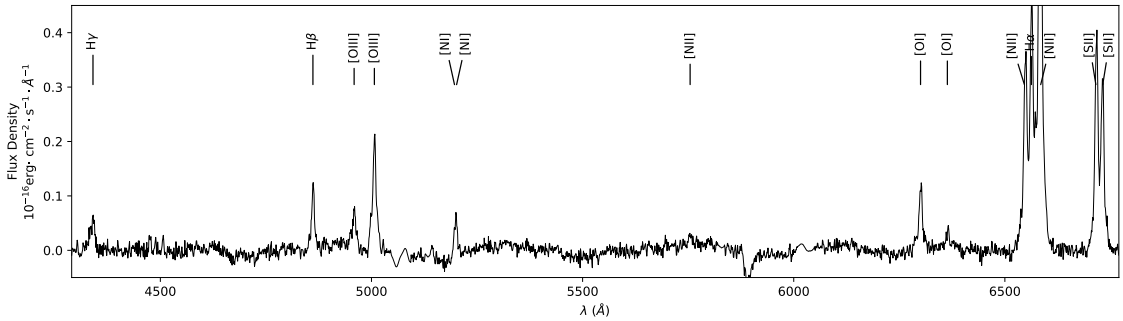

Figure 2. Absorption line free emission spectrum extracted at peak of the continuum. The most prominent emission lines are identified. More details of the kinematical nature of the lines can be seen in Fig. 4.

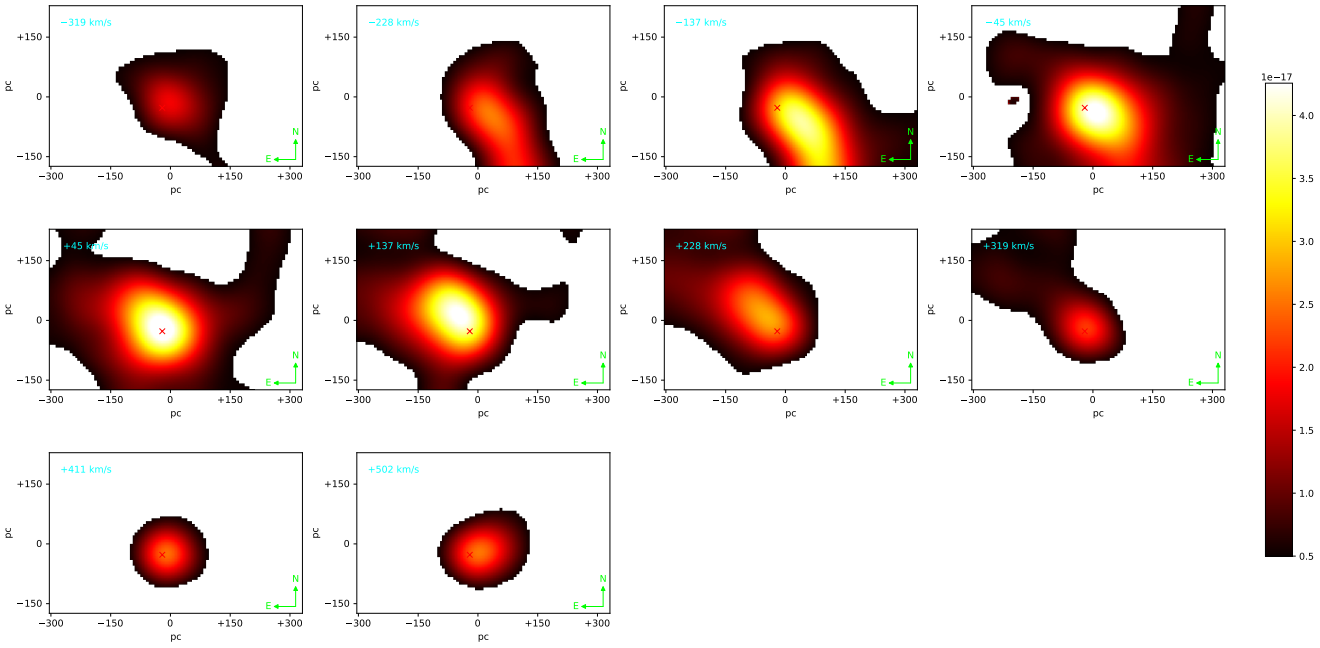

Figure 3. Channel maps for the Hα emission line using 2.0 Å (~91 km·s^{-1}) as our sampling width. We masked values smaller than three times the standard deviation as calculated in § 3. In the last map we can already see a contamination from the surrounding [N II] λ6583 Å. Interesting regions are marked with letters and are the same as in Fig. 4.

detected any ionized gas. This region can be more clearly seen in the +45 km·s^{-1} map.

4.1.2 Velocity and velocity dispersion maps

In Fig. 4 we present fits from different regions of our FoV, highlighting regions with "peculiar" components on the channel maps, it is worth mentioning that for all regions our fitting approach was able to properly reproduce the emission line profiles.

The centroid velocities and velocity dispersion for the narrow and broad components are presented in Fig. 5. It is clear from this figure that the narrow component broadens in the central regions, reaching ~ 140 km·s^{-1}, decreasing to ~ 90 km·s^{-1}. Looking at the centroid velocities of this component, one can infer that the central region of NGC 6868 hosts a disk of ionized gas, peaking at ~ ±150 km·s^{-1}. The centre of the rotation profile appears to coincide with the centre of NGC 6868, estimated in Paper I. The broader component appears to have a more diverse nature, with regions of the FoV with roughly the same velocity dispersion as the narrow component (NE region) but higher centroid velocities (~ 250 km·s^{-1}) and other reaching ~ 400 km·s^{-1}. We also notice that in the NW direction, a blueshifted (~ −100 km·s^{-1}) broader ~ 250 km·s^{-1} wing is apparent.

Previous studies have reported a rotating gas disc in NGC 6868, such as Caon et al. (2000). Our detection agrees with the orientation reported for their study, but they find profiles peaking at ~180 and 190 km·s^{-1}, slightly larger than reported here. As their modelling was much simpler than ours, they are probably having contamination of the high-velocity components that we also detect, mainly in PA=120° where they report a probable counter-rotating gas disc. It seems that

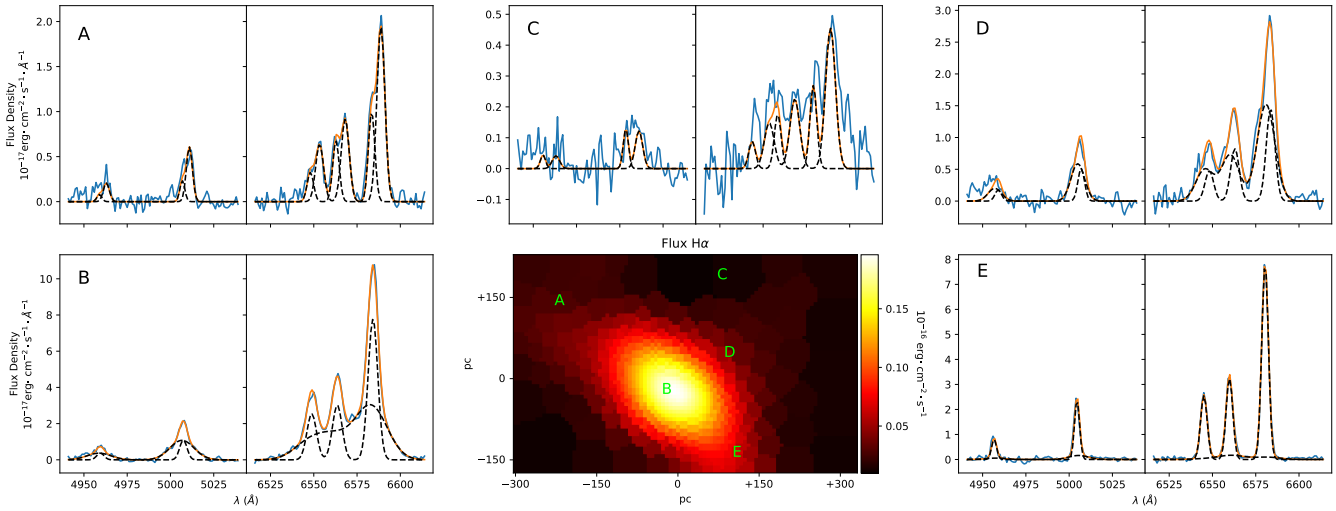

Figure 4. Different regions and the respective spectra showing, in blue, the observed profile of the [O III] (left) and Hα+[N II] (right), in dashed black lines, each modelled gaussian and, in orange, the total model. One can see the huge diversity among the line profiles, showing double peaks, broad, narrow and wing components. Our model proves to be successful to reproduce the line profiles.

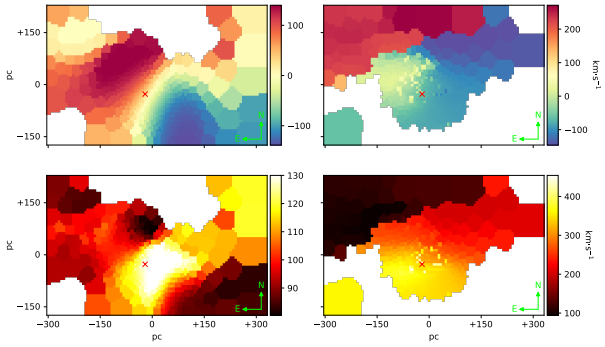

Figure 5. Kinematical results for the central region of NGC 6868. The top two panels show the centroid velocities for the narrow (left) and broad (right) and the bottom two panels show the velocity dispersion also from the narrow (left) and broad (right).

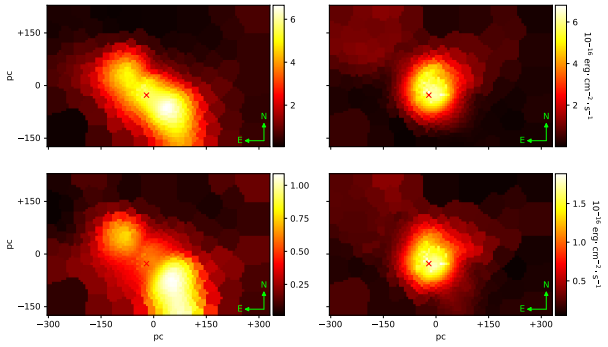

Figure 6. Flux distribution from narrow (left) and broad components (right) and [NII] λ6583 Å (top) and [OIII] λ5007 Å (bottom) emission lines. The components are fairly similar between the different lines. The profile from the broad component has more features when compared to the narrow.

they were detecting the contamination from the blueshifted broad component in the NW thus affecting their measurements.

The flux distributions derived are in Fig. 6. We decide to show only the [NII] λ6583 Å and [OIII] λ5007 Å emission lines flux distributions because [NII] is the most prominent line in our cube and most lines follow its distribution, except for [OIII] λ5007 Å which has some peculiarities.

The narrow component distribution appears in a flat distribution angled in the SW-NE direction, following the rotation profile described previously. In the [O III] line, however, it appears that the SW region is much more enhanced. This does not appear to be a feature from the fitting procedure, but rather some physical process enhancing it at this location. This can be roughly seen in Fig. 4 as it appears that in region E [O III] has the largest amplitude within all the spectra shown. The broader component shows a distribution diverse from the previous with a clear centrally concentrated flux distribution with two wings: one at NE and another at NW. Both of them originated in the components also detected in the channel maps and in the kinematical maps.

4.2 Ionized gas physical parameters

Using the fluxes derived in the previous sections we were able to derive physical parameters for the ionized gas through the python package PyNeb (Luridiana et al. 2015) as described in § 3.

First, using the Balmer recombination lines, we derived the reddening in the V band A_V. We decided to sum the fluxes from both components of each line to measure the A_V. Thus, having a single measurement of each property in each spaxel. PyNeb has a method to determine this parameter using line flux ratios. We used the Case B recombination so the code derives the emissivity given a temperature and density which we set as 10000 K and 100 cm^3, as a first approximation. Using the CCM extinction law (Cardelli et al. 1989), the A_V map is shown in Fig. 7.

The A_V reveals a dust lane that has already been reported in previous studies (see 1) and also in Paper I, having the same orientation and roughly the same spatial extension. The amplitude of such reddening however is enhanced, when you compare to these previous studies: in Paper I we found the dust distribution peaks at ~ 0.65 mag

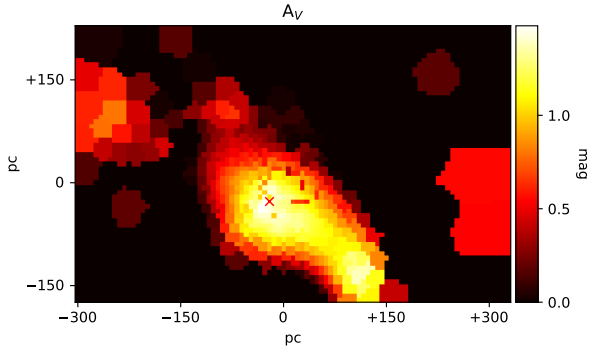

Figure 7. The reddening in the V band derived through the Balmer recombination lines ratio Hα/Hβ. A dust lane emerges in the centre, agreeing with past results found through stellar population synthesis.

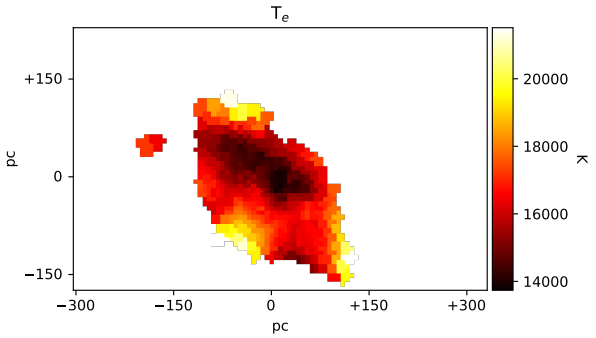

Figure 8. Temperature profile derived from the [N II] λ6583, 5755 Å line ratio corrected by the extinction. The temperature profile seems to display a negative gradient with values ranging from 14000 to 21000 K.

whereas the A_V derived here reaches $\sim$ 1.5 mag, more than doubling our previous result. This has been found in past studies, such as Riffel et al. (2021), with a ratio close to the one reported here. They interpret this finding as the fact that STARLIGHT uses a single extinction law to redden the whole stellar population, despite newer generations of stars being typically embedded in the dust reminiscent of the star-formation processes. Thus, in the synthesis, you end up underestimating the dust content mainly if old stellar populations dominate your galaxy. A similar scenario might be at play here, but, as we saw on Paper I this galaxy lacks any signs of recent star formation or a younger dust-embedded component. However, using the same reasoning, the ionising radiation might come from a more heavily dust-obscured region, not necessarily young stars, such as an AGN, or from the dustier gas ejected during the stellar evolution process. Using the A_V corrected emission line fluxes, we derived both the electronic temperature and density, respectively shown in Fig. 8 and Fig. 9.

We were not able to find any other measurement of the electronic temperature and density for NGC 6868, making this the first measurement. As can be seen in Fig. 8, the temperature profile of the ionized gas is co-spatial with the broader component flux distribution. Also, it appears that an outward gradient emerges, ranging from 14000 K to close to 21000 K in the borders of our detection, however, to confirm such a result higher spatial resolution observations would be necessary as the region where we can measure the temperature is slightly larger than our seeing.

We can provide density estimates, on the other hand, for the whole FoV separating the narrow and broad components in the [SII] λ6716, 6731 Å. In some regions, the [SII] λ6716, 6731 Å ratio is larger than 1.45 and density estimates are no longer valid. As this implies a low-density environment, when values exceeded 1.45, we set 100 cm^{-3} as the density in that spaxel.

For the narrow component, a ubiquitous low-density component is found, with values ranging from the lower limit 100 cm^{-3} to less than 500 cm^{-3}. This is not the case for the broader component with values similar to the ones found in the narrow component for the NE region and values in the central region reaching over 4000 cm^{-3}. Hansen et al. (1991) based on data from (Bonatto et al. 1989) has estimated the electron density as 800 cm^{-3}. As a kinematical decomposition was not carried out in those studies, the in-between value is most likely because they are treating the two components found in this work as one.

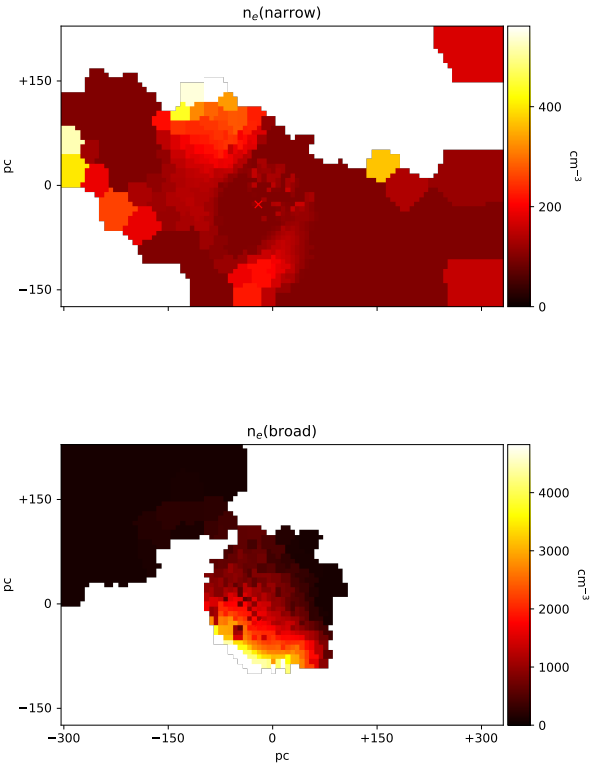

Figure 9. Electron density profile derived from the [N II] λ6716, 6731 Å line ratio corrected by extinction. **Top panel:** Density values for the narrow component with values ranging from 100 cm^{-3} to 500 cm^{-3}. **Bottom panel:** Broader component showing a large variation in the derived density values. In the central part of the FoV electron density is over 4000 cm^{-3} falling to similar values to the narrow component in the NE region.

Lastly, we estimate the total ionized gas mass using the relation

$$M_{gas} \approx 2.4 \times 10^5 \frac{L_{41}(H\alpha)}{n_3} M_\odot \quad (4)$$

as in do Nascimento et al. (2019), where $L_{41}(H\alpha)$ is the luminosity of Hα in units of 10^{41} erg·s^{-1} and n_3 is the electron density in units of 10^3 cm^{-3}. Using the extinction corrected Hα flux, the distance from table 1 and previously derived electron density, we estimated the total ionized gas mass in our FoV to be $\sim 4 \times 10^6$ M$_\odot$[4]. This however is a lower limit as the ionized gas component stretches beyond our FoV, as can be seen in Fig. 1. Hansen et al. (1991) using narrow band data to estimate the flux of Hα has estimate the H II mass as $\sim 2 \times 10^6$ M$_\odot$. They reported a value that is half of the value we found here. We attribute this difference due to several facts. They have used narrow band images to estimate the Hα using previously determined [N II] λ6583 Å/Hα ratios, instead of having the fine details spectroscopy can provide which enabled us to properly separate the [N II] and Hα emission. They use a fixed electron density value (800 cm^{-3}), which as can be seen in Fig. 9, is not correct. The fact that they are using a larger value for the density makes their estimate of the gas mass decrease (Eq. 4). Another difference between our estimate and theirs is the difference in the Hα flux. Our integrated Hα flux measurement is 9.12×10^{-13} erg· cm^{-2}·s^{-1}, whilst their reported value is 3.3×10^{-14} erg· cm^{-2}·s^{-1}. The reasons for this discrepancy also are many. Firstly, They did not apply any reddening corrections to their emission line fluxes. Also, they had a problem with their spectrophotometric standards, leading to a 30% error in their measurements. Despite all of these differences, both of our values have the same order of magnitude, further supporting our findings.

4.3 Emission line diagnostic diagrams

In order to assess the ionization mechanism present in the central region of NGC 6868, diagrams discerning the different ionization sources are needed. The most widely used diagrams in the literature are the Baldwin, Phillips & Terlevich (BPT, Baldwin et al. 1981) diagrams and rely on the [N II] λ6583 Å/Hα, [O III] λ5007 Å/Hβ, [S II] λ6716, 6731 Å/Hα and [O I] λ6300 Å/Hα line ratios to disentangle the possible ionization mechanisms. Kauffmann et al. (2003) and Kewley et al. (2006) have established calibrations to separate AGNs from LINERs and SF galaxies. Using these lines and the fluxes corrected previously derived, we mounted these diagnostics.

The BPT diagram for the [N II] λ6583 Å/Hα is seen in Fig. 10 for the components. Both diagrams classify the whole FoV as having LINER-like emission. This was expected as other studies already mentioned (§ 1) had detected the same signatures. As mentioned, shock-heated gas may be present in NGC 6868. Therefore shock models from Allen et al. (2008) were overplotted in the broad lines BPT. We used twice-solar metallicity models and a pre-shock density of 1 cm^{-3}, creating our grid with models of velocities between 300 and 1000 km·s^{-1}, and magnetic fields between 1.0 and 4.0 μG.

In order to make a deeper analysis of the nature of the ionization source of NGC 6868, we used the WHAN diagram (Cid Fernandes et al. 2011). It uses the equivalent width of the Hα (W$_{H\alpha}$) to measure if the light from hot low-mass evolved stars (HOLMES) is enough to reproduce the ionization levels of the observed emission lines, allowing for the distinction between true AGNs and retired galaxies.

[4] We have derived the M_{gas} using the $L_{41}(H\alpha)$ and n_3 in each spaxel and then summing over the whole FoV to get this final value

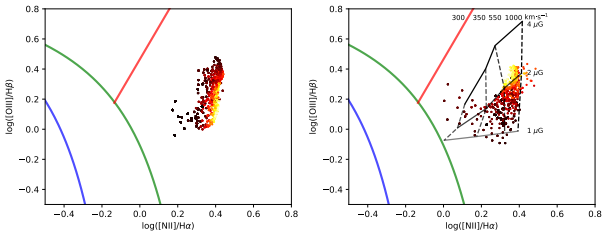

Figure 10. BPT diagram for the central region of NGC 6868 for the narrow (left panel) and broad (right panel). The points were colour-coded following the Hα flux in each spaxel, serving as a guide for interpreting the results. The whole FoV of our observation is kept within the LINER region, as expected. Shock grids were plotted with models of velocities between 300 and 1000 km·s^{-1}, and magnetic fields between 1.0 and 4.0 μG.

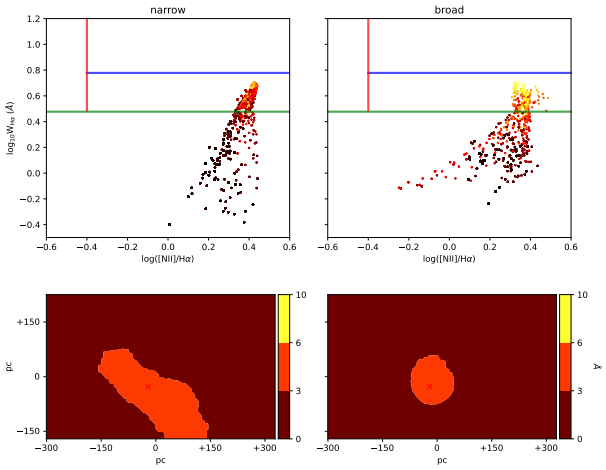

Figure 11. WHAN diagram showing the distribution of spaxels, going from the weak AGN region to the retired galaxies, displaying the diversity in the ionization nature from NGC 6868. The flux of Hα has been used to colour-code the points and serve as a guide. The central regions are ionized by an AGN whereas the outer parts are by the HOLMES with a transition region in between. Shocks cannot be ruled out and may also play a role in the ionization phenomena.

In Fig. 11 we show the WHAN diagram for each component with spatial identification of each region in the bottom panels, showing a more diverse scenario of the ionization phenomena in NGC 6868. Following Cid Fernandes et al. (2011), the centre is dominated by a strong AGN, followed by a transition region finally reaching the outermost parts of the FoV where the ionization is only due to HOLMES. The WHAN diagram cannot provide further information regarding shocks, which will be addressed in the following section.

5 DISCUSSION

5.1 Detection of an ionized gas disc

The kinematics from the ionized gas derived from our emission line fitting procedure can disentangle the different components that dominate the central region of NGC 6868. The narrow component that can be seen in Fig. 5 resembles a rotation profile. Therefore, we used a method within IFSCUBE to fit the disc model extracted from Bertola et al. (1991). It assumes the gas is orbiting in circular

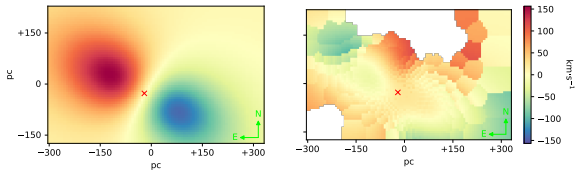

Figure 12. Left: Map containing the resulting fit from the kinematical map of the narrow component Fig. 5. Right: residuals from the fit. We can confidently model the gas disc as our residuals reach a maximum $\sim$ 50 km·s^{-1} for most of the FoV. The NW region is most likely disturbed by the other kinematical component

trajectories and follows a velocity field

$$v_r = A\frac{r}{(r^2+c_0^2)^{p/2}}. \quad (5)$$

Thus the projected velocity distribution follows

$$v(R,\Psi) = v_{\rm sys} + \frac{A\ R\ \cos(\Psi-\Psi_0)\sin\Theta\cos^p\Theta}{\left[R^2\left(\sin^2(\Psi-\Psi_0)+\cos^2\Theta\cos^2(\Psi-\Psi_0)\right)+c_0^2\cos^2\Theta\right]^{p/2}}. \quad (6)$$

The resulting fit is shown in Fig. 12 along with the residuals. As can be seen, we are able to properly model the ionized gas disc with residuals reaching at maximum $\sim$ 50 km·s^{-1}. The main exception is the region in the NW where larger values for the residuals are found. This is likely the result of a disturbance caused by inflowing material, described in the next section.

This ionized gas disc has already been reported in previous studies (see § 1). We can see that the A_V profile follows roughly the same spatial distribution as the gas disc. This linking had already been pointed in Hansen et al. (1991). The molecular gas already reported in NGC 6868 is found in distances compatible with our findings for the dust lane, therefore the dust is likely shielding the molecular gas from the ionising radiation present in the region.

5.2 What is the origin of the two components observed on the emission lines?

Rickes et al. (2008) using long slit spectroscopy had already raised the importance of shocks to explain the ionization phenomena, mainly in external regions (behind our FoV). Hansen et al. (1991) find evidence that NGC 6868 has recently captured a gas-rich companion using an FoV larger than ours. They detect gas filaments with spiral shapes. One of these filaments appears to connect with our FoV right where the high velocity ($\sim$ 250 km·s^{-1}) redshifted broader component is found in the NE region in Fig. 5.

We do not detect however this component approaching the centre of NGC 6868, therefore, allowing us to conclude this material is inflowing. We do however detect this behaviour with the blue-shifted component in the NW region. We propose that the redshifted component is a filament of material that goes through the ionized gas disc and bends backwards to be finally captured as inflowing material in the NW region. This would explain both the flux distribution and peculiar kinematics described previously and the higher residuals found in the disc fitting as this inflowing material is likely perturbing the gas. Also, the density radial profile (Fig. 9) shows that the density in the central region is larger than in the surrounding regions. This is likely the effect of the gas being compressed as it is being accreted.

Another evidence that this is likely inflowing material is that we have evidence of shocks. As can be seen in Fig. 13, [N II]/Hα and [S II]/Hα seem to be enhanced both on the NE towards the edge of the FoV and near the centre in the NW direction, right where we detect the peculiar kinematics, indicative of shock-heated gas.

5.3 What is driving the gas ionization in NGC 6868?

NGC 6868 displays an extended ionized gas component as can be seen in Fig. 1. It is classified as a LINER object in the BPT diagram, it has recently captured a gas-rich companion and is accreting the gas to its central region, therefore the contribution from shocks cannot be discarded. However, studies in other spectral regions have revealed that NGC 6868 hosts an LLAGN, such as the detection of a low-power flat spectrum radio source (Healey et al. 2007). Therefore, despite the non-detection of a broad component compatible with a broad-line region, we do believe an LLAGN is present in NGC 6868. In that sense, the central region must have at least part of its ionising photons coming from the AGN. This proves to be the case when looking at the WHAN diagram, where the central region does appear to have its ionization dominated by an AGN.

Thus, our interpretation of the ionization mechanism in NGC 6868 is that its nuclear region is predominantly ionized by an LLAGN, while the outskirts of our FoV are predominately ionized by HOLMES.

6 CONCLUSIONS

We analysed the central region of NGC 6868 using GMOS-IFU and mapped the properties of the ionized gas as well as the excitation mechanism behind the ionization observed. NGC 6868 proves to be an exciting laboratory to study the different mechanisms involved in LINERs. The main findings from our work are summarized below:

- Channel maps and line profiles reveal complex kinematics and morphology hinting at different processes acting on NGC 6868
- Emission line fitting has revealed two kinematic components a narrow and a broad. The narrow component traces an ionized gas disc and the broad component traces inflowing gas that is being driven to the vicinity of the LLAGN present in NGC 6868 and settling in a dispersion-dominated component. Flux distributions follow these findings.
- The reddening obtained from hydrogen recombination lines is consistent with the derived by the STARLIGHT in Paper I. With a larger amplitude. This is likely due to the obscuration of the ionizing source, mainly in the central regions (LLAGN).
- In this paper we report the first measurement of electron temperature in NGC 6868. We find a temperature of $\sim$ 14000 K for the central region with the outer parts surpassing the $\sim$ 20000 K. The density profile shows an inverse behaviour as the central regions show an enhancement ($\sim$ 800 cm^{-3}) when compared to the outer regions($\sim$ 100 cm^{-3}), hinting at a compression of the ionized gas.
- The whole FoV of our observation is kept within the LINER region in the BPT diagram. In the WHAN diagram, it appears that the central region is ionized mainly by an LLAGN and the HOLMES create an ionizing radiation field that is responsible for the ionization at larger scales.

ACKNOWLEDGEMENTS

This work was supported by Brazilian funding agencies Conselho Nacional de Desenvolvimento Científico e Tecnológico (CNPq) and Coordenação de Aperfeiçoamento de Pessoal de Nível Superior

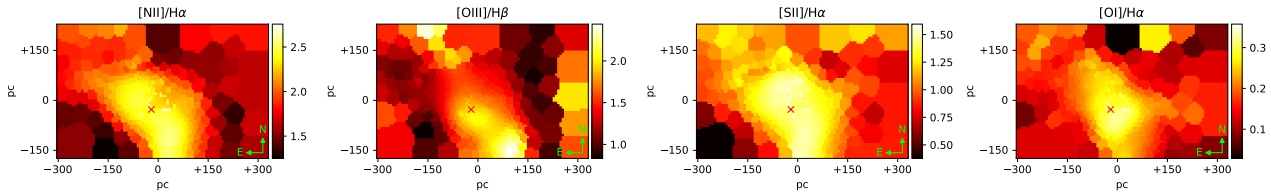

Figure 13. Maps of important emission line ratios. From left to right, [N II]/Hα, [O III]/Hβ, [S II]/Hα, [O I]/Hα. They were all corrected by extinction.

(CAPES) and by the *Programa de Pós-Graduação em Física* (PPGFis) at UFRGS. JPVB acknowledges financial support from CNPq and CAPES (Proj. 0001). RR thanks to CNPq (Proj. 311223/2020-6, 304927/2017-1 and 400352/2016-8), Fundação de amparo à pesquisa do Rio Grande do Sul (FAPERGS, Proj. 16/2551-0000251-7 and 19/1750-2) and CAPES (Proj. 0001). TVR thanks CNPq for support under grant 306790/2019-0. MT thanks the support of CNPq (process 312541/2021-0) and the program L'Oréal UNESCO ABC *Para Mulheres na Ciência*. RAR acknowledges the support from Conselho Nacional de Desenvolvimento Científico e Tecnológico and Fundação de Amparo à Pesquisa do Estado do Rio Grande do Sul. JAHJ acknowledges support from FAPESP, process number 2021/08920-8.

Based on observations obtained at the international Gemini Observatory and processed using the Gemini IRAF package, a program of NSF's NOIRLab, which is managed by the Association of Universities for Research in Astronomy (AURA) under a cooperative agreement with the National Science Foundation on behalf of the Gemini Observatory partnership: the National Science Foundation (United States), National Research Council (Canada), Agencia Nacional de Investigación y Desarrollo (Chile), Ministerio de Ciencia, Tecnología e Innovación (Argentina), Ministério da Ciência, Tecnologia, Inovações e Comunicações (Brazil), and Korea Astronomy and Space Science Institute (Republic of Korea).

DATA AVAILABILITY

The data are publicly available on GEMINI archive under the project GS-2013A-Q-52. The reduced and processed data can be made available under reasonable request.

REFERENCES

Allen M. G., Groves B. A., Dopita M. A., Sutherland R. S., Kewley L. J., 2008, The Astrophysical Journal Supplement Series, 178, 20
Babyk I. V., McNamara B. R., Nulsen P. E. J., Hogan M. T., Vantyghem A. N., Russell H. R., Pulido F. A., Edge A. C., 2018, The Astrophysical Journal, 857, 32
Baldwin J. A., Phillips M. M., Terlevich R., 1981, Publications of the Astronomical Society of the Pacific, 93, 5
Barth A. J., Shields J. C., 2000, Publications of the Astronomical Society of the Pacific, 112, 753
Belfiore F., et al., 2015, Monthly Notices of the Royal Astronomical Society, 449, 867
Belfiore F., et al., 2016, Monthly Notices of the Royal Astronomical Society, 461, 3111
Bertola F., Bettoni D., Danziger J., Sadler E., Sparke L., de Zeeuw T., 1991, The Astrophysical Journal, 373, 369
Binette L., Magris C. G., Stasińska G., Bruzual A. G., 1994, Astronomy and Astrophysics, 292, 13
Bonatto C., Bica E., Alloin D., 1989, Astronomy and Astrophysics, 226, 23
Bregman J. N., Snider B. A., Grego L., Cox C. V., 1998, The Astrophysical Journal, 499, 670
Buson L. M., et al., 1993, Astronomy and Astrophysics, 280, 409
Bönsch G., Potulski E., 1998, Metrologia, 35, 133
Caon N., Macchetto D., Pastoriza M., 2000, The Astrophysical Journal Supplement Series, 127, 39
Cappellari M., Copin Y., 2003, Monthly Notices of the Royal Astronomical Society, 342, 345
Cardelli J. A., Clayton G. C., Mathis J. S., 1989, The Astrophysical Journal, 345, 245
Carrasco E. R., Oliveira C. M. d., Infante L., 2006, The Astronomical Journal, 132, 1796
Cid Fernandes R., Stasińska G., Mateus A., Vale Asari N., 2011, Monthly Notices of the Royal Astronomical Society, 413, 1687
Constantin A., Vogeley M. S., 2006, The Astrophysical Journal, 650, 727
Croton D. J., et al., 2006, Monthly Notices of the Royal Astronomical Society, 365, 11
Dopita M. A., Sutherland R. S., 1995, The Astrophysical Journal, 455, 468
Eracleous M., Hwang J. A., Flohic H. M. L. G., 2010, The Astrophysical Journal, 711, 796
Fabian A., 2012, Annual Review of Astronomy and Astrophysics, 50, 455
Ferland G. J., Netzer H., 1983, The Astrophysical Journal, 264, 105
Ferrari F., Pastoriza M. G., Macchetto F., Caon N., 1999, Astronomy and Astrophysics Supplement Series, 136, 269
Ferrari F., Pastoriza M. G., Macchetto F. D., Bonatto C., Panagia N., Sparks W. B., 2002, Astronomy & Astrophysics, 389, 355
Filippenko A. V., 1982, Publications of the Astronomical Society of the Pacific, 94, 715
Flohic H. M. L. G., Eracleous M., Chartas G., Shields J. C., Moran E. C., 2006, The Astrophysical Journal, 647, 140
Gebhardt K., et al., 2000, The Astrophysical Journal, 539, L13
Girardi L., Bressan A., Bertelli G., Chiosi C., 2000, Astronomy and Astrophysics Supplement Series, 141, 371
Gomes J. M., et al., 2016, Astronomy & Astrophysics, 588, A68
Gonzalez R. C., Woods R. E., 2008, Digital image processing, 3rd ed edn. Prentice Hall, Upper Saddle River, N.J
Halpern J. P., Steiner J. E., 1983, The Astrophysical Journal, 269, L37
Hamuy M., Walker A. R., Suntzeff N. B., Gigoux P., Heathcote S. R., Phillips M. M., 1992, Publications of the Astronomical Society of the Pacific, 104, 533
Hansen L., Jorgensen H. E., Norgaard-Nielsen H. U., 1991, Astronomy and Astrophysics, 243, 49
Healey S. E., Romani R. W., Taylor G. B., Sadler E. M., Ricci R., Murphy T., Ulvestad J. S., Winn J. N., 2007, The Astrophysical Journal Supplement Series, 171, 61
Heckman T. M., 1980, Astronomy and Astrophysics, 87, 152
Heckman T. M., Best P. N., 2014, Annual Review of Astronomy and Astrophysics, 52, 589
Herpich F., Mateus A., Stasińska G., Cid Fernandes R., Vale Asari N., 2016,

Monthly Notices of the Royal Astronomical Society, 462, 1826
Ho L. C., 2008, Annual Review of Astronomy and Astrophysics, 46, 475
Ho L. C., Filippenko A. V., Sargent W. L. W., 1996, The Astrophysical Journal, 462, 183
Ho L. C., Filippenko A. V., Sargent W. L. W., Peng C. Y., 1997, The Astrophysical Journal Supplement Series, 112, 391
Ho I.-T., et al., 2014, Monthly Notices of the Royal Astronomical Society, 444, 3894
Ho I.-T., et al., 2016, Monthly Notices of the Royal Astronomical Society, 457, 1257
Hsieh B. C., et al., 2017, The Astrophysical Journal, 851, L24
Häring N., Rix H.-W., 2004, The Astrophysical Journal, 604, L89
Kauffmann G., et al., 2003, Monthly Notices of the Royal Astronomical Society, 341, 54
Kehrig C., et al., 2012, Astronomy & Astrophysics, 540, A11
Kewley L. J., Groves B., Kauffmann G., Heckman T., 2006, Monthly Notices of the Royal Astronomical Society, 372, 961
Kormendy J., Ho L. C., 2013, Annual Review of Astronomy and Astrophysics, 51, 511
Lagos P., et al., 2022, Monthly Notices of the Royal Astronomical Society
Lauberts A., Valentijn E. A., 1989, The surface photometry catalogue of the ESO-Uppsala galaxies. https://ui.adsabs.harvard.edu/abs/1989spce.book.....L
Loubser S. I., Soechting I. K., 2013, Monthly Notices of the Royal Astronomical Society, 431, 2933
Lucy L. B., 1974, The Astronomical Journal, 79, 745
Luridiana V., Morisset C., Shaw R. A., 2015, Astronomy & Astrophysics, 573, A42
Macchetto F., Pastoriza M., Caon N., Sparks W. B., Giavalisco M., Bender R., Capaccioli M., 1996, Astronomy and Astrophysics Supplement Series, 120, 463
Machacek M. E., O'Sullivan E., Randall S. W., Jones C., Forman W. R., 2010, The Astrophysical Journal, 711, 1316
Magorrian J., et al., 1998, The Astronomical Journal, 115, 2285
Mauch T., Murphy T., Buttery H. J., Curran J., Hunstead R. W., Piestrzynski B., Robertson J. G., Sadler E. M., 2003, Monthly Notices of the Royal Astronomical Society, 342, 1117
Menezes R. B., Ricci T. V., Steiner J. E., da Silva P., Ferrari F., Borges B. W., 2019, Monthly Notices of the Royal Astronomical Society, 483, 3700
Menezes R. B., Steiner J. E., Ricci T. V., da Silva P., 2022, Monthly Notices of the Royal Astronomical Society, 513, 5935
Muñoz L. H., Márquez I., Cazzoli S., Masegosa J., Agís-González B., 2022, Astronomy & Astrophysics, 660, A133
Nagar N. M., Falcke H., Wilson A. S., 2005, Astronomy & Astrophysics, 435, 521
Nayakshin S., Zubovas K., 2012, Monthly Notices of the Royal Astronomical Society, 427, 372
Osterbrock D. E., Ferland G. J., 2006, Astrophysics of gaseous nebulae and active galactic nuclei, 2nd ed edn. University Science Books, Sausalito, Calif
Papaderos P., et al., 2013, Astronomy & Astrophysics, 555, L1
Pizzella A., et al., 1997, Astronomy and Astrophysics, v.323, p.349-356, 323, 349
Ramella M., Focardi P., Geller M. J., 1996, Astronomy and Astrophysics, 312, 745
Ricci T. V., Steiner J. E., Menezes R. B., 2014a, Monthly Notices of the Royal Astronomical Society, 440, 2419
Ricci T. V., Steiner J. E., Menezes R. B., 2014b, Monthly Notices of the Royal Astronomical Society, 440, 2442
Ricci T. V., Steiner J. E., Menezes R. B., 2015a, Monthly Notices of the Royal Astronomical Society, 447, 1504
Ricci T. V., Steiner J. E., Menezes R. B., 2015b, Monthly Notices of the Royal Astronomical Society, 451, 3728
Richardson W. H., 1972, JOSA, 62, 55
Rickes M. G., Pastoriza M. G., Bonatto C., 2008, Monthly Notices of the Royal Astronomical Society, 384, 1427
Riffel R., et al., 2021, Monthly Notices of the Royal Astronomical Society, 501, 4064
Rose T., et al., 2019, Monthly Notices of the Royal Astronomical Society, 489, 349
Ruschel-Dutra D., Oliveira B. D. D., 2020, danielrd6/ifscube: Modeling, doi:10.5281/ZENODO.4065550, https://zenodo.org/record/4065550
Sarzi M., et al., 2010, Monthly Notices of the Royal Astronomical Society, 402, 2187
Schlafly E. F., Finkbeiner D. P., 2011, The Astrophysical Journal, 737, 103
Segers M. C., Schaye J., Bower R. G., Crain R. A., Schaller M., Theuns T., 2016, Monthly Notices of the Royal Astronomical Society: Letters, 461, L102
Singh R., et al., 2013, Astronomy & Astrophysics, 558, A43
Slee O. B., Sadler E. M., Reynolds J. E., Ekers R. D., 1994, Monthly Notices of the Royal Astronomical Society, 269, 928
Stasińska G., et al., 2008, Monthly Notices of the Royal Astronomical Society: Letters, 391, L29
Steiner J. E., Menezes R. B., Ricci T. V., Oliveira A. S., 2009, Monthly Notices of the Royal Astronomical Society, 395, 64
Steiner J. E., et al., 2022, Monthly Notices of the Royal Astronomical Society, 510, 5780
Tody D., 1986, in Crawford D. L., ed., Society of Photo-Optical Instrumentation Engineers (SPIE) Conference Series Vol. 627, Instrumentation in astronomy VI. Crawford, David L., Tucson, p. 733, doi:10.1117/12.968154, http://proceedings.spiedigitallibrary.org/proceeding.aspx?doi=10.1117/12.968154
Tody D., 1993, in Astronomical Data Analysis Software and Systems I. p. 173, https://ui.adsabs.harvard.edu/abs/1993ASPC...52..173T
Tully R. B., et al., 2013, The Astronomical Journal, 146, 86
Veron-Cetty M.-P., Veron P., 1988, Astronomy and Astrophysics, Vol. 204, p. 28-38 (1988), 204, 28
Yan R., Blanton M. R., 2012, The Astrophysical Journal, 747, 61
Zeilinger W. W., et al., 1996, Astronomy and Astrophysics Supplement Series, 120, 257
de Vaucouleurs G., de Vaucouleurs A., Corwin Herold G. J., Buta R. J., Paturel G., Fouque P., 1991, Third reference catalogue of bright galaxies. Springer-Verlag, New York
do Nascimento J. C., et al., 2019, Monthly Notices of the Royal Astronomical Society, 486, 5075
van Dokkum P., 2001, Publications of the Astronomical Society of the Pacific, 113, 1420

This paper has been typeset from a TEX/LATEX file prepared by the author.

6 Considerações Finais e perspectivas

Neste trabalho analisamos a região central da ETG NGC 6868 usando dados de GMOS-IFU para mapear o seu histórico de formação, a população estelar e as suas propriedades químicas, bem como o gás ionizado e o estado físico que este material se apresenta.

O estudo da população estelar nos revela que:

- Esta galáxia é dominada por uma população velha e rica em metais (12.6 Gyr; 1.0 e 1.6 $Z_{\odot}$) e apresenta um gradiente negativo em metalicidade. Isto é endossado pela distribuição espacial de [MgFe]'. Nós não encontramos sinais significativos de formação estelar para além de um único surto de formação estelar a cerca de 13 bilhões de anos.

- A aparente distorção na imagem do contínuo é devida à presença de uma faixa de poeira na linha de visada no centro de NGC 6868 e atinge um pico em $A_V \approx 0.65$ mag. Esta estrutura é coincidente com aquelas achadas em outros estudos.

- Não encontramos evidências de um FC, provavelmente devido ao fato do AGN no centro de NGC 6868 estar acretando matéria em taxas muito baixas.

- A cinemática estelar no centro de NGC 6868 é caracterizada por uma alta dispersão de velocidade e nenhuma rotação estelar é aparente.

- Os índices Mg_2, Mg_b, Fe3 e [MgFe]' apresentam perfis complexos, sendo que Mg_2 apresenta o maior gradiente. Ainda assim, ele é muito plano para ser consistente com um cenário de formação por um colapso monolítico.

- Três regiões distintas podem ser encontradas fazendo correlações entre os índices: anti-correlação para $R \lesssim 100$ pc e $R \gtrsim 220$ pc e correlação para 100 pc$\lesssim R \lesssim$ 220 pc. Isso revela diferentes mecanismos de enriquecimento do gás.

- O mapa de [α/Fe] não apresenta um gradiente claro. Porém, a mediana aparenta também estar dividida em três regiões: a região central (R<100 pc) e nas bordas do FoV (R>260 pc) parecem estar significativamente mais α-*enhanced* que na região intermediária.

Estes achados sugerem que NGC 6868 não formou-se através de apenas um colapso e evoluiu passivamente desde então. Na verdade, nós propomos que ela sofreu uma fusão no passado com outra galáxia. Isto pode explicar a distribuição do α-*enhancement* e as

diferentes correlações nos índices juntos com os da síntese de população estelar, como o gradiente na metalicidade e o fato dela ser completamente dominada por populações velhas. Nós não encontramos evidências de um componente cinemático diferente ou porque esta suposta fusão aconteceu há muito tempo atrás ou precisaríamos de um FoV maior para conseguirmos definir se esta região realmente é um KDC como outros estudos já reportaram.

Além das conclusões retiradas da população estelar, o gás ionizado em NGC 6868 prova ser um fonte muito interessante para se estudar os processos com características LINER. Os principais achados do nosso estudo estão citados abaixo:

- *Channel maps* e os perfis de linha revelam uma cinemática complexa indicando que diferentes processos estão atuando em NGC 6868.

- O ajuste das linhas de emissão revelou dois componentes cinemáticos: um estreito e um largo. O componente estreito traça um disco de gás ionizado e o componente largo traça provavelmente gás que está caindo em direção ao SMBH de NGC 6868 e se organizando em um componente dominado por dispersão. As distribuições de fluxo encontradas corroboram estes achados.

- O avermelhamento na banda V derivado através das linhas de recombinação do hidrogênio é consistente com o achado na síntese de população estelar derivado pelo STARLIGHT, considerando que a amplitude encontrada é maior. Provavelmente, isto é devido a um maior obscurecimento da fonte de ionização por poeira, possivelmente o LLAGN central.

- Reportamos também a primeira medição da temperatura eletrônica em NGC 6868. Encontramos uma temperatura de $\sim$ 14000 K para a região central com as partes mais externas passando os $\sim$ 20000 K. O perfil de densidade mostra um comportamento inverso uma vez que apresenta um pico em seu centro de $\sim$ 800 cm^{-3} caindo até $\sim$ 100 cm^{-3} nas partes externas do FoV, indicando uma compressão do gás.

- Todo o FoV das nossas observações está dentro da região LINER do diagrama BPT. Já no diagrama WHAN a região central aparenta se ionizar primariamente por um LLAGN e as HOLMES, criou um campo de radiação ionizante, que provavelmente também é o responsável pela ionização em maiores escalas. O perfil de temperatura que encontramos somado aos diagramas não descarta a possibilidade de choques também estarem envolvidos na ionização de NGC 6868.

Portanto, NGC 6868 prova ser um objeto com inúmeras peculiaridades e cujos cenários de formação, bem como os atuais processos que acontecem em seu centro são

muito complexos. Espera-se que o trabalho atual ajude a melhorar o entendimento sobre a formação das ETGs. Os resultados apresentados aqui, podem ser utilizados, por exemplo, para serem comparados com simulações de alta resolução (e.g. EAGLE) e cujo o resultado final é um "objeto" similar a NGC 6868. Assim, permitindo também avançar no entendimento sobre os diferentes processos de ionização em LINERs.

Com o domínio das diferentes técnicas necessárias para esse tipo de análise, bem como de um entendimento mais claro dos processos físicos que ocorrem nesse tipo de objetos pretendemos aumentar a amostra e fazer uma análise detalhada em objetos com diferentes massas e em diferentes ambientes.

Referências

ALLINGTON-SMITH, J. et al. Integral Field Spectroscopy with the Gemini Multiobject Spectrograph.I. Design, Construction, and Testing. *Publications of the Astronomical Society of the Pacific*, IOP Publishing, v. 114, n. 798, p. 892, jul. 2002. ISSN 1538-3873. Citado na página 29.

BABYK, I. V. et al. X-Ray Scaling Relations of Early-type Galaxies. *The Astrophysical Journal*, v. 857, p. 32, abr. 2018. ISSN 0004-637X. Citado na página 26.

BALDRY, I. K. et al. Quantifying the Bimodal Color-Magnitude Distribution of Galaxies. *The Astrophysical Journal*, v. 600, n. 2, p. 681–694, jan. 2004. ISSN 0004-637X, 1538-4357. Citado na página 21.

BARBERA, F. L. et al. SPIDER VIII – constraints on the stellar initial mass function of early-type galaxies from a variety of spectral features. *Monthly Notices of the Royal Astronomical Society*, v. 433, n. 4, p. 3017–3047, ago. 2013. ISSN 0035-8711. Citado na página 33.

BARTH, A. J.; SHIELDS, J. C. LINER/Hii "Transition" Nuclei and the Nature of NGC 4569. *Publications of the Astronomical Society of the Pacific*, IOP Publishing, v. 112, n. 772, p. 753, jun. 2000. ISSN 1538-3873. Citado na página 24.

BELFIORE, F. et al. P-MaNGA Galaxies: Emission-lines properties – gas ionization and chemical abundances from prototype observations. *Monthly Notices of the Royal Astronomical Society*, v. 449, n. 1, p. 867–900, maio 2015. ISSN 0035-8711. Citado na página 25.

BELFIORE, F. et al. SDSS IV MaNGA – spatially resolved diagnostic diagrams: A proof that many galaxies are LIERs. *Monthly Notices of the Royal Astronomical Society*, v. 461, n. 3, p. 3111–3134, set. 2016. ISSN 0035-8711. Citado na página 24.

BINETTE, L. et al. Photoionization in elliptical galaxies by old stars. *Astronomy and Astrophysics*, v. 292, p. 13–19, dez. 1994. ISSN 0004-6361. Citado na página 24.

BÖNSCH, G.; POTULSKI, E. Measurement of the refractive index of air and comparison with modified Edl n's formulae. *Metrologia*, v. 35, n. 2, p. 133–139, abr. 1998. ISSN 0026-1394. Citado na página 30.

BRAMMER, G. B. et al. THE DEAD SEQUENCE: A CLEAR BIMODALITY IN GALAXY COLORS FROM $z = 0$ to $z = 2.5$. *The Astrophysical Journal*, v. 706, n. 1, p. L173–L177, nov. 2009. ISSN 0004-637X, 1538-4357. Citado na página 21.

BREGMAN, J. N. et al. Far-Infrared Emission From E and E/S0 Galaxies. *The Astrophysical Journal*, IOP Publishing, v. 499, n. 2, p. 670, jun. 1998. ISSN 0004-637X. Citado na página 27.

BRUZUAL, G.; CHARLOT, S. Stellar population synthesis at the resolution of 2003. *Monthly Notices of the Royal Astronomical Society*, v. 344, n. 4, p. 1000–1028, out. 2003. ISSN 0035-8711. Citado na página 32.

BULLOCK, J. S.; BOYLAN-KOLCHIN, M. Small-Scale Challenges to the ΛCDM Paradigm. *Annual Review of Astronomy and Astrophysics*, v. 55, n. 1, p. 343–387, 2017. Citado na página 22.

BURTSCHER, L. et al. LLAMA: Stellar populations in the nuclei of ultra-hard X-ray-selected AGN and matched inactive galaxies. *Astronomy & Astrophysics*, EDP Sciences, v. 654, p. A132, out. 2021. ISSN 0004-6361, 1432-0746. Citado na página 24.

BUSON, L. M. et al. Tghe distribution of ionized gas in early-type galaxies. *Astronomy and Astrophysics*, v. 280, p. 409–425, dez. 1993. ISSN 0004-6361. Citado na página 27.

CALDWELL, N. A SURVEY OF 0II EMISSION IN ELLIPTICAL GALAXIES. *Publications of the Astronomical Society of the Pacific*, IOP Publishing, v. 96, n. 578, p. 287, abr. 1984. ISSN 1538-3873. Citado na página 22.

CANO-DÍAZ, M. et al. SPATIALLY RESOLVED STAR FORMATION MAIN SEQUENCE OF GALAXIES IN THE CALIFA SURVEY. *The Astrophysical Journal*, American Astronomical Society, v. 821, n. 2, p. L26, abr. 2016. ISSN 2041-8205. Citado na página 21.

CAON, N.; MACCHETTO, D.; PASTORIZA, M. A Survey of the Interstellar Medium in Early-Type Galaxies. III. Stellar and Gas Kinematics*. *The Astrophysical Journal Supplement Series*, IOP Publishing, v. 127, n. 1, p. 39, mar. 2000. ISSN 0067-0049. Citado 2 vezes nas páginas 27 e 35.

CAPPELLARI, M. Structure and Kinematics of Early-Type Galaxies from Integral Field Spectroscopy. *Annual Review of Astronomy and Astrophysics*, v. 54, p. 597–665, set. 2016. ISSN 0066-4146. Citado na página 21.

CAPPELLARI, M.; COPIN, Y. Adaptive spatial binning of integral-field spectroscopic data using Voronoi tessellations. *Monthly Notices of the Royal Astronomical Society*, v. 342, n. 2, p. 345–354, jun. 2003. ISSN 0035-8711. Citado na página 34.

CARDELLI, J. A.; CLAYTON, G. C.; MATHIS, J. S. The relationship between infrared, optical, and ultraviolet extinction. *The Astrophysical Journal*, v. 345, p. 245, out. 1989. ISSN 0004-637X, 1538-4357. Citado 3 vezes nas páginas 30, 32 e 36.

CARRASCO, E. R.; OLIVEIRA, C. M. de; INFANTE, L. The Dwarf Galaxy Population in Nearby Groups: The Data*. *The Astronomical Journal*, IOP Publishing, v. 132, n. 5, p. 1796, set. 2006. ISSN 1538-3881. Citado na página 26.

CONROY, C.; GUNN, J. E.; WHITE, M. THE PROPAGATION OF UNCERTAINTIES IN STELLAR POPULATION SYNTHESIS MODELING. I. THE RELEVANCE OF UNCERTAIN ASPECTS OF STELLAR EVOLUTION AND THE INITIAL MASS FUNCTION TO THE DERIVED PHYSICAL PROPERTIES OF GALAXIES. *The Astrophysical Journal*, v. 699, n. 1, p. 486–506, jul. 2009. ISSN 0004-637X, 1538-4357. Citado na página 32.

CONSTANTIN, A.; VOGELEY, M. S. The Clustering of Low-Luminosity Active Galactic Nuclei. *The Astrophysical Journal*, IOP Publishing, v. 650, n. 2, p. 727, out. 2006. ISSN 0004-637X. Citado na página 24.

CROTON, D. J. et al. The many lives of active galactic nuclei: Cooling flows, black holes and the luminosities and colours of galaxies. *Monthly Notices of the Royal Astronomical Society*, v. 365, n. 1, p. 11–28, jan. 2006. ISSN 0035-8711. Citado na página 23.

DAHMER-HAHN, L. G. et al. Stellar populations in local AGNs: Evidence for enhanced star formation in the inner 100 pc. *Monthly Notices of the Royal Astronomical Society*, v. 509, n. 3, p. 4653–4668, dez. 2021. ISSN 0035-8711, 1365-2966. Citado na página 24.

DEKEL, A.; BIRNBOIM, Y. Galaxy bimodality due to cold flows and shock heating. *Monthly Notices of the Royal Astronomical Society*, v. 368, n. 1, p. 2–20, maio 2006. ISSN 0035-8711. Citado na página 21.

DOKKUM, P. G. van. Cosmic-Ray Rejection by Laplacian Edge Detection. *Publications of the Astronomical Society of the Pacific*, v. 113, n. 789, p. 1420–1427, nov. 2001. ISSN 0004-6280, 1538-3873. Citado na página 29.

DOPITA, M. A.; SUTHERLAND, R. S. Spectral Signatures of Fast Shocks. II. Optical Diagnostic Diagrams. *The Astrophysical Journal*, v. 455, p. 468, dez. 1995. ISSN 0004-637X, 1538-4357. Citado na página 24.

ELLISON, S. L. et al. The EDGE–CALIFA survey: Central molecular gas depletion in AGN host galaxies – a smoking gun for quenching? *Monthly Notices of the Royal Astronomical Society: Letters*, v. 505, n. 1, p. L46–L51, jul. 2021. ISSN 1745-3925. Citado na página 23.

ERACLEOUS, M.; HWANG, J. A.; FLOHIC, H. M. L. G. AN ASSESSMENT OF THE ENERGY BUDGETS OF LOW-IONIZATION NUCLEAR EMISSION REGIONS. *The Astrophysical Journal*, American Astronomical Society, v. 711, n. 2, p. 796–807, fev. 2010. ISSN 0004-637X. Citado na página 25.

FABIAN, A. Observational Evidence of Active Galactic Nuclei Feedback. *Annual Review of Astronomy and Astrophysics*, v. 50, n. 1, p. 455–489, 2012. Citado na página 23.

FERLAND, G. J.; NETZER, H. Are there any shock-heated galaxies. *The Astrophysical Journal*, v. 264, p. 105, jan. 1983. ISSN 0004-637X, 1538-4357. Citado na página 24.

FERNANDES, R. C. On tests of full spectral fitting algorithms. *Monthly Notices of the Royal Astronomical Society*, v. 480, n. 4, p. 4480–4488, nov. 2018. ISSN 0035-8711. Citado na página 31.

FERNANDES, R. C. et al. The star formation history of Seyfert 2 nuclei. *Monthly Notices of the Royal Astronomical Society*, v. 355, n. 1, p. 273–296, nov. 2004. ISSN 0035-8711. Citado na página 31.

FERNANDES, R. C. et al. Semi-empirical analysis of Sloan Digital Sky Survey galaxies – I. Spectral synthesis method. *Monthly Notices of the Royal Astronomical Society*, v. 358, n. 2, p. 363–378, abr. 2005. ISSN 0035-8711. Citado 2 vezes nas páginas 31 e 32.

FERNANDES, R. C. et al. Resolving galaxies in time and space - I. Applying STARLIGHT to CALIFA datacubes. *Astronomy & Astrophysics*, EDP Sciences, v. 557, p. A86, set. 2013. ISSN 0004-6361, 1432-0746. Citado na página 31.

FERNANDES, R. C. et al. A comprehensive classification of galaxies in the Sloan Digital Sky Survey: How to tell true from fake AGN? *Monthly Notices of the Royal Astronomical Society*, v. 413, n. 3, p. 1687–1699, maio 2011. ISSN 0035-8711. Citado na página 24.

FERRARI, F. et al. Survey of the ISM in early-type galaxies - IV. The hot dust component. *Astronomy & Astrophysics*, EDP Sciences, v. 389, n. 2, p. 355–366, jul. 2002. ISSN 0004-6361, 1432-0746. Citado na página 27.

FILIPPENKO, A. V. The importance of atmospheric differential refraction in spectrophotometry. *Publications of the Astronomical Society of the Pacific*, v. 94, p. 715, ago. 1982. ISSN 0004-6280, 1538-3873. Citado na página 30.

FLOHIC, H. M. L. G. et al. The Central Engines of 19 LINERs as Viewed by$\less$i$\greater$Chandra$\less$/i$\greater$. *The Astrophysical Journal*, American Astronomical Society, v. 647, n. 1, p. 140–160, ago. 2006. ISSN 0004-637X. Citado na página 24.

GEBHARDT, K. et al. A Relationship between Nuclear Black Hole Mass and Galaxy Velocity Dispersion. *The Astrophysical Journal*, IOP Publishing, v. 539, n. 1, p. L13, ago. 2000. ISSN 0004-637X. Citado na página 23.

GIRARDI, L. et al. Evolutionary tracks and isochrones for low- and intermediate-mass stars: From 0.15 to 7 , and from to 0.03. *Astronomy and Astrophysics Supplement Series*, EDP Sciences, v. 141, n. 3, p. 371–383, fev. 2000. ISSN 0365-0138, 1286-4846. Citado na página 32.

GOMES, J. M. et al. Warm ionized gas in CALIFA early-type galaxies - 2D emission-line patterns and kinematics for 32 galaxies. *Astronomy & Astrophysics*, EDP Sciences, v. 588, p. A68, abr. 2016. ISSN 0004-6361, 1432-0746. Citado na página 25.

GONZALEZ, R. C.; WOODS, R. E. *Digital Image Processing*. 3rd ed. ed. Upper Saddle River, N.J: Prentice Hall, 2008. ISBN 978-0-13-168728-8. Citado na página 29.

HALPERN, J. P.; STEINER, J. E. Low-ionization active galactic nuclei - X-ray or shock heated? *The Astrophysical Journal*, v. 269, p. L37, jun. 1983. ISSN 0004-637X, 1538-4357. Citado na página 24.

HAMUY, M. et al. SOUTHERN SPECTROPHOTOMETRIC STANDARDS. I. *Publications of the Astronomical Society of the Pacific*, IOP Publishing, v. 104, n. 677, p. 533, jul. 1992. ISSN 1538-3873. Citado na página 29.

HANSEN, L.; JORGENSEN, H. E.; Norgaard-Nielsen, H. U. NGC 6868 : A merger with dust and extended Ly-alpha emission. *Astronomy and Astrophysics*, v. 243, p. 49, mar. 1991. ISSN 0004-6361. Citado na página 27.

HÄRING, N.; RIX, H.-W. On the Black Hole Mass-Bulge Mass Relation. *The Astrophysical Journal*, IOP Publishing, v. 604, n. 2, p. L89, mar. 2004. ISSN 0004-637X. Citado na página 23.

HARRISON, C. M. Impact of supermassive black hole growth on star formation. *Nature Astronomy*, Nature Publishing Group, v. 1, n. 7, p. 1–8, jul. 2017. ISSN 2397-3366. Citado na página 23.

HEALEY, S. E. et al. CRATES: An All-Sky Survey of Flat-Spectrum Radio Sources. *The Astrophysical Journal Supplement Series*, v. 171, p. 61–71, jul. 2007. ISSN 0067-0049. Citado 2 vezes nas páginas 26 e 27.

HECKMAN, T. M. An Optical and Radio Survey of the Nuclei of Bright Galaxies - Activity in the Normal Galactic Nuclei. *Astronomy and Astrophysics*, v. 87, p. 152, jul. 1980. ISSN 0004-6361. Citado na página 24.

HECKMAN, T. M.; BEST, P. N. The Coevolution of Galaxies and Supermassive Black Holes: Insights from Surveys of the Contemporary Universe. *Annual Review of Astronomy and Astrophysics*, v. 52, n. 1, p. 589–660, 2014. Citado na página 23.

HERPICH, F. et al. The many faces of LINER-like galaxies: A WISE view. *Monthly Notices of the Royal Astronomical Society*, v. 462, n. 2, p. 1826–1833, out. 2016. ISSN 0035-8711. Citado na página 25.

HO, I.-T. et al. The SAMI Galaxy Survey: Shocks and outflows in a normal star-forming galaxy. *Monthly Notices of the Royal Astronomical Society*, v. 444, n. 4, p. 3894–3910, nov. 2014. ISSN 1365-2966, 0035-8711. Citado na página 24.

HO, I.-T. et al. The SAMI Galaxy Survey: Extraplanar gas, galactic winds and their association with star formation history. *Monthly Notices of the Royal Astronomical Society*, v. 457, n. 2, p. 1257–1278, abr. 2016. ISSN 0035-8711, 1365-2966. Citado na página 24.

HO, L. C. Nuclear Activity in Nearby Galaxies. *Annual Review of Astronomy and Astrophysics*, v. 46, n. 1, p. 475–539, 2008. Citado na página 23.

HO, L. C.; FILIPPENKO, A. V.; SARGENT, W. L. W. New Insights into the Physical Nature of LINERs from a Multiwavelength Analysis of the Nucleus of M81. *The Astrophysical Journal*, v. 462, p. 183, maio 1996. ISSN 0004-637X, 1538-4357. Citado na página 24.

HO, L. C. et al. A Search for "Dwarf" Seyfert Nuclei. IV. Nuclei with Broad Hα Emission. *The Astrophysical Journal Supplement Series*, IOP Publishing, v. 112, n. 2, p. 391, out. 1997. ISSN 0067-0049. Citado na página 24.

HOOK, I. M. et al. The Gemini–North Multi-Object Spectrograph: Performance in Imaging, Long-Slit, and Multi-Object Spectroscopic Modes. *Publications of the Astronomical Society of the Pacific*, IOP Publishing, v. 116, n. 819, p. 425, abr. 2004. ISSN 1538-3873. Citado na página 29.

HOPKINS, P. F.; ELVIS, M. Quasar feedback: More bang for your buck. *Monthly Notices of the Royal Astronomical Society*, v. 401, n. 1, p. 7–14, jan. 2010. ISSN 0035-8711. Citado na página 23.

HSIEH, B. C. et al. SDSS-IV MaNGA: Spatially Resolved Star Formation Main Sequence and LI(N)ER Sequence. *The Astrophysical Journal*, American Astronomical Society, v. 851, n. 2, p. L24, dez. 2017. ISSN 2041-8205. Citado na página 25.

KAUFFMANN, G. et al. The dependence of star formation history and internal structure on stellar mass for 10^5 low-redshift galaxies. *Monthly Notices of the Royal Astronomical Society*, v. 341, n. 1, p. 54–69, maio 2003. ISSN 00358711, 13652966. Citado na página 21.

KEHRIG, C. et al. The ionized gas in the CALIFA early-type galaxies - I. Mapping two representative cases: NGC 6762 and NGC 5966. *Astronomy & Astrophysics*, EDP Sciences, v. 540, p. A11, abr. 2012. ISSN 0004-6361, 1432-0746. Citado na página 25.

KEREŠ, D. et al. How do galaxies get their gas? *Monthly Notices of the Royal Astronomical Society*, v. 363, n. 1, p. 2–28, out. 2005. ISSN 0035-8711. Citado na página 21.

KING, A.; POUNDS, K. Powerful Outflows and Feedback from Active Galactic Nuclei. *Annual Review of Astronomy and Astrophysics*, v. 53, n. 1, p. 115–154, ago. 2015. ISSN 0066-4146, 1545-4282. Citado na página 23.

KOKUSHO, T. et al. A star formation study of the ATLAS3D early-type galaxies with the AKARI all-sky survey. *Astronomy & Astrophysics*, EDP Sciences, v. 605, p. A74, set. 2017. ISSN 0004-6361, 1432-0746. Citado na página 22.

KORMENDY, J.; HO, L. C. Coevolution (Or Not) of Supermassive Black Holes and Host Galaxies. *Annual Review of Astronomy and Astrophysics*, v. 51, n. 1, p. 511–653, ago. 2013. ISSN 0066-4146, 1545-4282. Citado na página 23.

KROUPA, P. On the variation of the initial mass function. *Monthly Notices of the Royal Astronomical Society*, v. 322, n. 2, p. 231–246, abr. 2001. ISSN 0035-8711. Citado na página 32.

KUNTSCHNER, H. The stellar populations of early-type galaxies in the Fornax cluster. *Monthly Notices of the Royal Astronomical Society*, v. 315, n. 1, p. 184–208, jun. 2000. ISSN 0035-8711. Citado na página 33.

LAGOS, P. et al. Spatially-resolved properties of early-type group-dominant galaxies with MUSE: Gas content, ionisation mechanisms and metallicity gradients. *Monthly Notices of the Royal Astronomical Society*, arXiv, 2022. Citado na página 25.

LAUBERTS, A.; VALENTIJN, E. A. *The Surface Photometry Catalogue of the ESO-Uppsala Galaxies*. [S.l.: s.n.], 1989. Citado na página 26.

LOUBSER, S. I.; SOECHTING, I. K. The detailed nature of active central cluster galaxies. *Monthly Notices of the Royal Astronomical Society*, v. 431, n. 3, p. 2933–2959, maio 2013. ISSN 0035-8711. Citado na página 25.

LUCY, L. B. An iterative technique for the rectification of observed distributions. *The Astronomical Journal*, v. 79, p. 745, jun. 1974. ISSN 00046256. Citado na página 30.

LURIDIANA, V.; MORISSET, C.; SHAW, R. A. PyNeb: A new tool for analyzing emission lines - I. Code description and validation of results. *Astronomy & Astrophysics*, EDP Sciences, v. 573, p. A42, jan. 2015. ISSN 0004-6361, 1432-0746. Citado na página 36.

MACCHETTO, F. et al. A survey of the ISM in early-type galaxies. I. The ionized gas. *Astronomy and Astrophysics Supplement Series*, EDP Sciences, v. 120, n. 3, p. 463–488, dez. 1996. ISSN 0365-0138, 1286-4846. Citado na página 27.

MACHACEK, M. E. et al. THE MYSTERIOUS MERGER OF NGC 6868 AND NGC 6861 IN THE TELESCOPIUM GROUP. *The Astrophysical Journal*, v. 711, n. 2, p. 1316–1332, mar. 2010. ISSN 0004-637X, 1538-4357. Citado na página 27.

MAGORRIAN, J. et al. The Demography of Massive Dark Objects in Galaxy Centers. *The Astronomical Journal*, IOP Publishing, v. 115, n. 6, p. 2285, jun. 1998. ISSN 1538-3881. Citado na página 23.

MALLMANN, N. D. et al. The first 62 AGN observed with SDSS-IV MaNGA – II. Resolvedstellar populations. *Monthly Notices of the Royal Astronomical Society*, v. 478, n. 4, p. 5491–5504, ago. 2018. ISSN 0035-8711. Citado 2 vezes nas páginas 24 e 32.

MARASTON, C.; STRÖMBÄCK, G. Stellar population models at high spectral resolution. *Monthly Notices of the Royal Astronomical Society*, v. 418, n. 4, p. 2785–2811, dez. 2011. ISSN 0035-8711. Citado na página 32.

MATTEO, T. D.; SPRINGEL, V.; HERNQUIST, L. Energy input from quasars regulates the growth and activity of black holes and their host galaxies. *Nature*, Nature Publishing Group, v. 433, n. 7026, p. 604–607, fev. 2005. ISSN 1476-4687. Citado na página 23.

MAUCH, T. et al. SUMSS: A wide-field radio imaging survey of the southern sky – II. The source catalogue. *Monthly Notices of the Royal Astronomical Society*, v. 342, n. 4, p. 1117–1130, jul. 2003. ISSN 0035-8711. Citado na página 27.

MENEZES, R. B. et al. A treatment procedure for GMOS/IFU data cubes: Application to NGC 2835. *Monthly Notices of the Royal Astronomical Society*, v. 483, n. 3, p. 3700–3717, mar. 2019. ISSN 0035-8711. Citado na página 29.

MENEZES, R. B. et al. The DIVING3D Survey – Deep IFS view of nuclei of galaxies – II. First results: Nuclear emission-line properties of the mini-DIVING3D sample. *Monthly Notices of the Royal Astronomical Society*, v. 513, n. 4, p. 5935–5954, jul. 2022. ISSN 0035-8711. Citado na página 25.

MO, H.; BOSCH, F. van den; WHITE, S. *Galaxy Formation and Evolution*. Cambridge ; New York: Cambridge University Press, 2010. ISBN 978-0-521-85793-2. Citado na página 21.

MUÑOZ, L. H. et al. A search for ionised gas outflows in an Hα imaging atlas of nearby LINERs. *Astronomy & Astrophysics*, EDP Sciences, v. 660, p. A133, abr. 2022. ISSN 0004-6361, 1432-0746. Citado na página 24.

MUZZIN, A. et al. THE EVOLUTION OF THE STELLAR MASS FUNCTIONS OF STAR-FORMING AND QUIESCENT GALAXIES TO $z = 4$ FROM THE COSMOS/UltraVISTA SURVEY. *The Astrophysical Journal*, v. 777, n. 1, p. 18, out. 2013. ISSN 0004-637X, 1538-4357. Citado na página 21.

NAGAR, N. M.; FALCKE, H.; WILSON, A. S. Radio sources in low-luminosity active galactic nuclei - IV. Radio luminosity function, importance of jet power, and radio properties of the complete Palomar sample. *Astronomy & Astrophysics*, EDP Sciences, v. 435, n. 2, p. 521–543, maio 2005. ISSN 0004-6361, 1432-0746. Citado na página 24.

NAYAKSHIN, S.; ZUBOVAS, K. Quasar feedback: Accelerated star formation and chaotic accretion. *Monthly Notices of the Royal Astronomical Society*, v. 427, n. 1, p. 372–378, nov. 2012. ISSN 0035-8711. Citado na página 23.

NOESKE, K. G. et al. Star Formation in AEGIS Field Galaxies since $z = 1.1$: Staged Galaxy Formation and a Model of Mass-dependent Gas Exhaustion. *The Astrophysical Journal*, v. 660, n. 1, p. L47–L50, maio 2007. ISSN 0004-637X, 1538-4357. Citado na página 21.

OSTERBROCK, D. E.; FERLAND, G. J. *Astrophysics of Gaseous Nebulae and Active Galactic Nuclei*. 2nd ed. ed. Sausalito, Calif: University Science Books, 2006. ISBN 978-1-891389-34-4. Citado na página 35.

PAPADEROS, P. et al. Nebular emission and the Lyman continuum photon escape fraction in CALIFA early-type galaxies. *Astronomy & Astrophysics*, EDP Sciences, v. 555, p. L1, jul. 2013. ISSN 0004-6361, 1432-0746. Citado na página 25.

PHILLIPS, M. M. et al. Ionized gas in elliptical and SO galaxies. I. A survey for H alpha and N II emission. *The Astronomical Journal*, v. 91, p. 1062–1085, maio 1986. ISSN 0004-6256. Citado na página 22.

RAMELLA, M.; FOCARDI, P.; GELLER, M. J. The redshift-space neighborhoods of 13 SSRS groups of galaxies. *Astronomy and Astrophysics*, v. 312, p. 745–750, ago. 1996. ISSN 0004-6361. Citado na página 26.

RICCI, T. V.; STEINER, J. E.; MENEZES, R. B. IFU spectroscopy of 10 early-type galactic nuclei – II. Nuclear emission line properties. *Monthly Notices of the Royal Astronomical Society*, v. 440, n. 3, p. 2442–2456, maio 2014. ISSN 0035-8711. Citado 2 vezes nas páginas 25 e 29.

RICCI, T. V.; STEINER, J. E.; MENEZES, R. B. Integral field unit spectroscopy of 10 early-type galactic nuclei – I. Principal component analysis Tomography and nuclear activity. *Monthly Notices of the Royal Astronomical Society*, v. 440, n. 3, p. 2419–2441, maio 2014. ISSN 0035-8711. Citado na página 25.

RICCI, T. V.; STEINER, J. E.; MENEZES, R. B. Erratum: IFU spectroscopy of 10 early-type galactic nuclei – II. Nuclear emission line properties. *Monthly Notices of the Royal Astronomical Society*, v. 447, n. 2, p. 1504–1505, fev. 2015. ISSN 0035-8711. Citado na página 25.

RICCI, T. V.; STEINER, J. E.; MENEZES, R. B. IFU spectroscopy of 10 early-type galactic nuclei – III. Properties of the circumnuclear gas emission. *Monthly Notices of the Royal Astronomical Society*, v. 451, n. 4, p. 3728–3758, ago. 2015. ISSN 0035-8711. Citado na página 25.

RICHARDSON, W. H. Bayesian-Based Iterative Method of Image Restoration*. *JOSA*, Optica Publishing Group, v. 62, n. 1, p. 55–59, jan. 1972. Citado na página 30.

RICKES, M. G.; PASTORIZA, M. G.; BONATTO, C. Star formation, metallicity gradient and ionized gas: Clues to the formation of the elliptical galaxies NGC 6868 and 5903. *Monthly Notices of the Royal Astronomical Society*, v. 384, n. 4, p. 1427–1436, mar. 2008. ISSN 0035-8711. Citado na página 26.

RIFFEL, R. et al. Gemini NIFS survey of feeding and feedback processes in nearby active galaxies – VI. Stellar populations. *Monthly Notices of the Royal Astronomical Society*, v. 512, n. 3, p. 3906–3921, maio 2022. ISSN 0035-8711. Citado na página 24.

RIFFEL, R. et al. Determining star formation rates in active galactic nuclei hosts via stellar population synthesis. *Monthly Notices of the Royal Astronomical Society*, v. 501, n. 3, p. 4064–4079, mar. 2021. ISSN 0035-8711. Citado 4 vezes nas páginas 23, 24, 32 e 36.

RIFFEL, R. et al. Probing the near-infrared stellar population of Seyfert galaxies. *Monthly Notices of the Royal Astronomical Society*, v. 400, n. 1, p. 273–290, nov. 2009. ISSN 0035-8711. Citado na página 24.

RIFFEL, R. et al. Optical/NIR stellar absorption and emission-line indices from luminous infrared galaxies. *Monthly Notices of the Royal Astronomical Society*, v. 486, n. 3, p. 3228–3247, jul. 2019. ISSN 0035-8711. Citado na página 33.

RIFFEL, R.; VALE, T. B. Pacce: Perl algorithm to compute continuum and equivalent widths. *Astrophysics and Space Science*, v. 334, n. 2, p. 351–356, ago. 2011. ISSN 0004-640X, 1572-946X. Citado na página 33.

ROSA, I. G. de la et al. Truncated Star Formation in Compact Groups of Galaxies: A Stellar Population Study. *The Astronomical Journal*, v. 133, n. 1, p. 330–346, jan. 2007. ISSN 0004-6256, 1538-3881. Citado na página 33.

ROSE, T. et al. Constraining cold accretion on to supermassive black holes: Molecular gas in the cores of eight brightest cluster galaxies revealed by joint CO and CN absorption. *Monthly Notices of the Royal Astronomical Society*, v. 489, n. 1, p. 349–365, out. 2019. ISSN 0035-8711. Citado na página 27.

RUSCHEL-DUTRA, D. et al. Star formation in AGNs at the hundred parsec scale using MIR high-resolution images. *Monthly Notices of the Royal Astronomical Society*, v. 466, n. 3, p. 3353–3363, abr. 2017. ISSN 0035-8711. Citado na página 24.

RUSCHEL-DUTRA, D.; OLIVEIRA, B. D. D. *Danielrd6/Ifscube: Modeling*. 2020. Zenodo. Citado na página 35.

SARZI, M. et al. The SAURON project – XVI. On the sources of ionization for the gas in elliptical and lenticular galaxies. *Monthly Notices of the Royal Astronomical Society*, v. 402, n. 4, p. 2187–2210, mar. 2010. ISSN 0035-8711. Citado na página 25.

SCHAYE, J. et al. The EAGLE project: Simulating the evolution and assembly of galaxies and their environments. *Monthly Notices of the Royal Astronomical Society*, v. 446, n. 1, p. 521–554, jan. 2015. ISSN 0035-8711. Citado na página 23.

SCHLAFLY, E. F.; FINKBEINER, D. P. MEASURING REDDENING WITH SLOAN DIGITAL SKY SURVEY STELLAR SPECTRA AND RECALIBRATING SFD. *The Astrophysical Journal*, v. 737, n. 2, p. 103, ago. 2011. ISSN 0004-637X, 1538-4357. Citado 2 vezes nas páginas 26 e 30.

SEGERS, M. C. et al. The origin of the α-enhancement of massive galaxies. *Monthly Notices of the Royal Astronomical Society: Letters*, v. 461, n. 1, p. L102–L106, set. 2016. ISSN 1745-3925. Citado na página 23.

SINGH, R. et al. The nature of LINER galaxies: - Ubiquitous hot old stars and rare accreting black holes. *Astronomy & Astrophysics*, EDP Sciences, v. 558, p. A43, out. 2013. ISSN 0004-6361, 1432-0746. Citado 2 vezes nas páginas 24 e 25.

SLEE, O. B. et al. Parsec-scale radio cores in early-type galaxies. *Monthly Notices of the Royal Astronomical Society*, v. 269, n. 4, p. 928–946, ago. 1994. ISSN 0035-8711. Citado na página 27.

SPRINGEL, V. et al. Simulations of the formation, evolution and clustering of galaxies and quasars. *Nature*, Nature Publishing Group, v. 435, n. 7042, p. 629–636, jun. 2005. ISSN 1476-4687. Citado na página 23.

STASIŃSKA, G. et al. Can retired galaxies mimic active galaxies? Clues from the Sloan Digital Sky Survey. *Monthly Notices of the Royal Astronomical Society: Letters*, v. 391, n. 1, p. L29–L33, nov. 2008. ISSN 1745-3925. Citado na página 24.

STEINER, J. E. et al. PCA Tomography: How to extract information from data cubes. *Monthly Notices of the Royal Astronomical Society*, Oxford Academic, v. 395, n. 1, p. 64–75, maio 2009. ISSN 0035-8711. Citado na página 30.

STEINER, J. E. et al. The DIVING3D survey – Deep Integral Field Spectrograph View of Nuclei of Galaxies – I. Definition and sample presentation. *Monthly Notices of the Royal Astronomical Society*, v. 510, n. 4, p. 5780–5795, mar. 2022. ISSN 0035-8711. Citado na página 29.

STORCHI-BERGMANN, T.; SCHNORR-MÜLLER, A. Observational constraints on the feeding of supermassive black holes. *Nature Astronomy*, Nature Publishing Group, v. 3, n. 1, p. 48–61, jan. 2019. ISSN 2397-3366. Citado na página 23.

THOMAS, D.; MARASTON, C.; BENDER, R. Stellar population models of Lick indices with variable element abundance ratios. *Monthly Notices of the Royal Astronomical Society*, v. 339, n. 3, p. 897–911, mar. 2003. ISSN 0035-8711. Citado na página 33.

TODY, D. The Iraf Data Reduction And Analysis System. In: CRAWFORD, D. L. (Ed.). *Instrumentation in Astronomy VI*. Tucson: Crawford, David L., 1986. (Society of Photo-Optical Instrumentation Engineers (SPIE) Conference Series, v. 627), p. 733. Citado na página 29.

TODY, D. IRAF in the Nineties. In: *Astronomical Data Analysis Software and Systems I*. [S.l.: s.n.], 1993. (Astronomical Society of the Pacific Conference Series, v. 52), p. 173. Citado na página 29.

TREVISAN, M.; MAMON, G. A.; KHOSROSHAHI, H. G. Do the stellar populations of the brightest two group galaxies depend on the magnitude gap? *Monthly Notices of the Royal Astronomical Society*, v. 464, n. 4, p. 4593–4610, fev. 2017. ISSN 0035-8711. Citado na página 33.

TRUSSLER, J. et al. Both starvation and outflows drive galaxy quenching. *Monthly Notices of the Royal Astronomical Society*, v. 491, n. 4, p. 5406–5434, fev. 2020. ISSN 0035-8711. Citado na página 23.

TULLY, R. B. et al. COSMICFLOWS-2: THE DATA. *The Astronomical Journal*, American Astronomical Society, v. 146, n. 4, p. 86, set. 2013. ISSN 1538-3881. Citado na página 26.

VAUCOULEURS, G. de et al. *Third Reference Catalogue of Bright Galaxies*. New York: Springer-Verlag, 1991. Citado na página 26.

VAZDEKIS, A. et al. Evolutionary stellar population synthesis with MILES – II. Scaled-solar and α-enhanced models. *Monthly Notices of the Royal Astronomical Society*, v. 449, n. 2, p. 1177–1214, maio 2015. ISSN 0035-8711. Citado na página 33.

VAZDEKIS, A. et al. UV-extended E-MILES stellar population models: Young components in massive early-type galaxies. *Monthly Notices of the Royal Astronomical Society*, v. 463, n. 4, p. 3409–3436, dez. 2016. ISSN 0035-8711. Citado na página 32.

VERON-CETTY, M.-P.; VERON, P. Dust in early-type galaxies. *Astronomy and Astrophysics, Vol. 204, p. 28-38 (1988)*, v. 204, p. 28, out. 1988. ISSN 0004-6361. Citado na página 27.

WEL, A. van der et al. 3D-HST+CANDELS: THE EVOLUTION OF THE GALAXY SIZE-MASS DISTRIBUTION SINCE $z = 3$. *The Astrophysical Journal*, v. 788, n. 1, p. 28, maio 2014. ISSN 0004-637X, 1538-4357. Citado na página 21.

WETZEL, A. R.; TINKER, J. L.; CONROY, C. Galaxy evolution in groups and clusters: Star formation rates, red sequence fractions and the persistent bimodality: Galaxy evolution in groups and clusters. *Monthly Notices of the Royal Astronomical Society*, v. 424, n. 1, p. 232–243, jul. 2012. ISSN 00358711. Citado na página 21.

WORTHEY, G. et al. Old Stellar Populations. V. Absorption Feature Indices for the Complete Lick/IDS Sample of Stars. *The Astrophysical Journal Supplement Series*, v. 94, p. 687, out. 1994. ISSN 0067-0049. Citado na página 33.

YAN, R.; BLANTON, M. R. THE NATURE OF LINER-LIKE EMISSION IN RED GALAXIES. *The Astrophysical Journal*, American Astronomical Society, v. 747, n. 1, p. 61, fev. 2012. ISSN 0004-637X. Citado na página 24.

ZEILINGER, W. W. et al. The distribution of ionized gas in early-type galaxies. II. The velocity field of the ionized gas. *Astronomy and Astrophysics Supplement Series*, EDP Sciences, v. 120, n. 2, p. 257–266, dez. 1996. ISSN 0365-0138, 1286-4846. Citado 2 vezes nas páginas 27 e 35.

ZUBOVAS, K.; BOURNE, M. A. Do AGN outflows quench or enhance star formation? *Monthly Notices of the Royal Astronomical Society*, v. 468, n. 4, p. 4956–4967, jul. 2017. ISSN 0035-8711. Citado 2 vezes nas páginas 23 e 24.

Apêndices

APÊNDICE A – Press Release

A vida (nem tão) calma das galáxias elípticas: o caso de NGC 6868

Desde os primeiros estudos sobre galáxias por Hubble, já se sabe que elas se subdividem, de modo geral, em duas classes: as galáxias elípticas e as galáxias espirais. Estas últimas apresentam lindos braços espirais, cheios de centros de formação estelar que brilham com lindos tons azuis e vermelhos devido as jovens estrelas ionizando seu entorno, podendo também apresentar barras.

E, bem, também tem as galáxias elípticas... elas são esféricas ou redondas e um tom bege até um pouco desbotado. Enfim, acho que na competição de quem é o melhor *wallpaper* as espirais ganham não é? Devido a esta aparente falta de características interessantes estes objetos sempre foram pensados como sistemas muito simples, dominados apenas por dispersão de velocidades das estrelas velhas contidas neles.

Hoje em dia, porém já se sabe que estes sistemas podem ser muito mais complexos do que se imaginava: podendo apresentar poeira, gás, discos embebidos, jatos e muito mais! Além disso, hoje sabemos que as galáxias evoluem no decorrer da história do Universo, passando de formadoras de estrelas para aposentadas (sim, este é o termo mesmo!), sendo que este último é o caso da maioria das elípticas. Entender os processos físicos relevantes nesta transição é um dos maiores mistérios da astronomia moderna! E estudar estes sistemas mais "sem graça" pode nos dar boas pistas sobre esta transição.

Por isso, decidimos estudar a galáxia NGC 6868 que numa primeira vista não parece tão interessante assim. Porém, com as nossas observações fomos capazes de tirar algumas conclusões interessantes. Primeiramente, descobrimos que ela possui uma população muito velha e rica em metais, tudo esperado pra uma galáxia deste tipo. Contudo, nós descobrimos que ela possuiu uma variação na composição química da população estelar no seu centro, que é traçada utilizando o parâmetro $[\alpha/\mathrm{Fe}]$! Isto indica que no passado ela pode ter se fundido com alguma outra galáxia com composição estelar distinta, formando a estrutura que vemos atualmente.

Além disso, esta galáxia possui um disco de gás ionizado em seu centro, bem como influxo de gás, cuja fonte de ionização ainda é incerta. Baseado em outras observações e dos nossos dados, nós suspeitamos que esta galáxia tenha um núcleo ativo de baixa luminosidade em seu centro, mas que só é capaz de influenciar o seu entorno. Provavelmente, outros processos são os responsáveis pela ionização observada fora do seu centro. Além

disso, detectamos evidência de poeira no seu centro que, segundo outros estudos, deve ter vindo de uma galáxia que foi canibalizada por NGC 6868.

Nada mal para um objeto "sem graça"! Este estudo prova que as galáxias elípticas são laboratórios interessantes para entendermos a evolução das galáxias, bem como a sua aposentadoria. Esperamos replicar nossos estudos com outras galáxias para ajudar no nosso compreendimento sobre esta evolução.

Palavras-chave: Galáxias elípticas, NGC 6868